DISSERTATION

Put forward by
M.Sc. Sara Konrad
born in: Schwetzingen

Oral examination: 14 December 2020

COSMIC STRUCTURE FORMATION IN THE LIMIT OF SMALL SCALES WITHIN KINETIC FIELD THEORY

Referees: Matthias Bartelmann

Manfred Salmhofer

ABSTRACT

The amplitude and shape of the density fluctuation power spectrum today are determined by the initial conditions set after inflation, the properties of dark matter particles and the growth of structures due to the gravitational interaction in an expanding spacetime.

Since cosmic structure formation is highly non-linear, the impact of the properties of dark matter on today's structure or results from N-body simulations like the observed universal halo density profiles, are hard to understand with conventional analytical methods. While these approaches break down at small scales when particle streams cross, Kinetic Field Theory (KFT) operates with a generating functional in classical N-particle phase space, circumventing those problems.

In this work, we present novel asymptotic methods that apply to rapidly oscillating integrals with two large parameters. Applying these methods to KFT, we derive the asymptotic limit of the power spectrum on small scales in the Zel'dovich approximation. The power spectrum universally develops a k^{-3} tail, independent of the steepness of the initial spectrum, suggesting that scale-invariant structures form below a characteristic length scale already early in cosmic history. Finally, we derive the asymptotics of the factors of the factorized generating functional to guide their numerical implementation. These factors are indispensable for the numerical evaluation of perturbation theory and density correlation functions of high order within the framework of KFT.

ZUSAMMENFASSUNG

Die heutige Amplitude und Form des Leistungsspektrums kosmischer Dichtefluktuationen werden durch die Anfangsbedingungen nach der Inflation, die Eigenschaften der Teilchen dunkler Materie und das Strukturwachstum aufgrund gravitativer Wechselwirkung in einer expandierenden Raumzeit bestimmt.

Da kosmische Strukturentwicklung hochgradig nichtlinear verläuft, sind der Einfluss der Eigenschaften dunkler Materie auf die heutigen Strukturen sowie Ergebnisse aus N-Teilchen-Simulationen wie die beobachteten universellen Dichteprofile gebundener Strukturen mit konventionellen analytischen Methoden nur schwer zu verstehen. Während diese Herangehensweisen auf kleinen Skalen scheitern sobald sich Teilchenströme kreuzen, operiert die Kinetische Feldtheorie mit einem erzeugenden Funktional im klassischen N-Teilchen-Phasenraum und umgeht somit diese Probleme.

In dieser Arbeit präsentieren wir neue asymptotische Methoden, die auf stark oszillierende Integrale mit zwei großen Parametern anwendbar sind. Wir wenden diese Methoden auf KFT an und leiten im Rahmen der Zel'dovich-Näherung den asymptotischen Verlauf des Leistungsspektrums auf kleinen Skalen her. Das Leistungsspektrum strebt universell einem k^{-3}-Verhalten zu, unabhängig davon, wie steil das Anfangsleistungsspektrum war. Dies deutet darauf hin, dass sich unterhalb einer charakteristischen Längenskala skaleninvariante Strukturen bereits früh während der

kosmischen Geschichte bilden. Schließlich leiten wir die Asymptotik der Faktoren des faktorisierten erzeugenden Funktionals her, um Hinweise für deren numerische Implementierung zu gewinnen. Diese Faktoren sind unerlässlich, um Störungstheorie und Dichtekorrelationen höherer Ordnung im Rahmen von KFT zu berechnen.

PUBLICATIONS

Some ideas have appeared previously in the following publications:

[1] Matthias Bartelmann, Felix Fabis, Sara Konrad, Elena Kozlikin, Robert Lilow, Carsten Littek, and Johannes Dombrowski. "Analytic calculation of the non-linear cosmic density-fluctuation power spectrum in the Born approximation." In: 2017.

[2] Matthias Bartelmann, Elena Kozlikin, Robert Lilow, Carsten Littek, Felix Fabis, Ivan Kostyuk, Celia Viermann, Lavinia Heisenberg, Sara Konrad, and Daniel Geiss. "Cosmic structure formation with kinetic field theory." In: vol. 531. 11. Wiley Online Library, 2019, p. 1800446.

ACKNOWLEDGMENTS

CONTENTS

LIST OF FIGURES

LIST OF TABLES

This feeling of being lonely and very temporary visitors in the universe
is in flat contradiction to everything known about man
(and all other living organisms) in the sciences.
We do not "come into" this world;
we come out of it, as leaves from a tree.
As the ocean "waves," the universe "peoples."

— Alan Watts

In loving memory of my grandparents.

INTRODUCTION

Curious as we humans are, we seek to explore the world that we are part of and learn about the things that surround us. Throughout human history, changes in our scientific and philosophical world view go hand in hand with changes in the way how we think and how we see ourselves and how we conceive and articulate causal relations. Looking into the night sky and to the stars leads our gaze to the most extreme scales that we are able to explore.

What do we know today about our universe and what is still to be discovered?

We live in an expanding universe that appears isotropic and homogeneous if averaged over large enough scales [3, 50]. According to Einstein's theory of general relativity, the dynamics of spacetime depends on the matter-energy density of the universe [23]. However, only 5% of today's matter-energy content can be considered understood and are well described by the standard model of particle physics. For the remaining 95%, typically split into the two components dark energy and dark matter, we have only vague ideas about some of their properties [2]. Approximately 69% of today's matter-energy content are attributed to dark energy, a hypothetical substance that causes the accelerated expansion that the universe undergoes today [53, 55]. The remaining approximately 26% are associated to dark matter that reveals itself only via gravitational interaction. It differs from regular matter – so called baryonic matter – by the absence of any detectable interactions with electromagnetic radiation.

While we leave the search for dark energy to others, the goal of this work is to contribute to the ongoing endeavor to uncover the nature of dark matter, which might be particle-like, a modification of gravity, or something different.

Since dark matter is approximately five times more abundant than baryonic matter, it is supposed to dominate cosmic structure formation on large scales. The structures today are believed to have originated from small initial fluctuations set during the earliest stages of the universe [44]. If dark matter consists of an unknown particle species, the subsequent evolution of such structures until today depends on the particles' properties, such as their mass and interactions, as well as the background expansion of the universe. Hence, studying the evolution of the statistics of cosmic structures will guide us to a better understanding of the relation between these interactions, the growth of cosmic structures and to constrain possible dark matter particle candidates.

Since the differential equations that govern cosmic structure formation are highly non-linear and hard to solve analytically with conventional methods, the most detailed theoretical predictions today come from N-body simulations (see e.g. [59, 60, 63]). On the one hand, it is for example known from N-body simulations in combination with cosmological observations, that dark matter particles need to be non-relativistic and are to the largest extend collisionless. Otherwise the theoretical predictions would not match the structures we observe today. On the other hand, numerical simulations also bring up new problems and questions. An example is the observation that the density profiles of simulated dark matter halos always follow the same profile function,

independent of the halo mass and widely independent of the dark matter type [43, 46, 64]. Up to now, it is not known why these halo profiles are universal and structures therefore scale-free across many orders of magnitude. Even though we got many interesting insights about comic structure formation from simulations, they are also inherently limited in their applicability. For example, repeating simulations with many different cosmological parameters, initial conditions, dark matter models and across large scales requires large resources in time and energy. Moreover, extracting reliable values for higher-order statistics that serve as tests for non-Gaussianities turns out to be very difficult.

Due to their high computational cost and because gaining a fundamental understanding of physical processes from complex numerical simulations is limited, there is great need for analytical approaches with which cosmic structure formation can be calculated, especially in the non-linear regime. Common analytical approaches such as Eulerian and Lagrangian perturbation theory are successful in describing the largest structures in the regime of linear up to mildly nonlinear scales larger than approximately 20 h^{-1} Mpc. However, these theories break down when the particle streams of collisionless dark matter cross and the velocity fields are not uniquely defined any more (for an overview, see [11] and references therein). Thus, they cannot describe the evolution of the non-linear structures on small scales, which we wish to analyze.

For these reasons, we work in the framework of Kinetic Field Theory (KFT). KFT operates in the $6N$-dimensional phase space of correlated microscopic particles obeying Hamiltonian dynamics. Thus, the crossing of particle streams is no obstacle because the full phase space information always remains available [7, 9, 10]. Making use of the path integral formalism, the central objects of KFT are (i) the free generating functional, that governs free particle motion, and (ii) an interaction operator that has to be chosen appropriately. While correlation functions of macroscopic fields are obtained by the application of appropriate operators, interactions beyond free motion can be incorporated via perturbation theory or a mean field approach. KFT is a very flexible theory in which collisionless dark matter, other types of dark matter, baryonic physics, modified gravity and different cosmological models can be considered, while the computations can be performed on a standard computer within minutes or faster. For a recent review, we refer to [10]

When we started with this work, the basic equations of KFT, which govern the free evolution as well as perturbation theory, were already available. However, it was not possible to evaluate these expressions numerically at intermediate and small scales when the full initial momentum-momentum correlations were taken into account, not even for the free two-point statistics. The difficulties were due to the rapidly oscillating integrals that are delicate to handle numerically. To circumvent these obstacles, approximations in the initial correlations where typically applied. While these approximations yield numerically stable results, they are only valid in the large scale regime, where linear growth is expected to occur. At the other end of the spectrum, i.e. in the small-scale limit, no such approximation methods had been available, neither analytical nor numerical.

To eventually derive analytical and numerical results for the small-scale regime of cosmic structure formation from KFT, we pursue three major goals with this work.

(i) The development of novel asymptotic methods that apply to the rapidly oscillating integrals in KFT in Chapter 4. These methods might also find applications beyond KFT.

(ii) The application of these methods to KFT to derive the small-scale asymptotics of the free power spectrum in Chapter 6. Our main result is the proof that the free power spectrum at small scales always develops a k^{-3} tail, independent of the shape of the initial power spectrum.

(iii) To derive the asymptotic behavior of the factors of the free generating functional and to guide their numerical implementation in Chapter 7.

This work is organized as follows. In Chapter 2, we start with a summary of the cosmological standard model and review analytical approaches to cosmic structure formation. In the following Chapter 3, we review the basics of KFT and specifically those more recent results that are relevant to this work. In Chapter 4, we derive novel asymptotic methods for rapidly oscillating integrals with two large parameters, first in one and then in N dimensions. We then derive the asymptotics of the initial correlation functions of the cosmic density and velocity fields at large and small scales in Chapter 5. With the use of these results, we derive in Chapter 6 the small-scale k^{-3} asymptotics of the density fluctuation power spectrum. In Chapter 7, we derive the asymptotics of the factors of the free generating functional to enable the numerical evaluation and the implementation of higher order spectra and perturbation theory. Finally in Chapter 8, we give some concluding remarks and an outlook to future work.

Part I

FOUNDATIONS

STRUCTURES IN THE UNIVERSE

A hundred years ago, the western image of the cosmos was very different compared to the image we have today. It was widely believed that the universe was static and that all objects in it are located within the Milky Way, our own host galaxy. Modern cosmology begins with two scientific breakthroughs, one observational and one theoretical. In 1912, Henrietta Swan Leavitt discovered the relation between the period and the brightness of Cepheid variable stars [39]. This breakthrough in observational cosmology made it possible to quantify the distances to remote stars and later to prove the existence of other galaxies outside the Milky Way. In 1915, Albert Einstein lay the theoretical foundations of cosmology with the general theory of relativity, in which he explained gravity as a geometric phenomenon of spacetime [23]. These two findings marked the onset of a drastic change in our picture of the universe that finally led to the formulation of the standard model of cosmology.

In 1922 Alexander Friedmann published the equations for the dynamics of a homogeneous and isotropic universe, showing that the universe might not be static but expands [29, 30]. Independently, Georges Lemaître arrived the same prediction in 1927, and discussed its physical implications, in particular in the context of observations of redshifted galaxies [40]. The first observational proof for the expansion of the universe was provided by Edwin Hubble. He measured the redshifts of distant galaxies and quantified their distance with Cepheids. From these data, he found the linear relationship between distance and velocity, now known as Hubble-Lemaître law [37]. The more distant a galaxy, the higher the velocity with which it is driven away from us.

A few years later, Fritz Zwicky (1933) based on redshift observations of galaxies in clusters discovered first evidence for the existence of dark matter, a non-luminous substance that interacts gravitationally. By measuring the peculiar velocities of galaxies in the Coma cluster, he found that in order to be stable, the cluster had to contain much more mass than visible. In 1970, Vera Rubin confirmed the existence of dark matter on galaxy scales, where she found that the rotation curves measured from stellar velocities were flat [56]. These rotation curves cannot be explained by the observed distribution of luminous matter in the form of stars, gas or dust. Today we know that the universe is filled with approximately five times more dark than visible matter.

It is important to note that besides dark matter, our universe hosts another – even more puzzling and abundant – substance. Observations of supernovae of type 1A suggest that the universe today undergoes accelerated expansion [53, 55]. In general relativity, the unknown source of this acceleration needs to be attributed to a substance with negative pressure, known as dark energy that is the most abundant energy component in the universe today.

The discovery of the cosmic microwave background by Penzias and Wilson in 1965 marks another milestone in cosmology [52]. Since our universe expands today, going back in time implies higher densities and temperatures. Eventually, the density

and temperature reach a level at which the atoms in the universe ionize. Photons are tightly coupled to this hot optically thick plasma. When the temperature drops during cosmic expansion, atoms form and the universe becomes transparent, releasing the formerly trapped photons. This electromagnetic radiation is observed today as cosmic microwave background (CMB) radiation. Due to its thermal origin, it has a perfect Planck spectrum. The fluctuations in the cosmic density field during recombination are imprinted as tiny fluctuations of the CMB temperature. The statistics of these fluctuations can be used as an important tool for modern cosmology as they reveal crucial insights about the early universe as well as various processes that took place along the line of sight. For example, the low amplitude of these temperature fluctuations proves that a substantial amount of matter – that is dark matter – cannot interact with photons at all.

What is the origin of structures in the universe? According to the model of cosmic inflation, the structures we observe today were seeded by tiny quantum fluctuations [44]. These quantum fluctuations were massively enlarged during an early era of inflationary expansion. The origin and nature of the inflaton field, which is assumed to have driven this inflation, is still unknown. Once inflation ended, the seed fluctuations imprinted on the density field grew via gravitational instability. As we know today, this growth was largely dominated by the gravity of dark matter, whose dynamics shaped various properties of the present-day structures, such as their mass profiles or the amount of substructures. In order to understand the nature of dark matter, we have to understand how the formation of structures proceeds.

In the following, we give a brief introduction about the technical aspects of cosmology necessary for this work. This chapter is organized as follows. In the first section, we review the dynamics of the homogeneous and isotropic Friedmann universe. In the second section, we review how the growth of linear structures is described in the so-called Eulerian picture. In the third section, we show how Zel'dovich particle trajectories are derived in the Lagrangian picture. In the fourth section, we summarize the statistical description of density fluctuations and the connection to the halo picture. Finally, in the last section, we summarize these insights and discuss the need of an alternative analytical approach to cosmic structure formation that help us to understand the nature of dark matter and the emergence of universal halo density profiles.

Most parts of this chapter follow the description in [6].

2.1   THE HOMOGENEOUS UNIVERSE

Cosmology describes the universe as a whole, the natural language being the framework of general relativity. The dynamical variable that is considered is the metric $g_{\mu\nu}$. The metric is sourced in a set of non-linear second-order differential equations, known as the Einstein field equations

$$G_{\mu\nu} = \frac{8\pi G}{c^4} T_{\mu\nu} + \Lambda g_{\mu\nu} \,. \tag{2.1}$$

The Einstein tensor $G_{\mu\nu}$ on the left hand side represents the dynamics or (local) curvature of space time, containing second derivatives of the metric. The energy-momentum tensor is $T_{\mu\nu}$. When placed on the right hand side of the equation, the

cosmological constant term $\Lambda g_{\mu\nu}$ may be interpreted as an additional energy density with negative pressure. This term was originally introduced by Einstein to allow a static non-empty universe [24]. However, it is also possible to place this term on the left hand side of the equation and interpret it as a geometrical feature of spacetime.

On large scales, the universe appears to be homogeneous and isotropic. These two assumptions lead to the most general form of the metric, the Robertson-Walker line element

$$ds^2 = g_{\mu\nu}dx^\mu dx^\nu = -c^2 dt^2 + a^2(t)\left[dw^2 + f_K^2(w)\left(d\theta^2 + \sin^2\theta d\phi^2\right)\right] . \qquad (2.2)$$

The coordinates are chosen such that w is the radial co-moving coordinate of freely-falling fundamental observers who observe an isotropic universe. The time-dependent scale factor a describes the change in spatial length scales with cosmic time t. The coordinates can be chosen such that metric contains no terms g_{0i} with $i \in \{1,2,3\}$. If this was not possible, these terms would imply the flow of energy, contradicting isotropy. Analogously, if the coordinates cannot be chosen such that simultaneously the off-diagonal terms in the spatial part of the metric, i.e. g_{ij} with $i \neq j$, vanish, this would imply matter flows, which are forbidden, likewise. Due to homogeneity, the function f_K needs to be trigonometric, hyperbolic, or linear in the coordinate w,

$$f_K(w) = \begin{cases} K^{-1/2}\sin(\sqrt{K}w) & \text{for } K > 0 \\ w & \text{for } K = 0 \\ |K|^{-1/2}\sinh(\sqrt{|K|}w) & \text{for } K < 0 \end{cases} \qquad (2.3)$$

The constant K parameterises the curvature of spatial hypersurfaces. The only dynamical variable in the metric is therefore the scale factor a.

Due to homogeneity and isotropy, we can consider the matter-energy content of the universe as an ideal fluid with energy density ρ and pressure p. From Einstein's field equations and the Robertson-Walker line element, the Friedmann equations

$$H^2(a) := \left(\frac{\dot{a}}{a}\right)^2 = \frac{8\pi G}{3}\rho - \frac{Kc^2}{a^2} + \frac{\Lambda c^2}{3} , \qquad (2.4)$$

$$\frac{\ddot{a}}{a} = -\frac{4\pi G}{3}\left(\rho + \frac{3p}{c^2}\right) + \frac{\Lambda c^2}{3} \qquad (2.5)$$

follow. When a obeys the Friedmann equations, the metric in (2.2) is called the *Friedmann-Lemaître-Robertson-Walker metric*. The first Friedmann equation (2.4) defines the (squared) Hubble function H that quantifies the expansion rate. The second Friedmann equation (2.5) shows that any conventional energy content with positive pressure, like matter or radiation, slows down the expansion, while the cosmological constant leads to an acceleration of the expansion. Curvature has no effect on the acceleration of the scale factor. Note that one can combine both Friedmann equations (2.5)–(2.5) to get the adiabatic equation,

$$\frac{d}{dt}\left(a^3\rho c^2\right) + p\frac{d}{dt}\left(a^3\right) = 0 , \qquad (2.6)$$

which reflects local energy-momentum conservation.

In order to close the system of equations, an equation of state for the energy content is necessary. We use the ansatz

$$\rho = w\rho c^2 \, , \tag{2.7}$$

with the parameter w, characteristic for the specific type of energy considered. The energy density ρ and pressure p in the Friedmann equations are sums of different energy components

$$\rho = \sum_i \rho_i \, . \tag{2.8}$$

In the equations of motion, these energy components differ in their equation of state parameters w_i. For non-relativistic (dark) matter ρ_m, the pressure is negligible compared to the energy density, such that $w_m = 0$. Relativistic matter and radiation ρ_r are characterized by a trace-free energy momentum tensor, such that $w_r = \frac{1}{3}$ follows. An equation of state parameter can also be introduced for the cosmological constant, which yields $w_\Lambda = -1$. In this case, the cosmological constant is interpreted as an effective fluid component, that we call dark energy. Whether the presently observed acceleration of the cosmic expansion is governed by a cosmological constant or forms of dark energy is not known today. Alternative values for w_Λ or even a time-dependent equation of state, as are considered in so-called quintessence models, may be viable explanations as well.

The evolution of each density component with the scale factor a follows from the adiabatic equation (2.6) by inserting the corresponding equation of state parameter. Denoting the energy densities with a subscript 0 at $a = 1$, we obtain the equations

$$\rho_r(a) = \rho_{r0}a^{-4} \, , \quad \rho_m(a) = \rho_{m0}a^{-3} \quad \text{and} \quad \rho_\Lambda(a) = \rho_{\Lambda0} \equiv \frac{\Lambda c^2}{8\pi G} \, . \tag{2.9}$$

In order to express the densities by dimensionless parameters, it is convenient to define the critical density

$$\rho_{cr}(t) := \frac{3H^2(t)}{8\pi G} \quad \text{with} \quad \rho_{cr0} := \frac{3H_0^2}{8\pi G} \, . \tag{2.10}$$

The critical density has the following meaning: when the energy density of the universe, including the cosmological constant, is equal to the critical density, then the universe is spatially flat. We now define the dimensionless density parameters for radiation, matter and dark energy,

$$\Omega_i(t) := \frac{\rho_i(t)}{\rho_{cr}(t)} \quad \text{with} \quad \Omega_{i0} := \frac{\rho_{i0}}{\rho_{cr0}} \, . \tag{2.11}$$

The critical density also allows to define a curvature density parameter

$$\Omega_K := 1 - \Omega_r - \Omega_m - \Omega_\Lambda \, . \tag{2.12}$$

The values of these parameters today are shown in Table 2.2. With these parameters and (2.9) we can write the Hubble function (2.4) as

$$H(a) = H_0\sqrt{\Omega_{r0}a^{-4} + \Omega_{m0}a^{-3} + \Omega_{K0}a^{-2} + \Omega_{\Lambda0}} \tag{2.13}$$

$$=: H_0 E(a) \, , \tag{2.14}$$

which defines the *expansion function E*. This representation of the Hubble function shows that at very early times the expansion rate was governed by radiation. Since the energy density of radiation drops by a factor of a faster than that of matter, the scale factor $a_{eq} = \frac{\Omega_{r0}}{\Omega_{m0}}$ marks matter-radiation equality. As the matter density dilutes, the universe eventually reaches an era dominated by the cosmological constant. A summary of the evolution of the scale factor with cosmic time and of the expansion rate with scale factor is shown in Table 2.1.

era	$a(t)$	$H(a)$
radiation domination	$\propto t^{1/2}$	$\propto a^{-2}$
matter domination	$\propto t^{2/3}$	$\propto a^{-3/2}$
Λ domination	$\propto \exp(H_0\sqrt{\Omega_{\Lambda 0}}t)$	$\rightarrow$ const.

Table 2.1: The evolution of the scale factor a with cosmic time t and the evolution of the Hubble function H with the scale factor in the era of radiation, matter and Λ domination are shown.

2.2 LINEAR GROWTH OF LARGE-SCALE STRUCTURES

On scales $\gtrsim 100$ Mpc, the universe indeed appears to be homogeneous [57]. Below this scale, the matter in the universe is hierarchically structured. The largest gravitationally bound objects are the galaxy clusters, which are connected by the filamentary structure of the so-called *cosmic web*. The cosmic web is a network pattern of filaments, clusters and voids visible in the matter distribution on the largest observed scales. Galaxies and dwarf galaxies form on smaller scales, while smallest structures are globular clusters and finally stars and planets.

In order to describe the growth of the large-scale structures, one would need to do this in the framework of general relativity. However, since the structures we consider are small compared to the Hubble radius ($r_H \approx 3.01 \times 10^3 h^{-1}$ Mpc) and retardation effects are unimportant, Newtonian dynamics is appropriate to use.

We describe the dynamics of the inhomogeneous cosmic fluid by the equations of hydrodynamics

$$\frac{\partial \rho}{\partial t} + \vec{\nabla} \cdot \left(\rho \vec{v} \right) = 0 \,, \tag{2.15}$$

$$\frac{\partial \vec{v}}{\partial t} + \left(\vec{v} \cdot \vec{\nabla} \right) \vec{v} = -\frac{\vec{\nabla} p}{\rho} - \vec{\nabla}\Phi \,, \tag{2.16}$$

$$\vec{\nabla}^2 \Phi = 4\pi G \rho \,. \tag{2.17}$$

The continuity equation (2.15) ensures mass conservation. The Euler equation (2.16) expresses the conservation of momentum in the presence of pressure and gravitational forces and the Newtonian gravitational potential Φ satisfies Poisson's equation (2.17). These non-linear equations can in general not be solved analytically. However, when the amplitude of fluctuations in the density and velocity fields are small, (2.15)–(2.17) can be linearised in the fluctuations and then solved to yield linear growth. This procedure is called *(Eulerian) linear perturbation theory*.

parameter	symbol	value
Hubble constant	H_0	67.4 ± 0.5 km s^{-1} Mpc^{-1}
age of the universe	t_H	13.801 ± 0.024 Gyr
redshift at recombination	z^*	1089.80 ± 0.21
age at recombination	t^*	377700 ± 3200 yr
variance at 8 h^{-1}Mpc	σ_8	0.811 ± 0.006
spectral index	n_s	0.965 ± 0.004
matter density parameter	Ω_{m0}	0.315 ± 0.007
baryon density parameter	Ω_{b0}	0.0486 ± 0.0010
radiation density parameter	Ω_{r0}	
curvature density parameter	Ω_{K0}	0.001 ± 0.002
dark energy density parameter	$\Omega_{\Lambda0}$	0.6889 ± 0.0056
dark energy eos parameter	w_Λ	-1.03 ± 0.03

Table 2.2: Cosmological parameters, taken from the Planck collaboration [2].

To this end, we split the density and the velocity field into their mean values, indicated by a subscript 0, and their fluctuations

$$\rho = \rho_0 + \delta\rho \quad \text{and} \quad \vec{v} = \vec{v}_0 + \delta\vec{v} \, . \tag{2.18}$$

The introduction of a non-vanishing mean velocity might seem to contradict the isotropy assumption. However, when we consider the physical spatial coordinate $\vec{r}$ and the comoving coordinate $\vec{q} = \vec{r}/a$, the velocity can be split into a comoving and a peculiar part,

$$\vec{v} = \dot{\vec{r}} = \dot{a}\vec{q} + a\dot{\vec{q}} = H\vec{r} + a\dot{\vec{q}} = \vec{v}_0 + \delta\vec{v} \, . \tag{2.19}$$

Thus, two observers who are comoving with the Hubble flow and separated by the comoving vector $\vec{q}$, will measure a relative velocity $\vec{v}_0 = H\vec{r}$ in physical coordinates due to the Hubble expansion.

Next, we define the density contrast

$$\delta(\vec{r},t) := \frac{\rho(\vec{r},t) - \rho_0(t)}{\rho_0(t)} = \frac{\delta\rho(\vec{r},t)}{\rho_0(t)} \tag{2.20}$$

that quantifies the relative over- or under-density relative to the mean density and the peculiar velocity $\vec{u} := \frac{\delta\vec{v}}{a}$.

Linearizing the perturbed equations (2.15)–(2.17) and considering that the mean background fields satisfy those equations individually, we arrive at

$$\dot{\delta} + \vec{\nabla} \cdot \vec{u} = 0 \, , \tag{2.21}$$

$$\dot{\vec{u}} + 2H\vec{u} = -\frac{\vec{\nabla}\delta p}{a^2\rho_0} - \frac{\vec{\nabla}\delta\Phi}{a^2} \, , \tag{2.22}$$

$$\vec{\nabla}^2\delta\Phi = 4\pi G\rho_0 a^2\delta \, . \tag{2.23}$$

We relate fluctuations in the pressure to fluctuations in the density field via the sound speed c_s by $\delta p = c_s^2 \rho_0 \delta$, (2.21)–(2.23) can be combined to yield the linear second-order equation for the dynamics of the density contrast of non-relativistic matter

$$\ddot{\delta} + 2H\dot{\delta} = 4\pi G\rho_0\delta + \frac{c_s^2\vec{\nabla}^2\delta}{a} \ . \tag{2.24}$$

Decomposing the density contrast into plane waves yields

$$\ddot{\hat{\delta}} + 2H\dot{\hat{\delta}} = \left(4\pi G\rho_0 - \frac{c_s^2k^2}{a}\right)\hat{\delta} \ . \tag{2.25}$$

For a pressureless non-relativistic fluid like dark matter that dominates cosmic structure formation, (2.25) simplifies to

$$\ddot{\hat{\delta}} + 2H\dot{\hat{\delta}} = \frac{3}{2}H^2\Omega_m\hat{\delta} \ . \tag{2.26}$$

Since modes are uncoupled in the linear theory, every mode evolves independently with the same rate. Thus, the solution to (2.25) has the form $\hat{\delta}(\vec{k}, t) = \hat{\delta}(\vec{k}, t_0)D(t)$, with $D(t_0) = 1$. Since (2.25) is a linear second-order equation, the function D has two independent solutions. Considering collisionless dark matter in the matter dominated era, the solutions to (2.26) are a growing solution $D_+(a) \propto a$ and a decaying solution $D_-(a) \propto a^{-3/2}$. In general, any linear combination of the two solutions then solves (2.25). The single constraint $D(t_0) = 1$ removes one degree of freedom in the combination of these solutions, but is not sufficient to uniquely determine the final form. Since we are interested in the growth of structures, only the growth factor D_+ will be considered for any practical purposes and we write

$$\delta(t) = \delta(t_0)\frac{D_+(t)}{D_+(t_0)} \ . \tag{2.27}$$

In Table 2.3 we show the solutions for relativistic matter, pressure-less non-relativistic matter and non-relativistic matter with pressure in the radiation dominated era.

matter type	non-growing solution	growing solution	scales
relativistic	$\propto a^{-2}$ osc. $\omega = \frac{ck}{\sqrt{3}aH}$	$\propto a^2$	$k \ll 2\sqrt{3}Hc^{-1}$ $k \gg 2\sqrt{3}Hc^{-1}$
non-relelativistic (pressure-less)	$\propto$ const.	$\propto \ln a$	all
non-relativistic (with pressure)	$\propto$ const. osc. $\omega = \frac{ck}{aH}$	$\propto \ln a$	$k \ll 2Hc^{-1}$ $k \gg 2Hc^{-1}$

Table 2.3: The linear growth of density perturbations during the radiation dominated era for different types of matter is scale-dependent. Large-scale perturbations in relativistic matter grow like a^2, while small-scale perturbations oscillate. Perturbations in pressure-less non-relativistic matter grow logarithmically at all scales. Large-scale perturbations in non-relativistic matter with pressure also grow logarithmically, while small-scale perturbations oscillate.

A good approximation for the post-matter dominated era, when $\Omega_m + \Omega_\Lambda = 1$, while $\Omega_m \neq 1$ is given by

$$D_+(a) \approx \frac{5a}{2}\Omega_m \left[\Omega_m^{4/7} - \Omega_\Lambda + \left(1 + \frac{1}{2}\Omega_m\right)\left(1 + \frac{1}{70}\Omega_\Lambda\right)\right]^{-1} . \tag{2.28}$$

The linear growth of velocity perturbations in co-moving coordinates $\vec{q}$ can be derived from the ansatz

$$\vec{u}(\vec{q}, t) = u(t)\vec{\nabla}\delta\Phi(\vec{q}, t) , \tag{2.29}$$

and the linear growth of density perturbations (2.27), when the initial field $\vec{u}^{(i)}$ is a Gaussian random field, correlated with $\delta^{(i)}$. Ignoring pressure gradients in (2.22), which is appropriate for collisionless dark matter, the linear velocity perturbations become

$$\vec{u} = -\frac{2}{3}\frac{f}{a^2 H \Omega_m}\vec{\nabla}\delta\Phi , \tag{2.30}$$

with the logarithmic derivative of the growth function $f = \mathrm{d}\ln D_+ / \mathrm{d}\ln a$. The ansatz (2.29) for the perturbations in the velocity field implies a curl-free velocity field, since $\vec{u}$ is proportional to the gradient of the perturbations in the gravitational field. If the initial velocity perturbations contained a non-vanishing vorticity part, i.e. $\vec{\nabla} \times \vec{u}(t_0) \neq 0$, linear perturbation theory yields only a decaying solution $\propto a^{-1}$ for the vorticity [11]. Since the rotational part of velocity perturbations is suppressed during linear growth, we neglect any rotational velocities at initial times for the growth of structures. Thus, we can write the initial velocity field as the gradient of a velocity potential $\vec{u}^{(i)} = \vec{\nabla}\psi$.

2.3 ZEL'DOVICH APPROXIMATION

Another analytic approach to describe the growth of cosmic structures is given by Lagrangian perturbation theory. While Eulerian perturbation theory considers the dynamics of the density and velocity fields in a spatial rest-frame, the Lagrangian picture follows the spatial trajectories of particles. The central object of Lagrangian perturbation theory is the displacement field $\vec{\Psi}$, which describes a map between the initial and the final position of a particle

$$\vec{q}^{(i)} \rightarrow \vec{q}^{(i)} + \vec{\Psi}(\vec{q}^{(i)}, t) . \tag{2.31}$$

The equations of motion for the particle positions can then be solved perturbatively. For details, we refer to [11]. The first-order solution is given by

$$\vec{\nabla} \cdot \vec{\Psi}^{(1)}(\vec{q}, t)\Big|_{\vec{q}=\vec{q}^{(i)}} = -D_+(t) \cdot \delta(\vec{q}^{(i)}) . \tag{2.32}$$

The divergence of the displacement field is linearly related to the initial density contrast by the growth factor. When we assume that the initial vorticity of the velocity field vanishes, (2.32) completely determines the displacement field to linear order.

Lagrangian perturbation theory breaks down, when particle trajectories cross such that caustics form in the density field. In the Zel'dovich approximation particle

trajectories are set to follow the first-order solution of Lagrangian perturbation theory beyond the range of validity. We review the derivation of particle trajectories in the Zel'dovich approximation as presented in [6]. We consider the map $\vec{q} \to \vec{r}(\vec{q}, t)$ from initial comoving coordinates $\vec{q}$ to late time coordinates $\vec{r}$ in real space with the ansatz

$$\vec{r}(\vec{q}, t) = a(t)\vec{q} + b(t)\vec{f}(\vec{q}) \, . \tag{2.33}$$

Comparing to this expression to the mapping (2.31) implies that $b/a\vec{f}$ corresponds to the displacement field $\vec{\Psi}$. The ansatz (2.33) implies straight particle trajectories at all times.[1] As long as particle trajectories do not cross, the time-evolved density is then related to the initial density by

$$\rho = \rho_0 \det{}^{-1}\left[\frac{\partial r_i}{\partial q_j}\right] \, , \tag{2.34}$$

where the linearized map of $\vec{q} \to \vec{r}$ is given by

$$\frac{\partial r_i}{\partial q_j} = a(t)\delta_{ij} + b(t)\frac{\partial f_i(\vec{q})}{\partial q_j} \, . \tag{2.35}$$

Taking the time derivative of (2.33) yields

$$\dot{\vec{r}}(\vec{q}, t) = \dot{a}(t)\vec{q} + \dot{b}(t)\vec{f}(\vec{q}) \, , \tag{2.36}$$

where we identify the peculiar velocity $\vec{u} = \frac{b}{a}\vec{f}$. Since we assume $\vec{u}$ to be curl-free, as discussed in Section 2.2, this implies the existence of an initial velocity potential ψ such that $\vec{f} = \vec{\nabla}\psi$. We now denote the eigenvalues of $(\vec{\nabla} \otimes \vec{\nabla})\psi(\vec{q})$ by $(\lambda_1, \lambda_2, \lambda_3)$ and express the determinant of the Jacobian as

$$\det\left[\frac{\partial r_i}{\partial q_j}\right] = \left(a(t) + b(t)\lambda_1\right)\left(a(t) + b(t)\lambda_2\right)\left(a(t) + b(t)\lambda_3\right) \, . \tag{2.37}$$

Using this result in (2.34) together with the definition of the density contrast (2.20), we arrive at

$$\begin{aligned}
\delta &= \frac{a^3(t)}{\left(a(t) + b(t)\lambda_1\right)\left(a(t) + b(t)\lambda_2\right)\left(a(t) + b(t)\lambda_3\right)} - 1 \\
&\approx -\frac{b(t)}{a(t)}\left(\lambda_1 + \lambda_2 + \lambda_3\right) \\
&= -\frac{b(t)}{a(t)}\vec{\nabla} \cdot \vec{f}(\vec{q}) \, ,
\end{aligned} \tag{2.38}$$

where the approximation holds for low densities, i.e. when $\frac{b}{a}\lambda_i \ll 1$. Since $\vec{\nabla}\vec{f}$ is time-independent and $\frac{b}{a}$ independent of position, a comparison with our known solution of linear growth (2.27) yields the identification

$$\frac{b(t)}{a(t)} = \frac{D_+(t)}{D_+(t_0)} \, , \quad \text{and} \quad \delta(\vec{q}, t_0) = -\vec{\nabla} \cdot \vec{f}(\vec{q}) \, . \tag{2.39}$$

Inserting this result in (2.33) and adjusting the normalization of the velocity potential ψ finally yields the *Zel'dovich trajectories*

$$\vec{r}(\vec{q}, t) = a(t)\left[\vec{q} + D_+(t)\vec{\nabla}\psi\right] \, . \tag{2.40}$$

---

1 The evolution of trajectories for a more general ansatz is discussed in [14].

2.4   STATISTICS OF FLUCTUATIONS

The fluctuations in the cosmic density field can be characterized by the n-point statistics of the density contrast. As long as the density contrast is a Gaussian random field, its statistics is completely described by the two-point correlations: The one-point statistics, the average density contrast, $\langle \delta \rangle = 0$ vanishes by definition, and any higher order even cumulants of the field can be expressed as products of the two-point function, while cumulants of odd order vanish.

The two-point correlation function of density fluctuations is defined as

$$\xi_{\delta\delta}(y) := \langle \delta(\vec{x})\delta(\vec{x}+\vec{y}) \rangle \,, \tag{2.41}$$

where the average is performed over all positions $\vec{x}$ and orientations of $\vec{y}$.

The *power spectrum P* is defined by the two-point correlation function of density fluctuations in Fourier space

$$\langle \hat{\delta}(\vec{k})\hat{\delta}^*(\vec{k}') \rangle =: (2\pi)^3 \delta_D(\vec{k}-\vec{k}')P_\delta(k) \,, \tag{2.42}$$

where the star superscript indicates complex conjugation. Homogeneity requires that modes of different wave numbers are uncorrelated in Fourier space, which is the reason for the Dirac delta distribution. Isotropy demands that the power spectrum depends only on the absolute value of the wave vector k.

The time-evolved density fluctuation power spectrum during linear evolution then follows from (2.27) and (2.42)

$$P_\delta(k,t) = \frac{D_+^2(t)}{D_+(t^{(i)})}P_\delta^{(i)}(k) \,, \tag{2.43}$$

where $P_\delta^{(i)}$ denotes the power spectrum at an initial time. For practical purposes, the power spectrum at recombination is an excellent choice for $P_\delta^{(i)}$ for at least two reasons: (i) structure formation is expected to occur linearly at this early time, and (ii) the shape of the power spectrum at large scales, i.e. small wave numbers, is very well known from measurements of the CMB while the shape at smaller scales, i.e. larger wave number, is known from measurements of the Lyman-α forest.

The two-point correlation function and the power spectrum are related by the Fourier transform

$$\xi_{\delta\delta}(y) = \int \frac{\mathrm{d}^3 k}{(2\pi)^3} P_\delta(k) \mathrm{e}^{i\vec{k}\cdot\vec{y}} = \frac{1}{2\pi^2} \int \mathrm{d}k \, k^2 P_\delta(k) \frac{\sin ky}{ky} \,. \tag{2.44}$$

The variance σ of the density contrast δ is given by $\xi_{\delta\delta}(0)$. In practice, the variance σ_R of the filtered density field is considered, where R denotes the filter scale. Then, σ_R can be expressed in terms of the power spectrum and the Fourier transform $\hat{W}_R$ of filter function W_R in real space

$$\sigma_R^2 = \frac{1}{2\pi^2} \int \mathrm{d}k \, k^2 P_\delta(k) \hat{W}_R^2(k) \,. \tag{2.45}$$

The value of the variance σ_8 at $R = 8h^{-1}\mathrm{Mpc}$ is shown in Table 2.2.

Another way to approach the two-point statistics of the density fluctuations is by considering how matter is actually distributed. Cosmological *N*-body simulations and observations suggest that most of the dark matter today is bound in halos[2]. While in general difficult to measure in the real world, simulations have shown that the density profiles of individual halos have a universal shape. This universal shape was first found and characterized in [46] with the fit-function

$$\rho^{\text{NFW}}(r|M) = \frac{\rho_s r_s^3}{r(r+r_s)^2} \, ,\tag{2.46}$$

where the scale radius r_s and the scale density ρ_s depend on the virialized halo mass M. A recent numerical study suggests that this so-called *NFW profile* is valid in simulated halos across 20 orders of magnitude in halo mass [64]. Considering that most of the dark matter today is organized in halos, the power spectrum can roughly be split into two contributions[3],

$$P_\delta(k) \approx P_\delta^{1h}(k) + P_\delta^{2h}(k) \, .\tag{2.47}$$

The one-halo term P^{1h} takes correlations from the density profiles of individual halos into account. Let $n(M)$ denote the number density of halos of a given mass M, then the one-halo term is given by

$$P^{1h}(k) = \int \mathrm{d}M \, n(M) \left(\frac{M}{\bar{\rho}} \right)^2 |u(k|M)|^2 \, ,\tag{2.48}$$

where $u(k|M)$ denotes the Fourier transform of the density profile of a halo with mass M. If the positions of halos were completely uncorrelated, the power spectrum would be completely determined by P^{1h}. The correlation of halo positions is taken into account by the two-halo term P^{2h}. For more details on the halo picture, we refer to [22] and the references therein.

Figure 2.1 shows the dimensionless nonlinear power spectrum $\Delta(k) = k^3 P_\delta(k)/(2\pi^2)$ from a fit function (PD) together with the linear power spectrum (lin), the one-halo term P^{1h}, and the two-halo term P^2 for today. For small scales, i.e. large wave numbers above $1 \, \text{h Mpc}^{-1}$, the non-linear power spectrum is completely determined by the one-halo term.

2.5 SUMMARY AND DISCUSSION

The largest portion of the matter-energy content that fills our universe today consists of substances that we know very little of. While dark energy reveals itself in the accelerated expansion of universe, the existence of dark matter - a substance that does not interact with light - becomes apparent to us through its gravitational effects and the unexpectedly small fluctuations in the cosmic microwave background. We can learn more about the nature of dark matter by studying the properties of cosmic

---

2 It is estimated that the amount of dark matter that is not bound in halos is less than 20 % (see e.g. [69] and references therein).

3 A more thorough analyis that incorporates the rich substructures of halos and takes the redhisft dependence of (2.46) and the statistical scattering of the mass dependence of r_s and ρ_s into account is presented in [34].
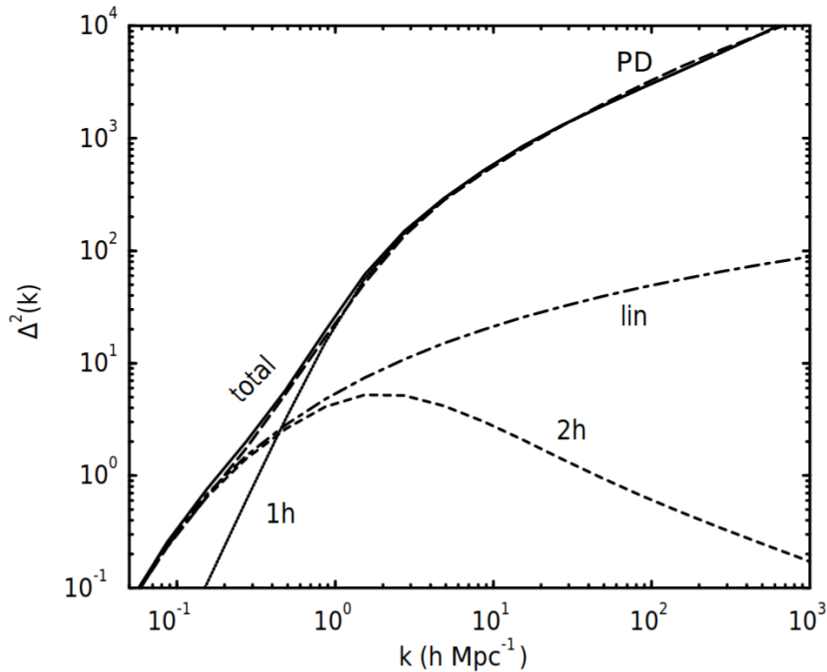
Figure 2.1: The dimensionless power spectrum of the dark matter density field at the present time. The curve labeled 'PD' shows the fitting formula of reference [210] in [22]. The dot dashed curve labeled 'lin' shows the linear power spectrum. The dotted and short dashed curves show the two terms which sum to give the total power (solid line) in the halo model. The figure and caption are taken from [22]. The wording of the caption is slightly changed.

structures and investigating how they must have formed; and in particular, how different properties of dark matter affect this formation process.

Linear theory is very successful to quantify the growth of density perturbations on the largest scales, even until today. However, non-linear evolution sets in at small scales already at early times. This leads to a break-down of linear theory, which cannot explain the diverse structures we observe today or the development of halos with a universal density profile. As time progresses, the non-linearity in the power spectrum arises at successively smaller wave numbers, implying the growth of non-linear structures first on small and then on larger scales. Here, two fundamental questions arise:

- How can we find an analytical description of the non-linear dark matter power spectrum?

- Why do dark matter halos attain a universal density profile?

Rigorous analytical descriptions on how the non-linear power spectrum emerges are still missing. Cosmological *N*-body simulations are time and energy consuming, especially when one wishes to repeat the simulation for different parameters. Furthermore, they suffer from their own issues like limited resolution, the formation of spurious features, the implementation of initial conditions or the limited box size, to name a few.

Describing the growth of cosmic structures with Eulerian perturbation theory has several limitations. First, linear theory is valid only for small perturbations, i.e. $\delta \ll 1$.

This assumption can be relaxed to some degree by incorporating higher orders in the perturbations. This leads to non-linear equations that couple modes, such that modes no longer evolve independently. However, the standard perturbation series does not converge. Second, treating cosmic structures in the picture of hydrodynamics restricts the theory to single-valued velocity fields. This is a valid assumption for fluids for which the mean free path of particles is small compared to the scales under consideration. This assumption does in general not hold for collisionless dark matter, which develops flows with crossing particle streams, such that the velocity can no longer be described by a single-valued continuous field. While hydrodynamics predicts the formation of shocks, which prevent the crossing of streams, stream crossing is actually important for cosmic structure formation. Similar problems arise in Lagrangian perturbation theory, where the functional determinant becomes singular when streams cross. The non-linear Zel'dovich power spectrum, which can be obtained by extrapolating the particle trajectories from first-order Lagrangian perturbation theory beyond its validity, i.e. shell crossing, underestimates structures at late times even more than the linear power spectrum does.

In this work, we make use of another analytical approach to cosmic structure formation, which circumvents the aforementioned problems: Kinetic Field Theory (KFT) is an analytical approach to cosmic structure formation that operates in the particle picture. The dynamics of the particles phase space trajectories is governed by the Hamiltonian flow in $6N$-dimensional phase space, thus avoiding problems with stream crossing, as trajectories in phase space do not cross. In the next chapter, we review the most important aspects of KFT, relevant to this work.

3

KINETIC FIELD THEORY FOR COSMIC STRUCTURE FORMATION

Kinetic field theory (KFT) is a statistical field theory for ensembles of classical particles in or out of equilibrium. The central object in KFT is the generating functional Z. Similar to the partition function in classical thermodynamics, it contains all information about the probability distribution $P(\varphi)$ of system states φ

$$Z = \int \mathcal{D}\varphi \, P(\varphi) \, . \tag{3.1}$$

In general, the system states φ are continuous fields of time, which requires the use of a path integral. In this chapter, we review the foundations of KFT for cosmic structure formation. Since KFT became a very diverse theory with various formulations and applications in cosmology, astrophysics and beyond, we restrict this review to those results that are relevant for this work. We recommend the recent review on KFT [10] to the interested reader.

In the first section, we introduce the tensor notation that is used througout this work. In the second section, we review, in the spirit of [35] and [51], how classical mechanics can be formulated with path integrals. In the third section, we specify the particle dynamics appropriate for cosmic structure formation in KFT by considering an expanding space time and gravitational interactions. In the fourth section, we introduce the initial phase space distribution for cosmic structures. Finally, in the last section, we summarize the current state of the theory of free density moments with initial momentum correlations in KFT.

3.1 NOTATION

We consider a set of N point particles in the classical $6N$ dimensional phase space Γ. The trajectory of each particle $1 \leq j \leq N$ in phase space is the tuple of position $\vec{q}_j$ and momentum $\vec{p}_j$, which we denote by

$$x_j := \begin{pmatrix} \vec{q}_j \\ \vec{p}_j \end{pmatrix} \, . \tag{3.2}$$

Note that the following notations are equivalent $\vec{q}_j \equiv \vec{x}_{q_j}$, $\vec{p}_j \equiv \vec{x}_{p_j}$.

To compactify notation, we collect the trajectories of all particles in the tensorial object

$$\mathbf{x} := x_j \otimes e_j \, , \tag{3.3}$$

where summation over j is implied, and $e_j \in \mathbb{R}^N$ with $(e_j)_i = \delta_{ij}$, $1 \leq i \leq N$. Furthermore, when we consider the collection of all particle positions or momenta separately, we write

$$\mathbf{x}_q := \vec{q}_j \otimes e_j \, , \tag{3.4}$$

$$\mathbf{x}_p := \vec{p}_j \otimes e_j \, , \tag{3.5}$$

respectively. Unless otherwise stated, we use bold letters without index (e.g. $\mathbf{J}$, $\mathbf{x}$) to denote $6N$-dimensional vectors. We can split these vectors into the $3N$ dimensional position component (e.g. $\mathbf{J}_q$, $\mathbf{x}_q$) and a $3N$-dimensional momentum component (e.g. $\mathbf{J}_p$, $\mathbf{x}_p$). When we use the same letter non-bold with integer index (e.g. J_j, x_j), we mean the 6-dimensional phase space tuple of one specific particle. In order to indicate the 3-dimensional position/momentum component of an individual particle, we use non-bold symbols with vector arrow, position/momentum label and integer particle index (e.g. $\vec{J}_{q_j}$, $\vec{J}_{p_j}$, $\vec{x}_{q_j}$, $\vec{x}_{p_j}$).

With these conventions, any bold vector $\mathbf{J}$ can be written as

$$\mathbf{J} = \begin{pmatrix} \vec{J}_{q_j} \\ \vec{J}_{p_j} \end{pmatrix} \otimes e_j \; . \tag{3.6}$$

We introduce the scalar product

$$\langle \mathbf{J}, \mathbf{x} \rangle := (J_j \otimes e_j) \cdot (x_i \otimes e_i) = J_j \cdot x_j \equiv \langle \mathbf{J}_q, \mathbf{x}_q \rangle + \langle \mathbf{J}_p, \mathbf{x}_p \rangle \; , \tag{3.7}$$

and define the symplectic two-form

$$\mathcal{J} := \begin{pmatrix} 0 & \mathbb{I}_3 \\ -\mathbb{I}_3 & 0 \end{pmatrix} \otimes \mathbb{I}_N \; . \tag{3.8}$$

We define the gradient with respect to the phase space coordinates of all particles

$$\nabla_{\mathbf{x}} := \begin{pmatrix} \vec{\nabla}_{q_j} \\ \vec{\nabla}_{p_j} \end{pmatrix} \otimes e_j \; , \tag{3.9}$$

such that the application to any scalar function f of the particles' phase space coordinates can be written as

$$\nabla_{\mathbf{x}} f(\mathbf{x}) = \sum_{j=1}^{N} \begin{pmatrix} \frac{\partial}{\partial q_{j,x}} \\ \frac{\partial}{\partial q_{j,y}} \\ \frac{\partial}{\partial q_{j,z}} \end{pmatrix} f(\mathbf{x}) + \sum_{j=1}^{N} \begin{pmatrix} \frac{\partial}{\partial p_{j,x}} \\ \frac{\partial}{\partial p_{j,y}} \\ \frac{\partial}{\partial p_{j,z}} \end{pmatrix} f(\mathbf{x}) \; . \tag{3.10}$$

To write equations more compactly, we introduce the following notion for integrals over k in Fourier space and over q in real space, respectively,

$$\int_k := \int_{\mathbb{R}^3} \frac{\mathrm{d}^3 k}{(2\pi)^3} \quad \text{and} \quad \int_q := \int_{\mathbb{R}^3} \mathrm{d}^3 q \; . \tag{3.11}$$

3.2   CLASSICAL MECHANICS WITH PATH INTEGRALS

A path-integral formulation for classical Hamiltonian dynamics was developed in [35] and a perturbation theory via Feynman diagrams in [51]. In this section, we review the key ideas that appear in these works which also enter the foundations of KFT. We show how the generating functional is set up for a classical Hamiltonian system of many point-like particles, the role of operators, and how the split of free motion and interactions leads to perturbation theory.

3.2.1 *Generating Functional*

For a classical (canonical) ensemble of N point particles, the system states φ are described by the trajectories $\mathbf{x}$ in the classical $6N$-dimensional phase space Γ, as defined in (3.3). We write the generating functional (3.1) as

$$Z = \int \mathcal{D}\mathbf{x}\, P(\mathbf{x}) \,. \tag{3.12}$$

Note that $P(\mathbf{x})$ is the probability distribution for *trajectories* in classical phase space, and not the probability distribution to find the system in a specific configuration at a given time.

For a given probability distribution of initial conditions $\mathbf{x}^{(i)}$ at some initial time, we can write

$$P(\mathbf{x}) = \int d\mathbf{x}^{(i)}\, P(\mathbf{x}|\mathbf{x}^{(i)}) P(\mathbf{x}^{(i)}) =: \int d\Gamma^{(i)} P(\mathbf{x}|\mathbf{x}^{(i)}) \,. \tag{3.13}$$

For now, we assume that the initial state of the system is known and we omit the integration over initial conditions until Ection 3.4, when we introduce the probability distribution of the initial phase space coordinates relevant for dark matter particles in cosmology.

In classical phase space, trajectories do not cross and are uniquely constrained by the initial conditions because they follow the Hamiltonian flow. For a given Hamiltonian $\mathcal{H}$, the equations of motion (e.o.m.) are given by

$$\dot{\mathbf{x}}(t) = \mathcal{J}\nabla_{\mathbf{x}}\mathcal{H}\left[\mathbf{x}(t)\right] \,, \tag{3.14}$$

with the symplectic two-form $\mathcal{J}$ defined in (3.8) and the phase space gradient $\nabla_{\mathbf{x}}$ defined in (3.9).

For specified initial conditions $\mathbf{x}^{(i)}$, we denote the formal solution to the e.o.m. by $\mathbf{x}_{\mathrm{cl}}(t;\mathbf{x}^{(i)})$ and call them *classical trajectories*. Clearly, $P(\mathbf{x}|\mathbf{x}^{(i)})$ is non-zero only if $\mathbf{x}$ solves the e.o.m., and zero otherwise, such that we can write

$$P(\mathbf{x},t|\mathbf{x}^{(i)},t^{(i)}) = \delta_D\left[\mathbf{x} - \mathbf{x}_{\mathrm{cl}}(t;\mathbf{x}^{(i)})\right] \,. \tag{3.15}$$

The functional Dirac delta distribution can be written in terms of the e.o.m.,

$$\delta_D\left[\mathbf{x} - \mathbf{x}_{\mathrm{cl}}\right] = \delta_D\left[\dot{\mathbf{x}} - \mathcal{J}\nabla_{\mathbf{x}}\mathcal{H}\right] \det\left[\partial_t \delta_b^a - \mathcal{J}^{ac}\partial_c\nabla_b\mathcal{H}\right] \,, \tag{3.16}$$

where the determinant can be formally proven to be equal to unity [35], which is the statement of Liouville's theorem. We now write the generating functional (3.2) in terms of the e.o.m.,

$$\begin{aligned}
Z &= \int \mathcal{D}\mathbf{x}\, P(\mathbf{x}|\mathbf{x}^{(i)}) \\
&= \int \mathcal{D}\mathbf{x}\, \delta_D\left[\dot{\mathbf{x}} - \mathcal{J}\nabla_{\mathbf{x}}\mathcal{H}\right] \\
&= \int \mathcal{D}\mathbf{x}\, \mathcal{D}\chi\, \exp\left[i\int_0^\infty dt\, \left(\langle\chi, \dot{\mathbf{x}} - \mathcal{J}\nabla_{\mathbf{x}}\mathcal{H}\rangle\right)\right] \,,
\end{aligned} \tag{3.17}$$

expressing the Dirac delta distribution as a functional Fourier integral with respect to an auxiliary field χ in the last step.[1]

In order to generate moments of phase space coordinates from the generating functional, we introduce two source fields

$$\mathbf{J} := \begin{pmatrix} \vec{J}_{q_j} \\ \vec{J}_{p_j} \end{pmatrix} \otimes e_j \quad \text{and} \quad \mathbf{K} := \begin{pmatrix} \vec{K}_{q_j} \\ \vec{K}_{p_j} \end{pmatrix} \otimes e_j , \tag{3.18}$$

turning the generating functional into the expression

$$Z[\mathbf{J}, \mathbf{K}] = \int \mathcal{D}\mathbf{x}\, \mathcal{D}\chi \, \exp\left[\mathrm{i} \int_0^\infty \mathrm{d}t \left(\langle \chi, \dot{\mathbf{x}} - \mathcal{J}\nabla_{\mathbf{x}}\mathcal{H} \rangle + \langle \mathbf{J}, \mathbf{x} \rangle + \langle \mathbf{K}, \chi \rangle \right) \right] . \tag{3.19}$$

We define the Lagrangian as in [51],

$$\mathcal{L} := \langle \chi, \dot{\mathbf{x}} - \mathcal{J}\nabla_{\mathbf{x}}\mathcal{H} \rangle , \tag{3.20}$$

such that we arrive at the following compact expression for the generating functional including source fields,

$$Z[\mathbf{J}, \mathbf{K}] = \int \mathcal{D}\mathbf{x}\, \mathcal{D}\chi \, \exp\left[\mathrm{i} \int_0^\infty \mathrm{d}t \left(\mathcal{L} + \langle \mathbf{J}, \mathbf{x} \rangle + \langle \mathbf{K}, \chi \rangle \right) \right] . \tag{3.21}$$

3.2.2 *Operators*

By applying differential operators to the generating functional and setting the source fields to zero afterwards, functions of the phase space trajectories can be generated. In the simplest case, applying a functional derivative with respect to the source field $\mathbf{J}(t)$, generates phase space trajectories

$$-\mathrm{i} \left. \frac{\delta Z[\mathbf{J}, \mathbf{K}]}{\delta \mathbf{J}(t)} \right|_{\mathbf{J}=0=\mathbf{K}} = \mathbf{x}(t) . \tag{3.22}$$

More generally, we apply operators in form of functions of functional derivatives with respect to the field components, to generate functions of the phase spase trajectories.

$$f(\mathbf{x}) = \hat{f}\left(-\mathrm{i}\frac{\delta}{\delta \mathbf{J}} \right) Z[\mathbf{J}, \mathbf{K}]\big|_{\mathbf{J}=0=\mathbf{K}} . \tag{3.23}$$

Note that since the particle trajectories evolve deterministically and we consider specified initial conditions here, the application of operators returns actual functions rather than averages of functions of the phase space trajectories. Only later, when we integrate over initial conditions, do we generate averages.

One important operator is the particle density operator in Fourier space. The number

---

1 Note that (3.17) is a conditional generating functional with respect to the initial conditions. In Section 3.4, we complete the expression by incorporating the integral over initial conditions, appropriate to cosmology.

density $\rho(q, t)$ of N point particles with positions $\vec{q}_j(t)$ at time t is given by a sum of Dirac delta distributions,

$$\rho(\vec{q}, t) = \sum_{j=1}^{N} \delta_D(\vec{q} - \vec{q}_j(t)) \, . \tag{3.24}$$

In Fourier space, the density becomes

$$\tilde{\rho}(\vec{k}, t) = \sum_{j=1}^{N} e^{i\vec{k}\cdot\vec{q}_j(t)} \, . \tag{3.25}$$

We define the one-particle number density as

$$\tilde{\rho}_j(\vec{k}, t) = e^{i\vec{k}\cdot\vec{q}_j(t)} \, , \tag{3.26}$$

and the corresponding operator follows from (3.23),

$$\hat{\rho}_j(\vec{k}, t) = e^{-\vec{k}\cdot\frac{\delta}{\delta \vec{J}_{q_j}(t)}} \, . \tag{3.27}$$

Because of its exponential form, acting with a one-particle density operator on the generating functional shifts the corresponding source field as follows,

$$\hat{\rho}_j(\vec{k}_j, t_j)Z[\mathbf{J}, \mathbf{K}] : \quad \vec{J}_{q_j}(t) \to \vec{J}_{q_j}(t) - \delta_D(t - t_j)\vec{k}_j \, . \tag{3.28}$$

In order to generate products of one particle number densities from the generating functional, we have to apply the corresponding operator (3.27) multiple times,

$$
\begin{aligned}
\tilde{\rho}_1(\vec{k}_1, t_1) \cdots \tilde{\rho}_r(\vec{k}_r, t_r) &= \hat{\rho}_1(\vec{k}_1, t_1) \cdots \hat{\rho}_r(\vec{k}_r, t_r) \, Z[\mathbf{J}, \mathbf{K}]\big|_{\mathbf{J}=0=\mathbf{K}} \\
&= e^{-\vec{k}_1 \frac{\delta}{\delta \vec{J}_{q_1}(t_1)} - \cdots - \vec{k}_r \frac{\delta}{\delta \vec{J}_{q_r}(t_r)}} \, Z[\mathbf{J}, \mathbf{K}]\big|_{\mathbf{J}=0=\mathbf{K}} \, .
\end{aligned}
\tag{3.29}
$$

To describe the shifts (3.29), we define

$$\mathbf{k} := \sum_{j=1}^{r} \delta_D(t_j - t) \begin{pmatrix} \vec{k}_j \\ \vec{0} \end{pmatrix} \otimes e_j \, , \tag{3.30}$$

such that the product of the one-particle densities (3.29) becomes

$$\tilde{\rho}_1(\vec{k}_1, t_1) \cdots \tilde{\rho}_r(\vec{k}_r, t_r) = Z[\mathbf{k}, 0] = \prod_{j=1}^{r} e^{i\vec{k}_j \cdot \vec{q}_j(t_j)} \, , \tag{3.31}$$

in agreement with (3.26).

3.2.3 *Free Generating Functional*

In the last section we showed how functions of the phase space trajectories can be generated by applying differential operators to the generating functional. However, in order to actually evaluate these expressions, the solution to the equations of motion is needed. This solution can in general not be obtained exactly. The idea of the path integral formulation of classical mechanics is to first introduce a reduced

or *free* Hamiltonian for which the equations of motion can be solved and the path integral can be performed, to arrive at the *free generating functional*. In the next step an operator is derived from the remaining or *interaction* part of the Hamiltonian. With this resulting interaction operator, the solution of the equations of motion can be calculated perturbatively.

First, we consider a system of non-interacting particles with the free Hamiltonian

$$\mathcal{H}_0 = \frac{\mathbf{p}^2}{2m(t)} \,, \tag{3.32}$$

where we allow the particles to have a time-dependent mass $m(t)$. With (3.20), we arrive at the free Lagrangian

$$\mathcal{L}_0 = \langle \chi, \dot{\mathbf{x}} - \mathcal{J}\nabla_{\mathbf{x}}\mathcal{H}_0 \rangle = \langle \chi, \dot{\mathbf{x}}^{\alpha} \rangle - \frac{1}{m(t)}\langle \chi_q, \mathbf{p} \rangle \,, \tag{3.33}$$

which leads to the *free generating functional*

$$Z_0[\mathbf{J}, \mathbf{K}] = \int \mathcal{D}\mathbf{x} \, \mathcal{D}\chi \, \exp\left[i \int_0^\infty dt \left(\langle \chi, \dot{\mathbf{x}} \rangle - \frac{1}{m(t)}\langle \chi_q, \mathbf{p} \rangle + \langle \chi, \mathbf{K} \rangle + \langle \mathbf{J}, \mathbf{x} \rangle \right) \right] \,. \tag{3.34}$$

Next, we bring (3.34) in a form, such that we can perform the path integral. To this end, we define a modified free Lagrangian by including the $\langle \chi, \mathbf{K} \rangle$ term

$$\begin{aligned} \mathcal{L}_0' &= \langle \chi, \dot{\mathbf{x}} \rangle - \frac{1}{m(t)}\langle \chi_q, \mathbf{p} \rangle + \langle \chi, \mathbf{K} \rangle \\ &= \langle \chi, \dot{\mathbf{x}} \rangle - \langle \chi, \mathcal{J}\nabla_{\mathbf{x}}\mathcal{H}_0' \rangle \,, \end{aligned} \tag{3.35}$$

with the modified free Hamiltonian

$$\begin{aligned} \mathcal{H}_0' &= \sum_{j=1}^{N} \left(\frac{\vec{p}_j^2}{2m(t)} - \vec{K}_{q,j} \cdot \vec{p}_j + \vec{K}_{p,j} \cdot \vec{q}_j \right) \\ &= \frac{\mathbf{p}^2}{2m(t)} - \langle \mathbf{K}, \mathcal{J}\mathbf{x} \rangle \,, \end{aligned} \tag{3.36}$$

including the source field $\mathbf{K}$. Because of their linearity, we can solve

$$\dot{\mathbf{q}} = \partial_p \mathcal{H}_0' = \frac{1}{m(t)}\mathbf{p} - \mathbf{K}_q \,, \tag{3.37}$$

$$\dot{\mathbf{p}} = -\partial_q \mathcal{H}_0' = -\mathbf{K}_p \tag{3.38}$$

with a Green's function $\mathcal{G}$,

$$\mathbf{x}(t) = \mathcal{G}(t, t^{(i)})\mathbf{x}^{(i)} - \int_0^\infty dt' \mathcal{G}(t, t')\mathbf{K}(t') \,, \tag{3.39}$$

where the Green's function can be written as

$$\mathcal{G}(t, t') = G(t, t') \otimes \mathbb{I}_N \,, \tag{3.40}$$

and

$$G(t, t') = \begin{pmatrix} g_{qq}(t, t')\mathbb{I}_3 & g_{qp}(t, t')\mathbb{I}_3 \\ g_{pq}(t, t')\mathbb{I}_3 & g_{pp}(t, t')\mathbb{I}_3 \end{pmatrix} \tag{3.41}$$

is a 6×6-dimensional matrix. The propagators

$$g_{qq}(t,t') = \Theta(t-t') = g_{pp}(t,t') , \tag{3.42}$$

$$g_{pq}(t,t') = 0 , \tag{3.43}$$

$$g_{qp}(t,t') = \int_{t'}^{t} \frac{dt''}{m(t'')} \tag{3.44}$$

are scalar functions, where Θ denotes the Heaviside step function. A derivation of these propagators is shown in Appendix A.1. We denote the free particle motion by $\mathbf{x}_0(t)$ with spatial and momentum components with

$$\mathbf{q}_0(t) = \mathbf{q}^{(i)} + g_{qp}(t,t')\mathbf{p}^{(i)} , \tag{3.45}$$

$$\mathbf{p}_0(t) = \mathbf{p}^{(i)} . \tag{3.46}$$

This allows us to evaluate the path integral , yielding the free generating functional

$$Z_0[\mathbf{J},\mathbf{K}] = \exp\left[i \int_0^\infty dt \langle \mathbf{J}(t), \mathbf{x}_0(t)\rangle - i \int dt\, dt' \langle \mathbf{J}(t), \mathcal{G}(t,t')\mathbf{K}(t')\rangle \right] . \tag{3.47}$$

Note that by applying functional derivatives with respect to the source fields $\mathbf{J}$ and $\mathbf{K}$, we generate the propagators,

$$(-i)^2 \frac{\delta^2 Z_0[\mathbf{J},\mathbf{K}]}{\delta \vec{J}_{a_j}(t)\delta \vec{K}_{b_i}(t')}\bigg|_{\mathbf{J}=0=\mathbf{K}} = i\,\delta_{ij}\, g_{ab}(t,t')\, \mathbb{I}_3 , \tag{3.48}$$

where $a,b \in \{q,p\}$.

3.2.4 *Interactions*

In the previous section, we considered free particle motion for which we solved the e.o.m. and derived the free generating functional. Now, we consider a Hamiltonian that includes an *interaction* part $\mathcal{H}_I$, which we allow to depend on both the particle positions $\mathbf{q}$ and momenta $\mathbf{p}$,

$$\mathcal{H} = \mathcal{H}_0 + \mathcal{H}_I(\mathbf{p},\mathbf{q}) . \tag{3.49}$$

Analogously to the free system, the modified Lagrangian (3.35) now becomes

$$\mathcal{L}' = \langle \chi, \dot{\mathbf{x}} - \mathcal{J}\nabla_\mathbf{x}\mathcal{H}_0' \rangle - \langle \chi, \mathcal{J}\nabla_\mathbf{x}\mathcal{H}_I(\mathbf{p},\mathbf{q})\rangle . \tag{3.50}$$

We define the interaction-Lagrangian

$$\mathcal{L}_I(\chi,\mathbf{x}) := -\langle \chi, \mathcal{J}\nabla_\mathbf{x}\mathcal{H}_I(\mathbf{p},\mathbf{q})\rangle , \tag{3.51}$$

and write the generating functional (3.19) as

$$Z[\mathbf{J},\mathbf{K}] = \int \mathcal{D}\mathbf{x}\,\mathcal{D}\chi \exp\left[i \int_0^\infty dt\, \left(\mathcal{L}_0' + \mathcal{L}_I(\chi,\mathbf{x}) + \langle \mathbf{J},\mathbf{x}\rangle\right) \right] . \tag{3.52}$$

Since we introduced $\mathbf{K}$ as source field for χ in (3.19), functional derivatives with respect to $\mathbf{K}$ generate χ, the same way as functional derivatives with respect to $\mathbf{J}$ generate the

particle trajectories $\mathbf{x}$. As a consequence, we can transform the part in (3.52) containing the interaction-Lagrangian into an interaction operator

$$\int_0^\infty \mathrm{d}t \mathcal{L}_I \left(\chi, \mathbf{x} \right) \to \hat{S}_I = \int_0^\infty \mathrm{d}t \mathcal{L}_I \left(-\mathrm{i}\frac{\delta}{\delta \mathbf{K}(t)}, -\mathrm{i}\frac{\delta}{\delta \mathbf{J}(t)} \right) . \tag{3.53}$$

We pull the interaction operator in front of the integral and arrive at the full generating functional, which is now expressed as the free generating functional with the interaction operator in the exponential applied to it,

$$Z[\mathbf{J}, \mathbf{K}] = \mathrm{e}^{\mathrm{i}\hat{S}_I} Z_0[\mathbf{J}, \mathbf{K}] . \tag{3.54}$$

In general, the interaction operator is not linear in the functional derivatives, such that a direct application of $\mathrm{e}^{\mathrm{i}\hat{S}_I}$ to the free generating functional can not be evaluated exactly. However, expanding the exponential,

$$\mathrm{e}^{\mathrm{i}\hat{S}_I} \approx 1 + \mathrm{i}\hat{S}_I + \cdots , \tag{3.55}$$

leads to a perturbative series in the interaction, as illustrated in the following example.

Example 3.1. *We consider the phase space trajectories (3.22) with the generating functional (3.54)*

$$\mathbf{x}(t) = -\mathrm{i}\frac{\delta}{\delta \mathbf{J}(t)} \mathrm{e}^{\mathrm{i}\hat{S}_I} Z_0[\mathbf{J}, \mathbf{K}]\big|_{\mathbf{J}=0=\mathbf{K}} . \tag{3.56}$$

By expanding the exponential (3.55), we arrive at a perturbative series for the phase space trajectories,

$$\mathbf{x}(t) \approx -\mathrm{i}\frac{\delta}{\delta \mathbf{J}(t)} \left(1 + \mathrm{i}\hat{S}_I + ... \right) Z_0[\mathbf{J}, \mathbf{K}]\big|_{\mathbf{J}=0=\mathbf{K}} \tag{3.57}$$

$$= \mathbf{x}_0(t) + \mathbf{x}^{(1)}(t) + ... , \tag{3.58}$$

where

$$\mathbf{x}_0(t) = -\mathrm{i}\frac{\delta}{\delta \mathbf{J}(t)} Z_0[\mathbf{J}, \mathbf{K}]\big|_{\mathbf{J}=0=\mathbf{K}} \tag{3.59}$$

describes free motion, and the first perturbative term

$$\mathbf{x}^{(1)}(t) = -\mathrm{i}\frac{\delta}{\delta \mathbf{J}(t)} \mathrm{i}\hat{S}_I Z_0[\mathbf{J}, \mathbf{K}]\big|_{\mathbf{J}=0=\mathbf{K}} \tag{3.60}$$

corresponds to the application of one interaction operator. The n-th pertubative term is given by

$$\mathbf{x}^{(n)}(t) = -\mathrm{i}\frac{\delta}{\delta \mathbf{J}(t)} \frac{\mathrm{i}^n}{n!} \hat{S}_I^n Z_0[\mathbf{J}, \mathbf{K}]\big|_{\mathbf{J}=0=\mathbf{K}} , \tag{3.61}$$

where $\hat{S}_I^n$ has the meaning of applying the interaction operator n times.

In the last section, we reviewed how classical mechanics can generally be formulated in the path integral formalism. In this section, we review how the dynamics of collisionless particles in an expanding spacetime under the influence of Newtonian gravity is specified.

Since the splitting of the Hamiltonian into a free and an interaction part is in general not unique, we are free in our choice of the propagators. We review the representation of the Hamiltonian as well as the propagators in the Newtonian case and when free motion is specified to Zel'dovich trajectories, as derived in [5]. Furthermore, we derive the interaction operator similar to [7] and show how the choice of the propagator changes the interaction operator by an additional propagator correction operator.

3.3.1   *Hamiltonian*

For our considerations, the Newtonian limit is appropriate, since it is the limiting case that applies to scales that are small compared to the Hubble length cH^{-1} and large compared to the Schwarzschild radii of any collapsed objects [50]. We review the derivation of the Hamiltonian for particles under the influence of gravity in an expanding spacetime in Appendix A.2. In summary, the key steps are as follows. (i) We derive the Lagrangian of a single particle in an expanding spacetime with a time-dependent gravitational field in comoving coordinates q. (ii) We transform the time coordinate such that the linear growth factor D_+, which is a monotonic function of time, is our new time coordinate ($t = D_+ - D_+^{(\mathrm{i})}$). Because of the expanding spacetime, the particle mass becomes effectively time-dependent. (iii) Finally, we perform a Legendre transform of the Lagrangian to obtain the Hamiltonian for the single-particle system (A.26). We finally arrive at the N-particle Hamiltonian

$$\mathcal{H}(\mathbf{q},\mathbf{p}) = \frac{\mathbf{p}^2}{2m(t)} + V(\mathbf{q},t) \; . \tag{3.62}$$

The effective particle mass is

$$m(t) = a^2 \frac{H}{H_0} D_+ f \; , \tag{3.63}$$

where H and f denote the usual Hubble function and growth rate, respectively,

$$H = \frac{a'}{a} \quad \text{and} \quad f = \frac{\mathrm{d}\ln D_+}{\mathrm{d}\ln a} \; , \tag{3.64}$$

and a' denotes the derivative of the scale factor with respect to the original time coordinate. H_0 is the value of H evaluated at the time when $a = 1$. The total potential V is the sum of all potentials φ at the positions of individual particles

$$V(\mathbf{q},t) = \frac{1}{2} \sum_{j=1}^{N} \varphi(\vec{q}_j,t) \; , \tag{3.65}$$

where φ satisfies the Poisson equation

$$\vec{\nabla}_q^2 \varphi(\vec{q},t) = \frac{4\pi G a(t)}{H_0^2 m(t)} \left[\rho_{\mathrm{m}}(\vec{q},t) - \bar{\rho}_{\mathrm{m}} \right] \; , \tag{3.66}$$

ρ_{m} is the comoving mass density and $\bar{\rho}_{\mathrm{m}}$ the spatially averaged comoving mass density, which is constant in time. With the density contrast

$$\delta(\vec{q}, t) := \frac{\rho_{\mathrm{m}}(\vec{q}, t) - \bar{\rho}_{\mathrm{m}}}{\bar{\rho}_{\mathrm{m}}} \tag{3.67}$$

and the dimensionless matter density parameter

$$\Omega_{\mathrm{m0}} = \frac{8\pi G}{3H_0^2} \bar{\rho} \tag{3.68}$$

at $a = 1$, we can write (3.66) now as

$$\vec{\nabla}_q^2 \varphi(\vec{q}, t) = \frac{3}{2} \frac{a(t)}{m(t)} \Omega_{\mathrm{m0}} \delta(t) . \tag{3.69}$$

3.3.2   *Interaction Operator*

In KFT, we are free in our choice of how to split the Hamiltonian into a free and an interaction part. Starting with (3.62) suggests to choose $\mathcal{H}_0 = \frac{\mathbf{p}^2}{2m(t)}$ as free Hamiltonian, such that free trajectories are given by (3.45) and (3.46), with the Newtonian propagator (3.44) and the effective particle mass (3.63). A much better choice to reproduce the observed linear growth at large scales are Zel'dovich trajectories with the Zel'dovich propagator

$$g_{qp}^Z(t, t') = (t - t')\Theta(t - t') . \tag{3.70}$$

A comparison with (3.44) implies $m(t) = 1$ for the free motion and hence implies the free Zel'dovich Hamiltonian

$$\mathcal{H}_0^Z = \frac{\mathbf{p}^2}{2} . \tag{3.71}$$

We therefore split the Hamiltonian (3.62) in the following way,

$$\mathcal{H}(\mathbf{q}, \mathbf{p}) = \frac{\mathbf{p}^2}{2} + \left(\frac{1}{m(t)} - 1\right) \frac{\mathbf{p}^2}{2} + V(\mathbf{q}, t) , \tag{3.72}$$

and define the Zel'dovich interaction Hamiltonian

$$\mathcal{H}_I^Z(\mathbf{p}, \mathbf{q}) := \left(\frac{1}{m(t)} - 1\right) \frac{\mathbf{p}^2}{2} + V(\mathbf{q}, t) . \tag{3.73}$$

The Zel'dovich interaction Lagrangian (3.51) then turns into

$$\mathcal{L}_I^Z = -\langle \chi, \mathcal{J}\nabla_{\mathbf{x}}\mathcal{H}_I(\mathbf{p}, \mathbf{q})\rangle \tag{3.74}$$

$$= -\left(\frac{1}{m(t)} - 1\right) \langle \chi_q, \mathbf{p}\rangle + \langle \chi_p, \nabla_q V(\mathbf{q}, t)\rangle \tag{3.75}$$

$$= -\mathcal{C}(\chi_q, \mathbf{p}) + \mathcal{V}(\chi_p, \mathbf{q}) . \tag{3.76}$$

In the last step, we defined the potential part

$$\mathcal{V}(\chi_p, \mathbf{q}) := \langle \chi_p, \nabla_q V(\mathbf{q}, t)\rangle \tag{3.77}$$

and the propagator correction part

$$
\mathcal{C}(\chi_q, \mathbf{p}) := \left(\frac{1}{m(t)} - 1 \right) \langle \chi_q, \mathbf{p} \rangle .
\tag{3.78}
$$

With this Lagrangian, the interaction operator (3.53) becomes

$$
\begin{aligned}
\hat{S}_I := & \int_0^\infty \mathrm{d}t \left(\frac{1}{m(t)} - 1 \right) \left\langle \frac{\delta}{\delta \mathbf{K}_q(t)}, \frac{\delta}{\delta \mathbf{J}_p(t)} \right\rangle \\
& - \int_0^\infty \mathrm{d}t \, \hat{\mathcal{V}} \left(-\mathrm{i} \frac{\partial}{\partial \mathbf{J}_q(t)}, -\mathrm{i} \frac{\partial}{\partial \mathbf{K}_p(t)} \right) .
\end{aligned}
\tag{3.79}
$$

The interaction operator now consists of two parts. The potential part $\mathcal{V}$ generates the interactions due to the pairwise interaction potentials. The propagator correction part $\mathcal{C}$ subtracts those interactions that are already taken into account in the Zel'dovich trajectories.

For collisionless point particles like cold dark matter, the interaction potential V is given by the sum of gravitational potentials acting between all individual particle pairs. More generally, when the potential only depends on the pairwise distances of particles and has a time-dependent amplitude $A(t)$, we write V as

$$
V(\mathbf{q}, t) = A(t) \sum_{1 \leq i \leq j \leq N} v \left(|\vec{q}_i(t) - \vec{q}_j(t)| \right) ,
\tag{3.80}
$$

where v is the potential acting between individual pairs of particles, which scales like $|\vec{q}|^{-1}$ for gravity.

As shown in Appendix A.3, we can express the potential operator in terms of the single-particle density operators (3.27),

$$
\hat{\mathcal{V}} \left(-\mathrm{i} \frac{\partial}{\partial \mathbf{J}_q(t)}, -\mathrm{i} \frac{\partial}{\partial \mathbf{K}_p(t)} \right) = A(t) \sum_{k=1}^N \sum_{i \neq k} \int_k \hat{\rho}_i(\vec{k}, t) \tilde{v}(\vec{k}) \hat{\rho}_k(-\vec{k}, t) \vec{k} \cdot \frac{\delta}{\delta \vec{K}_{p_k}(t)} ,
\tag{3.81}
$$

where $\tilde{v}$ is the Fourier transform of the potential function v, which is k^{-2} for gravity. The time-dependent amplitude

$$
A(t) = \frac{3}{2} \frac{a(t)}{m(t)} \frac{\Omega_{\mathrm{m}0}}{\bar{\rho}}
\tag{3.82}
$$

follows from (3.69), with the time-independent comoving particle number density $\bar{\rho}$.

Although the potential and the correction parts in (3.79) should always be kept together in order to generate coherent orders of perturbations, we illustrate the action of $\mathcal{C}$ in the perturbative calculation of $\mathbf{q}$, neglecting $\mathcal{V}$ in the following example.

Example 3.2 (Propagator Correction Operator). *We consider N particles with the Hamiltonian*

$$
\mathcal{H} = \frac{\mathbf{p}^2}{2m(t)} .
\tag{3.83}
$$

We computed the solution to the e.o.m.s (3.45) and (3.46) with the propagator (3.44). We now introduce a split $\mathcal{H} = \mathcal{H}_0^Z + \mathcal{H}_I^Z$ to force the free motion to follow Zel'dovich trajectories,

$$
\mathcal{H}_0(\mathbf{p}) = \frac{\mathbf{p}^2}{2} \quad and \quad \mathcal{H}_I(\mathbf{p}) = \left(\frac{1}{m(t)} - 1 \right) \frac{\mathbf{p}^2}{2} .
\tag{3.84}
$$

The free motion is now determined by the Zel'dovich propagator (3.70), such that the free particle positions are

$$\mathbf{q}_0(t) = \mathbf{q}^{(i)} + t\mathbf{p}^{(i)} \, . \tag{3.85}$$

To compute the deviation from the Zel'dovich trajectories due to the time-dependent mass, we consider the $\mathbf{q}$-part of (3.56) with $\hat{S}_I$ from (3.79) without the potential part $\mathcal{V}$,

$$\mathbf{q}(t) = -\mathrm{i}\frac{\delta}{\delta\mathbf{J}_q(t)}\exp\left[\mathrm{i}\int \mathrm{d}t' \left(\frac{1}{m(t')} - 1\right)\left\langle\frac{\delta}{\delta\mathbf{K}_q(t')}, \frac{\delta}{\delta\mathbf{J}_p(t')}\right\rangle\right] Z_0[\mathbf{J}, \mathbf{K}]\big|_{\mathbf{J}=0=\mathbf{K}} \, . \tag{3.86}$$

We compute the first perturbative term (3.60) in Appendix A.4 and arrive at

$$\begin{aligned}
\mathbf{q}^{(1)}(t) &= \frac{\delta}{\delta\mathbf{J}_q(t)}\int \mathrm{d}t'\left(\frac{1}{m(t')} - 1\right)\left\langle\frac{\delta}{\delta\mathbf{K}_q(t')}, \frac{\delta}{\delta\mathbf{J}_p(t')}\right\rangle Z_0[\mathbf{J}, \mathbf{K}]\big|_{\mathbf{J}=0=\mathbf{K}} \\
&= -t\mathbf{p}^{(i)} + \mathbf{p}^{(i)}\int_0^t \mathrm{d}t'\frac{1}{m(t')} \, .
\end{aligned} \tag{3.87}$$

Adding this first-order perturbation term to the free solution (3.85) yields the exact solution of (3.83),

$$\mathbf{q}_0(t) + \mathbf{q}^{(1)}(t) = \mathbf{q}^{(i)} + \int_0^t \mathrm{d}t'\frac{1}{m(t')}\mathbf{p}^{(i)} \, . \tag{3.88}$$

Example 3.3 (First-order Perturbation Theory). *We consider the full Hamiltonian (3.72) with the free Zel'dovich trajectories (3.85). Then, the first-order correction to the trajectory of particle 1 due to the time-dependent mass, as in the previous example, and due to gravitational interactions, is given by*

$$\begin{aligned}
\vec{q}_1^{(1)}(t) &= -t\vec{p}_1^{(i)} + \int_0^t \mathrm{d}t'\frac{1}{m(t')}\vec{p}_1^{(i)} \\
&\quad + \sum_{j=2}^N \int \mathrm{d}t'' \, A(t'')g_{qp}(t, t'')\frac{\vec{q}_{0,1}(t'') - \vec{q}_{0,j}(t'')}{|\vec{q}_{0,1}(t'') - \vec{q}_{0,j}(t'')|^3} \, .
\end{aligned} \tag{3.89}$$

Note that the gravitational contribution in the second line takes the form of Born's approximation: the force the particle experiences is evaluated along the free trajectory.

3.4 INITIAL PHASE SPACE DISTRIBUTION

Up to here, we considered classical N-particle systems where the particles attain definite initial positions and momenta. In general, however, the exact initial conditions are not known but obey certain statistics. This implies a probability distribution density $P(\mathbf{x}^{(i)})$ for the initial state in phase space. The initial phase space measure in (3.13) is generally given by

$$\mathrm{d}\Gamma^{(i)} := P(\mathbf{q}^{(i)}, \mathbf{p}^{(i)})\mathrm{d}\mathbf{q}^{(i)}\mathrm{d}\mathbf{p}^{(i)} \, . \tag{3.90}$$

In order to arrive at the complete generating functional for cosmic structure formation, we have to modify the free generating functional (3.47) by including the

integration over the initial phase space distribution while the interaction operator remains unchanged,

$$Z_0[\mathbf{J}, \mathbf{K}] = \int d\Gamma^{(i)} \exp\left[i \int_0^\infty dt \langle \mathbf{J}(t), \mathbf{x}_0(t) \rangle - i \int dt \, dt' \langle \mathbf{J}(t), \mathcal{G}(t, t') \mathbf{K}(t') \rangle \right] . \quad (3.91)$$

In this section, we review the initial phase space distribution for cosmic structures as derived in [7] and show how parts of the initial conditions can be integrated out in the generating functional.

From now on, we drop the superscript (i) that indicates initial particle positions and initial particle momenta. To avoid confusion, time-evolved quantities are always written with a time argument.

3.4.1 Initial Correlations

We review the initial conditions that apply to cosmology [7]. First, we consider the initial probability distribution of the initial density contrast and momenta $P(\delta, \mathbf{p})$, where $\delta = \delta_j \otimes e_j$, and δ_j denotes the density contrast at the position of particle j. As shown in the appendix of [7], the intial phase space distribution can be obtained from Poisson sampling, such that

$$P(\mathbf{q}, \mathbf{p}) = V^{-N} \int d\delta \prod_{j=1}^N (1 + \delta_j) P(\delta, \mathbf{p}) . \quad (3.92)$$

Initially, we assume a Gaussian random field,

$$P(\delta, \mathbf{p}) = \frac{1}{\sqrt{(2\pi)^{4N} \det C}} \exp\left(-\frac{1}{2} (\delta^\mathsf{T}, \mathbf{p}^\mathsf{T}) C^{-1} \begin{pmatrix} \delta \\ \mathbf{p} \end{pmatrix} \right) , \quad (3.93)$$

with the $4N \times 4N$ dimensional correlation matrix

$$C := \begin{pmatrix} \langle \delta_j \delta_k \rangle & \langle \delta_j \vec{p}_k^\mathsf{T} \rangle \\ \langle \vec{p}_j \delta_k \rangle & \langle \vec{p}_j \otimes \vec{p}_k \rangle \end{pmatrix} \otimes e_j \otimes e_k . \quad (3.94)$$

The two-particle density contrast correlation function depends on the relative particle distance and is given by the Fourier transform of the initial density perturbation power spectrum $P_\delta^{(i)}$,

$$\begin{aligned} \langle \delta_i \delta_j \rangle &= \xi_{\delta\delta}(\vec{q}_i - \vec{q}_j) \\ &= \int_k P_\delta^{(i)}(k) e^{i\vec{k} \cdot (\vec{q}_i - \vec{q}_j)} \\ &=: C_{\delta\delta}(q_{ij}) . \end{aligned} \quad (3.95)$$

Since we initially consider only the curl-free part of the velocity field, we introduce a velocity potential field ψ such that the initial momentum of particle j at position $\vec{q}_j$ can be expressed as

$$\vec{p}_j = \left. \vec{\nabla}_q \psi(\vec{q}) \right|_{q = q_j} . \quad (3.96)$$

(2.23) and (2.30) imply that the power spectrum of the initial velocity potential is related to the initial density fluctuation power spectrum by a factor k^{-4},

$$P_\psi^{(i)}(k) = k^{-4} P_\delta^{(i)}(k) .$$ (3.97)

We conclude that the initial density-momentum correlations are given by

$$
\begin{aligned}
\langle \delta_i \vec{p}_j \rangle &= -\mathrm{i} \int_k \vec{k} \frac{P_\delta^{(i)}(k)}{k^2} \mathrm{e}^{\mathrm{i}\vec{k}\cdot(\vec{q}_i - \vec{q}_j)} \\
&= \vec{\nabla}_{q_j} \int_k \frac{P_\delta^{(i)}(k)}{k^2} \mathrm{e}^{\mathrm{i}\vec{k}\cdot(\vec{q}_i - \vec{q}_j)} \\
&=: \vec{C}_{\delta p}(q_{ij}) .
\end{aligned}
$$ (3.98)

Similarly, we obtain for the initial momentum-momentum correlations

$$
\begin{aligned}
\langle \vec{p}_i \otimes \vec{p}_j \rangle &= \int_k \vec{k} \otimes \vec{k} \frac{P_\delta^{(i)}(k)}{k^4} \mathrm{e}^{\mathrm{i}\vec{k}\cdot(\vec{q}_i - \vec{q}_j)} \\
&= \vec{\nabla}_{q_i} \otimes \vec{\nabla}_{q_j} \int_k \frac{P_\delta^{(i)}(k)}{k^4} \mathrm{e}^{\mathrm{i}\vec{k}\cdot(\vec{q}_i - \vec{q}_j)} \\
&=: \hat{C}_{pp}(q_{ij}) .
\end{aligned}
$$ (3.99)

We discuss the specific properties in the large- and small-scale limits in detail in Chapter 5.

3.4.2 *Generating Functional with Initial Correlations*

The initial conditions can partially be integrated out in the free generating functional. First, we introduce a source vector $\mathbf{t}_\delta$ for δ and rewrite the initial probability distribution (3.92) as

$$
\begin{aligned}
P(\mathbf{q}, \mathbf{p}) &= V^{-N} \int \mathrm{d}\delta \prod_{j=1}^{N}(1 + \delta_j) P(\delta, \mathbf{p}) \\
&= V^{-N} \prod_{j=1}^{N}\left(1 - \mathrm{i}\frac{\partial}{\partial t_{\delta_j}}\right) \int \mathrm{d}\delta\, P(\delta, \mathbf{p}) \mathrm{e}^{\mathrm{i}\delta\cdot\mathbf{t}_\delta} \Bigg|_{\mathbf{t}_\delta = 0} .
\end{aligned}
$$ (3.100)

Next, we define the vectors

$$\tilde{\mathbf{J}}_q := \int \mathrm{d}t\, \mathbf{J}_q(t) ,$$ (3.101)

$$\tilde{\mathbf{J}}_p := \int \mathrm{d}t \left(g_{qp}(t,0)\mathbf{J}_q(t) + \mathbf{J}_p(t)\right) ,$$ (3.102)

and rewrite the free generating functional (3.91) in terms of the free trajectories (3.45) and (3.46),

$$
\begin{aligned}
Z_0[\mathbf{J}, \mathbf{K}] &= \int \mathrm{d}\Gamma^{(i)} \exp\left[\mathrm{i}\int \mathrm{d}t\langle \mathbf{J}(t), \mathbf{x}_0(t)\rangle - \mathrm{i}\int \mathrm{d}t\mathrm{d}t'\langle \mathbf{J}(t), \mathcal{G}(t,t')\mathbf{K}(t')\rangle\right] \\
&= \int \mathrm{d}\Gamma^{(i)} \exp\left[\mathrm{i}\langle\tilde{\mathbf{J}}_q, \mathbf{q}\rangle + \mathrm{i}\langle\tilde{\mathbf{J}}_p, \mathbf{p}\rangle - \mathrm{i}\int \mathrm{d}t\mathrm{d}t'\langle \mathbf{J}(t), \mathcal{G}(t,t')\mathbf{K}(t')\rangle\right] .
\end{aligned}
$$ (3.103)

Now, we can perform the integration over initial momenta and initial density contrasts,

$$
\int d\Gamma^{(i)} e^{i\langle \tilde{J}_q, \mathbf{q}\rangle + i\langle \tilde{J}_p, \mathbf{p}\rangle}
$$

$$
= V^{-N} \prod_{j=1}^{N} \left(1 - i\frac{\partial}{\partial t_{\delta_j}}\right) \int d\delta d\mathbf{q} d\mathbf{p}\, P(\delta, \mathbf{p}) e^{i\langle \mathbf{t}_\delta, \delta\rangle + i\langle \tilde{J}_q, \mathbf{q}\rangle + i\langle \tilde{J}_p, \mathbf{p}\rangle}\Bigg|_{\mathbf{t}_\delta = 0} \tag{3.104}
$$

$$
= V^{-N} \prod_{j=1}^{N} \left(1 - i\frac{\partial}{\partial t_{\delta_j}}\right) \int d\mathbf{q}\, \exp\left(-\frac{1}{2}(\mathbf{t}_\delta^{\mathsf{T}}, \tilde{J}_p^{\mathsf{T}})C(\mathbf{q})\begin{pmatrix}\mathbf{t}_\delta\\ \tilde{J}_p\end{pmatrix} + i\langle \tilde{J}_q, \mathbf{q}\rangle\right)\Bigg|_{\mathbf{t}_\delta = 0}.
$$

Note that the initial correlation matrix C explicitly depends on the initial (relative) particle positions $\mathbf{q}$. We define the sub matrices

$$
C_{\delta\delta}(\mathbf{q}) := \langle \delta_j \delta_k\rangle \otimes e_j \otimes e_k, \tag{3.105}
$$
$$
C_{\delta p}(\mathbf{q}) = C_{p\delta}^{\mathsf{T}}(\mathbf{q}) := \langle \delta_j \vec{p}_k^{\mathsf{T}}\rangle \otimes e_j \otimes e_k, \tag{3.106}
$$
$$
C_{pp}(\mathbf{q}) := \langle \vec{p}_j \otimes \vec{p}_k\rangle \otimes e_j \otimes e_k, \tag{3.107}
$$

and arrive at

$$
\int d\Gamma^{(i)} e^{i\langle \tilde{J}_q, \mathbf{q}\rangle + i\langle \tilde{J}_p, \mathbf{p}\rangle}
$$

$$
= V^{-N} \prod_{j=1}^{N} \left(1 - i\frac{\partial}{\partial t_{\delta_j}}\right) \int d\mathbf{q}\, \left\{\exp\left(-\frac{1}{2}\mathbf{t}_\delta^{\mathsf{T}} C_{\delta\delta}(\mathbf{q})\mathbf{t}_\delta\right)\right. \tag{3.108}
$$

$$
\left. \times \exp\left(-\mathbf{t}_\delta^{\mathsf{T}} C_{\delta p}(\mathbf{q})\tilde{J}_p - \frac{1}{2}\tilde{J}_p^{\mathsf{T}} C_{pp}(\mathbf{q})\tilde{J}_p + i\langle \tilde{J}_q, \mathbf{q}\rangle\right)\right\}\Bigg|_{\mathbf{t}_\delta = 0}.
$$

A comprehensive analysis of the series that is induced by the differential operator is given in [27].

Let us note that in [7] it was shown that the initial phase space distribution $P(\mathbf{q}, \mathbf{p})$ can also be expressed in terms of the initial momentum correlations together with an operator $\mathcal{C}$ that generates the initial density and momentum-density correlations,

$$
P(\mathbf{q}, \mathbf{p}) = \frac{V^{-N}}{\sqrt{(2\pi)^{3N}\det C_{pp}(\mathbf{q})}} \mathcal{C}\left(\mathbf{q}, -i\frac{\partial}{\partial \mathbf{p}}\right)\exp\left(-\frac{1}{2}\mathbf{p}^{\mathsf{T}} C_{pp}^{-1}(\mathbf{q})\mathbf{p}\right). \tag{3.109}
$$

For the evaluation of quantities at late times, we can assume $\mathcal{C} \approx 1$ when working with the Zel'dovich propagator (3.70) [7, 27]. The reason is that at late times, when the propagator g_{qp} becomes large, and at linear scales the contributions from initial density correlations $C_{\delta\delta}$ and initial momentum-density correlations $C_{p\delta}$ are relatively suppressed by g_{qp}^{-2} and g_{qp}^{-1}, respectively, compared to the initial momentum correlations C_{pp}. The initial phase space distribution is then approximated by

$$
P(\mathbf{q}, \mathbf{p}) \approx \frac{V^{-N}}{\sqrt{(2\pi)^{3N}\det C_{pp}(\mathbf{q})}}\exp\left(-\frac{1}{2}\mathbf{p}^{\mathsf{T}} C_{pp}^{-1}(\mathbf{q})\mathbf{p}\right). \tag{3.110}
$$

We therefore consider only the effect of initial momentum correlations for structure growth throughout this work, unless otherwise stated. Furthermore, we derive results

for free streaming, i.e. we do not consider any interactions, apart from those that are already included in the Zel'dovich approximation. Therefore, we can set $\mathbf{K} = 0$ and arrive at the free streaming generating functional for particles with initial Gaussian momentum correlations,

$$Z_0[\mathbf{J}, 0] = V^{-N} \int \mathrm{d}\mathbf{q} \, \exp\left(-\frac{1}{2}\tilde{\mathbf{J}}_p^{\mathsf{T}} C_{pp}(\mathbf{q})\tilde{\mathbf{J}}_p + \mathrm{i}\langle\tilde{\mathbf{J}}_q, \mathbf{q}\rangle\right) \, . \tag{3.111}$$

3.5   FREE DENSITY CORRELATORS

In this section, we review the factorized expression for the free density correlators as derived in [9], and point out an erroneous expression in the same work that concerns correlators of third and higher order.

3.5.1   *Free Correlators*

For a more compact notation, we denote wave vector and time arguments by a single symbol in the following way,

$$f(1) \equiv f(\vec{k}_1, t_1) \, , \quad \text{in general:} \quad f(n) \equiv f(\vec{k}_n, t_n) \, . \tag{3.112}$$

Correlators of the density field are computed by applying density operators (3.27) to the generating functional. We denote the r-point density correlation function in Fourier space, which is obtained by the application of r density operators, by

$$
\begin{aligned}
G_{\rho\rho\cdots\rho}(1, 2, \ldots, r) &:= \langle\tilde{\rho}(1)\tilde{\rho}(2)\cdots\tilde{\rho}(r)\rangle \\
&= \hat{\rho}(1)\hat{\rho}(2)\cdots\hat{\rho}(r) \, Z[\mathbf{J}, \mathbf{K}]\big|_{\mathbf{J}=0=\mathbf{K}} \, .
\end{aligned}
\tag{3.113}
$$

Recall that every density operator is a sum of one-particle density operators,

$$\hat{\rho}(1)\hat{\rho}(2)\cdots\hat{\rho}(r) = \sum_{j_1=1}^{N} \sum_{j_2=1}^{N} \cdots \sum_{j_r=1}^{N} \hat{\rho}_{j_1}(1)\hat{\rho}_{j_2}(2)\cdots\hat{\rho}_{j_r}(r) \, . \tag{3.114}$$

The r point density correlator is then a sum of N^r terms, which can be grouped into N one-particle, $N(N-1)$ two-particle, etc., up to $\frac{N!}{(N-r)!}$ r-particle contributions. We define the vector $\mathbf{L}$ with components

$$\mathbf{L}_q := \sum_{s=1}^{r} \vec{k}_s \otimes e_{j_s} \, , \tag{3.115}$$

$$\mathbf{L}_p := \sum_{s=1}^{r} g_{qp}(t_s, 0)\vec{k}_s \otimes e_{j_s} \, , \tag{3.116}$$

and the single particle components

$$\vec{L}_{q_j} = \sum_{s=1}^{r} \vec{k}_s \delta_{jj_s} \, , \tag{3.117}$$

$$\vec{L}_{p_j} = \sum_{s=1}^{r} g_{qp}(t_s, 0)\vec{k}_s \delta_{jj_s} \, . \tag{3.118}$$

With these definitions, we write an l-particle term as

$$Z_0[\mathbf{L}] = V^{-l} \left(\prod_{j=1}^{l} \int_{q_j} \right) \exp \left(-\frac{1}{2} \mathbf{L}_p^{\mathsf{T}} C_{pp}(\mathbf{q}) \mathbf{L}_p + \mathrm{i} \sum_{j=1}^{l} \vec{L}_{q_j} \cdot \vec{q}_j \right) , \tag{3.119}$$

where we already integrated out the initial positions of the $N - l$ non-contributing particles.

3.5.2 *Factorization*

Since C_{pp} only depends on the relative particle positions, we introduce coordinates relative to the initial position of the first particle $\vec{q}_{j1} := \vec{q}_j - \vec{q}_1$. Integration over the initial position of the first particle leads to a Dirac delta distribution, indicating statistical homogeneity, and the l-particle term becomes

$$Z_0[\mathbf{L}] = \frac{(2\pi)^3}{V^l} \delta_D \left(\sum_{j=1}^{l} \vec{L}_{q_j} \right) \left(\prod_{j=2}^{l} \int_{q_{j1}} \right) \exp \left(-\frac{1}{2} \mathbf{L}_p^{\mathsf{T}} C_{pp}(\mathbf{q}) \mathbf{L}_p + \mathrm{i} \sum_{j=2}^{l} \vec{L}_{q_j} \cdot \vec{q}_{j1} \right) . \tag{3.120}$$

See also reference [9], (B3).

The integral (3.120) can be factorized. First, we introduce relative coordinates between all l involved particles, and write (3.120) as

$$Z_0[\mathbf{L}] = \frac{(2\pi)^3}{V^l} \delta_D \left(\sum_{j=1}^{l} \vec{L}_{q_j} \right) \left(\prod_{2 \leq b < a \leq l} \int_{k'_{ab}} \right) \left(\prod_{1 \leq k < j \leq l} \int_{q_{jk}} \right)$$
$$\times \exp \left(-\frac{1}{2} \mathbf{L}_p^{\mathsf{T}} C_{pp}(\mathbf{q}) \mathbf{L}_p + \mathrm{i} \sum_{j=2}^{l} \vec{L}_{q_j} \cdot \vec{q}_{j1} + \mathrm{i} \sum_{2 \leq b < a \leq r} \vec{k}'_{ab} \cdot (\vec{q}_{ab} - \vec{q}_{a1} + \vec{q}_{b1}) \right) . \tag{3.121}$$

Then, we define the internal wave vectors

$$\vec{k}_{jk} := \begin{cases} \vec{L}_{q_j} - \sum_{b=2}^{j-1} \vec{k}'_{jb} + \sum_{a=j+1}^{l} \vec{k}'_{aj} & \text{for } k = 1, \, j = 2, \dots, l \\ \vec{k}'_{jk} & \text{for } k = 2, \dots, (l-1), \, j = (k+1), \dots, l , \end{cases} \tag{3.122}$$

such that the l-particle contribution to the free correlator can be written in the factorized form

$$Z_0[\mathbf{L}] = \frac{(2\pi)^3}{V^l} \delta_D \left(\sum_{j=1}^{l} \vec{L}_{q_j} \right) \exp \left(-\frac{\sigma_1^2}{6} \sum_{j=1}^{l} \vec{L}_{p_j}^2 \right)$$
$$\times \left(\prod_{2 \leq b < a < l} \int_{k'_{ab}} \right) \prod_{1 \leq k < j \leq l} I_{jk}(\vec{L}_{p_j}, \vec{L}_{p_k}, \vec{k}_{jk}) , \tag{3.123}$$

where we defined the factors

$$I_{jk}(\vec{L}_{p_j}, \vec{L}_{p_k}, \vec{k}_{jk}) := \int_{q_{jk}} e^{-\vec{L}_{p_j}^{\mathsf{T}} \hat{C}_{pp}(\vec{q}_{jk}) \vec{L}_{p_k} + i\vec{k}_{jk} \cdot \vec{q}_{jk}} \ , \tag{3.124}$$

and

$$\sigma_1^2 := \int_k k^2 P_\psi^{(i)}(k) \tag{3.125}$$

denotes the initial velocity dispersion. In (3.124) $\hat{C}_{pp}(\vec{q})$ denotes the 3×3-dimensional momentum correlation matrix of two particles separated by $\vec{q}$, as defined in (3.99). The terms I_{jk} can be interpreted as the two-particle correlation of particles j and k that contribute to the l-particle correlator (3.121). The integral over the wave vectors k'_{ab} connects the contributions from all particle pairs. Note that the structure of (3.120) is the same as the structure of the free generating functional (3.111), implying that the free generating functional can be factorized in the same way. We discuss the asymptotics of the factors I_{jk} in the limit of small scales in Chapter 7.

We would like to point out that the expression for $\vec{L}_{p_j}^{\mathsf{T}} \hat{C}_{pp}(\vec{q}_{jk}) \vec{L}_{p_k}$ in the kernel of I_{jk} in terms of the functions $a_\parallel$ and $a_\perp$ derived in Appendix B.3 of [9] is erroneous. For two-point correlation functions, the results are correct. In general, however, the transformation using the projection operators shown there, is not valid as shown in Appendix A.5 of this work. The correct coordinate representation of the momentum correlation matrix, which is also derived in [9], is given by

$$\begin{aligned} \hat{C}_{pp}(\vec{q}_{jk}) &= -\vec{\nabla}_{q_{jk}} \otimes \vec{\nabla}_{q_{jk}} \int_k \frac{P_\delta^{(i)}(k)}{k^4} e^{i\vec{k} \cdot \vec{q}_{jk}} \\ &= -\frac{\vec{q}_{jk} \otimes \vec{q}_{jk}}{q_{jk}^2} a_2(q_{jk}) - \mathbb{I}_3 a_1(\vec{q}_{jk}) \ , \end{aligned} \tag{3.126}$$

where we defined the functions

$$a_1(q) := \frac{\xi_\psi'(q)}{q} = -\frac{1}{2\pi^2} \int_0^\infty dk \ P_\delta^{(i)}(k) \frac{j_1(kq)}{kq} \ , \tag{3.127}$$

$$a_2(q) := \xi_\psi''(q) - \frac{\xi_\psi'(q)}{q} = \frac{1}{2\pi^2} \int_0^\infty dk \ P_\delta^{(i)}(k) j_2(kq) \ , \tag{3.128}$$

with the velocity potential correlation function ξ_ψ and the spherical Bessel functions of the first kind j_1 and j_2.

3.5.3 *Free Power Spectrum*

Finally, we have a closer look at two-point correlations. Using the definition of the density fluctuation power spectrum P_δ,

$$\langle \tilde{\delta}(\vec{k}_1, t) \tilde{\delta}(\vec{k}_2, t) \rangle = (2\pi)^3 \delta_D(\vec{k}_1 + \vec{k}_2) P_\delta(k, t) \ , \tag{3.129}$$

and

$$(2\pi)^3 \delta_D(\vec{k}_1 + \vec{k}_2) P_\delta(k, t) = \bar{\rho}^{-2} G_{\rho\rho}(12) - \bar{\rho}^{-1} G_\rho(1) - \bar{\rho}^{-1} G_\rho(2) + 1 \ , \tag{3.130}$$

with $t_1 = t_2 = t$, the free power spectrum becomes

$$\mathcal{P}(k,t) = e^{-\frac{\sigma_1^2}{3}k^2 g_{qp}^2(t,0)} \int d^3q \left(e^{-\vec{L}_{p_1}^\mathsf{T} \hat{C}_{pp}(\vec{q})\vec{L}_{p_2}} - 1 \right) e^{i\vec{k}\cdot\vec{q}} . \tag{3.131}$$

When we choose the Zel'dovich propagator this expression is equivalent to the nonlinear Zel'dovich power spectrum [58]. In Chapter 6, we discuss the properties of the free power spectrum in the limit of small scales, i.e. large wave numbers k, in detail.

For Zel'dovich trajectories, the free power spectrum behaves asymptotically like the linear power spectrum [7]. To summarize this result, the large-scale limit is obtained by a Taylor expansion of the exponential in the kernel of (3.131). There are at least two reasons why this expansion leads to the correct limit. First, the momentum correlation matrix is bounded for all q, implying that for fixed g_{qp} and arbitrarily small k the exponent itself becomes arbitrarily small, which in turn justifies a Taylor expansion of the exponential. And second, we expect that the dominant contribution to the large-scale limit comes from the integrand at large q. Since C_{pp} falls off like q^{-n_s-1} for large q with $n_s \leq 1$ (see Chapter 5), the behavior of the kernel in this regime is well approximated by the Taylor expansion. Thus, as $k \to 0$ (3.131) assumes the asymptotic expansion

$$\mathcal{P}(k,t) = e^{-\frac{\sigma_1^2}{3}k^2 g_{qp}^2(t,0)} \int d^3q \sum_{n=1}^{\infty} \frac{\left(g_{qp}^2(t,0)\vec{k}^\mathsf{T} \hat{C}_{pp}(\vec{q})\vec{k} \right)^n}{n!} e^{i\vec{k}\cdot\vec{q}}$$

$$\sim e^{-\frac{\sigma_1^2}{3}k^2 g_{qp}^2(t,0)} \left[g_{gp}^2(t,0) P_\delta^{(i)}(k) + \frac{g_{qp}^4(t,0)}{2} \int_{k'} P_\delta^{(i)}(k') P_\delta^{(i)}(|\vec{k}-\vec{k}'|) + \cdots \right] . \tag{3.132}$$

Since we choose Zel'dovich trajectories the propagator is equal to the linear growth factor $g_{qp}^Z(t,0) = D_+(t) - D_+(t^{(i)})$ and we indeed recover linear growth. However, this result deviates from standard perturbation theory by the damping term $e^{-\frac{\sigma_1^2}{3}k^2 g_{qp}^2(t,0)}$ in front of the series. It is legitimate to ask about the physical relevance of this factor. On the one hand, in [41] it was shown that by resummation, this damping can be removed. On the other hand, we deliberately expanded the integral for small k such that any statement about the damping factor at scales where it becomes relevant may be out of the scope of this expansion. In Chapter 6, we derive an asymptotic expansion of the free power spectrum at small scales and discuss the implications for the growth of cosmic structures in detail.

3.6 SUMMARY AND DISCUSSION

In this chapter, we summarized the basic foundations of KFT that apply to cosmic structure formation. We started with a review on how classical mechanics can be formulated in the framework of path integrals. The central object is the generating functional $Z[\mathbf{J}, \mathbf{K}]$ which can be split into a free generating functional and an interaction operator applied to it. This split is not unique, such that the propagators that describe free motion can be chosen arbitrarily. Changes in the choice of the propagators are then compensated in the interaction operator. By applying operators to

the generating functional, functions of the phase space coordinates at arbitrary times can be generated. However, in general, it is not possible to calculate the effect of the complete interaction operator. A perturbation series can be obtained by a Taylor expansion of the interaction operator to include higher orders in the interactions. Another way to include higher interaction orders is the use of an averaged interaction operator. This strategy turned out to be quite successful for the calculation of the non-linear density fluctuation power spectrum of cosmic structures [8].

Next, we reviewed the dynamics that apply to collisionless particles in an expanding spacetime and derived the interaction operator for pair-wise gravitational interactions. We also showed how the choice of free Zel'dovich trajectories changes the interaction operator and how this effects the particle trajectories in first-order perturbation theory.

We then reviewed the initial conditions that apply to the cosmic fluid at early times. Assuming initially a Gaussian random field as well as the linear continuity equation, the probability distribution of density and momentum fluctuations depends only on the initial density perturbation power spectrum. The probability distribution in phase space is then obtained by a Poisson sampling in the initial fields. For large scales and large propagators g_{qp}, only the initial momentum correlations are relevant when using Zel'dovich propagators. In Chapter 5, we derive the characteristics of the initial correlation functions in the limit of small and large scales in detail.

Finally, we reviewed how density correlation functions can be obtained by the factorization of the generating functional. We discussed an error in an earlier publication [9] that concerns the kernel of correlation functions of order three and higher. When the factorization was originally introduced, it was hoped that these expressions facilitate the numerical evaluation of higher-order density correlation functions. The idea was to first tabulate the factors I_{jk} such that the remaining convolution of these factors can be efficiently computed. Up to now, it was not possible to successfully implement such an algorithm for general factors. One problem was the error in the kernel that we resolved. In Chapter 7, we discuss further reasons for the still outstanding successful implementation and resolve some of the major issues.

The two point density fluctuation power spectrum in the free theory of KFT recovers the non-linear Zel'dovich power spectrum when the Zel'dovich propagator is used. Thus, in order to obtain a non-linear power spectrum with KFT, we can start at lowest order with the non-linear Zel'dovich power spectrum. Then, we can use perturbation theory or an averaged interaction operator to include more interactions. Before stream crossing, the Zel'dovich power spectrum is in very good agreement with power spectra obtained from N-body simulations. The exact behavior of this power spectrum during stream crossing and afterwards, when re-expansion occurs, is important for the understanding of early structure formation. However, the free power spectrum is hard to implement numerically for large wave numbers, because of the oscillating integral and the same problem arises for the factors I_{jk}. In Chapter 6, we derive the asymptotic series of the free power spectrum in KFT for large wave numbers at arbitrary times. Since, to our knowledge, no asymptotic methods dealing with integrals of these types exist yet – the large parameter k in the kernel appears with different powers in the exponent – we derive in Chapter 4 a new method that applies to these integrals.

Part II

RESULTS

INTERLUDE: ASYMPTOTICS OF CERTAIN TYPES OF INTEGRALS

Integrals over rapidly oscillating integrands occur frequently in physics and are often difficult to handle numerically. Their asymptotic behaviour for large parameter values (e.g. large wave numbers) is interesting in view of estimates, studies of limiting behaviour, and testing numerical solutions. In this chapter, we derive the asymptotics of integrals of the form

$$P(k) = \int_\Omega g(x) e^{-k^s f(x)} e^{ik \cdot x} dx , \tag{4.1}$$

for large parameters $k \to \infty$, where $\Omega \subset \mathbb{R}^N$, $N \geq 1$, and $s \geq 1$, real. There are asymptotic methods for certain special choices of s in the literature. For example for $s = 1$, the method of stationary phase or the method of steepest descent can typically be applied. Without the phase function e^{ikx} in the kernel, Laplace's method is used. For $s = 0$, there are methods that deal with the asymptotic expansion of Fourier or Hankel transforms. However, for more general values of s, the large parameter k appears with different powers in the exponent of the integration kernel. When f and g are monomials, a coordinate transformation, e.g. $k \cdot x \to y$, can be performed and one of the forementioned methods can be applied. For general values of s as well as functions f and g, to our knowledge, no general techniques are known to derive the asymptotics of the integral (4.1). Our goal is to narrow this gap by providing a technique that is valid for a broad class of functions f and g as well as a wide range of parameters s. For the techniques we present, s needs to exceed a lower bound that depends on f.

We introduce in the first section some notation and definitions related to asymptotics and multi-indices. In the second section, we derive the asymptotics for one-dimensional integrals over finite intervals. In the third section we derive the asymptotics for N-dimensional integrals over finite regions. In the fourth part, we show that for quadratically integrable, bounded functions f with a unique minimum at $x = 0$, the derived asymptotics is valid for integration over the whole $\mathbb{R}^N$, even when the integral (4.1) is not absolutely convergent.

4.1 NOTATION AND DEFINITIONS

4.1.1 *Asymptotics*

We start by defining the order symbols and asymptotic equality as in [17] and [49].

Definition 4.1 (O-Notation). *Suppose f, g are real-valued functions over a space $\mathbb{X}$ and x_0 a limit point.*
(i) As $x \to x_0$ in $\mathbb{X}$,

$$f(x) = o\left(g(x)\right) :\Leftrightarrow \frac{f(x)}{g(x)} \to 0 . \tag{4.2}$$

In this case f is said to be „little-oh" of g as $x \to x_0$.
(ii) As $x \to x_0$ in $\mathbb{X}$,

$$f(x) = \mathcal{O}\left(g(x)\right) :\Leftrightarrow \left|\frac{f(x)}{g(x)}\right| \text{ is bounded .} \tag{4.3}$$

In this case, f is said to be „big-oh" of g as $x \to x_0$. When $\lim_{x \to x_0} \frac{f(x)}{g(x)} \neq 0$, then f is said to be „of order" g.

The o and $\mathcal{O}$ symbols are also known as *Landau symbols*.

Definition 4.2 (Asymptotic Equality). *Suppose f, g are real-valued functions over a space $\mathbb{X}$ and x_0 a limit point. As $x \to x_0$ in $\mathbb{X}$,*

$$f(x) \sim g(x) \Leftrightarrow \frac{f(x)}{g(x)} \to 1 . \tag{4.4}$$

In this case, we say f and g are asymptotically equal.

Note that this use of the term „asymptotic equality" differs from the use by some other authors who define two functions to be asymptotically equal if and only if they possess identical asymptotic expansions (see below). One can show that the difference of two asymptotically equal functions is of lower order,

$$f(x) \sim g(x) \quad \Leftrightarrow \quad f(x) - g(x) = o\left(g(x)\right) , \quad \text{as } x \to x_0 . \tag{4.5}$$

This leads us to the definitions of an asymptotic sequence and a generalized asymptotic expansion, which we take from Wong [68].

Definition 4.3 (Asymptotic Sequence). *Let $\{f_n\}_{n \in \mathbb{N}}$ be a sequence of functions defined on a common space $\mathbb{X}$ and x_0 a limit point of $\mathbb{X}$. We say that $\{f_n\}_{n \in \mathbb{N}}$ is an asymptotic sequence as $x \to x_0$ in $\mathbb{X}$ if for all $n \geq 0$*

$$f_{n+1}(x) = o\left(f_n(x)\right) , \quad \text{as } x \to x_0 . \tag{4.6}$$

Definition 4.4 (Generalized Asymptotic Expansion). *Let f and f_n, $n = 0, 1, 2, \ldots$, be functions defined on $\mathbb{X}$. The formal series $\sum f_n$ is called a generalized asymptotic expansion of f with respect to the asymptotic sequence $\{\varphi_n\}_{n \in \mathbb{N}}$, as $x \to x_0$, if*

$$f(x) = \sum_{n=0}^{N} f_n(x) + o\left(\varphi_N(x)\right) , \tag{4.7}$$

for every fixed $N \geq 0$. In this case, we write

$$f(x) \sim \sum_{n=0}^{\infty} f_n(x) ; \quad \{\varphi_n\}_{n \in \mathbb{N}} , \quad \text{as } x \to x_0 . \tag{4.8}$$

Note that Definition 4.4 implies that the asymptotic expansion of a function f is not unique. For $x \neq x_0$, the asymptotic expansion of a function may not be a convergent series. Nevertheless, in some cases it is possible to get good estimates for the function value in the vicinity of the limit point by optimal truncation. We adopt the definition of the *optimal truncation rule* as stated by Boyd [13].

Definition 4.5 (Optimal Truncation Rule). *Consider a generalized asymptotic expansion as in the previous definition. Then, for a given x, the minimum error in an asymptotic series is usually achieved by truncating the series so as to retain the smallest term in the series, discarding all terms of higher degree.*

As stated by Boyd, the imprecise adjective „usually" indicates that this is not true in general and there are simple counter-examples. However, the optimal truncation rule can be rigorously proven for some classes of asymptotic series. Apart from these special classes, it is an empirical rule that turned out to be very useful in practice. [1] The shorter term *superasymptotic* was introduced by Berry and Howls (see [13] and references therein).

Definition 4.6 (Superasymptotic). *An optimally-truncated asymptotic series is a superasymptotic approximation.*

4.1.2   Multi-Index Notation

A multi-index $\alpha = (\alpha_1, \alpha_2, \ldots, \alpha_N) \in \mathbb{N}_0^N$ is an N-tuple of non-negative integers. Multi-indices compactify the notation a lot. The following list of notation and formulas will be useful throughout this chapter.

- Absolute value

$$|\alpha| := \alpha_1 + \alpha_2 + \ldots + \alpha_N .\tag{4.9}$$

- Factorial

$$\alpha! := \alpha_1!\, \alpha_2! \cdots \alpha_N! .\tag{4.10}$$

- The sum of two multi-indices $\alpha, \beta \in \mathbb{N}_0^N$

$$\alpha + \beta := (\alpha_1 + \beta_1, \alpha_2 + \beta_2 + \ldots + \alpha_N + \beta_N) .\tag{4.11}$$

- The binomial of two multi-indices $\alpha, \beta \in \mathbb{N}_0^N$

$$\binom{\alpha}{\beta} := \binom{\alpha_1}{\beta_1}\binom{\alpha_2}{\beta_2} \cdots \binom{\alpha_N}{\beta_N} .\tag{4.12}$$

- Gamma function

$$\Gamma(\alpha) := \Gamma(\alpha_1)\Gamma(\alpha_2) \cdots \Gamma(\alpha_N) .\tag{4.13}$$

- Multi-index applied to a vector $x = (x_1, x_2, \ldots, x_N) \in \mathbb{C}^N$

$$x^\alpha := x_1^{\alpha_1} x_2^{\alpha_2} \cdots x_N^{\alpha_N} .\tag{4.14}$$

---

[1] Carl Bender once stated in a seminar he held in Heidelberg about asymptotics that physics is typically nice. For this reason and since in this work we check all our results numerically, we adopt this rule unless contradictions arise.

- Multi-index applied to a function of a multi-index $\mu \in \mathbb{N}^N$

$$f^{\alpha}(\mu) := f^{\alpha_1}(\mu_1) f^{\alpha_2}(\mu_2) \cdots f^{\alpha_N}(\mu_N) .\qquad(4.15)$$

or more specific, as used below

$$\left(\frac{2}{\mu}\right)^{(\alpha+1)/2} := \left(\frac{2}{\mu_1}\right)^{(\alpha_1+1)/2} \left(\frac{2}{\mu_2}\right)^{(\alpha_2+1)/2} \cdots \left(\frac{2}{\mu_N}\right)^{(\alpha_N+1)/2} .\qquad(4.16)$$

- Applied to a differential operator

$$D^{\alpha} G(y_0) := \left(\frac{\partial^{|\alpha|}}{\partial y_1^{\alpha_1} \cdots \partial y_N^{\alpha_N}} \right) G(y) \Bigg|_{y=y_0} .\qquad(4.17)$$

- Leibniz formula for two functions f, g

$$D^{\alpha}(fg) = \sum_{\beta+\gamma=\alpha} \binom{\alpha}{\beta} (D^{\beta}f)(D^{\gamma}g) .\qquad(4.18)$$

4.2 ONE-DIMENSIONAL INTEGRALS

In one dimension, we start by considering for $s \geq 1$ and $\beta > 0$ integrals of the form

$$I(k) = \int_0^b \mathrm{d}x \, \mathrm{e}^{-k^s f(x)} x^{\beta-1} \mathrm{e}^{ikx} ,\qquad(4.19)$$

in the limit of large parameters $k \to \infty$.

We begin our analysis with Laplace's method as stated by Erdélyi [25], using the formulation from Nemes [47], slightly adapted. For a proofs of Laplace's method, we refer to [25, 68].

Theorem 4.1 (Erdélyi's Theorem). *Consider for real-valued functions f and real- or complex-valued functions g the following integral,*

$$I(\lambda) = \int_a^b \mathrm{e}^{-\lambda f(x)} g(x) \mathrm{d}x, \quad \text{as } \lambda \to \infty ,\qquad(4.20)$$

for which we assume that

1. *$f(x) > f(a)$ for $x \in (a,b)$ and*

$$\inf_{x \in [a+\delta,b)} \{ f(x) - f(a) \} > 0 ,\qquad(4.21)$$

    for all $\delta > 0$;

2. *$f'(x)$ and $g(x)$ are continuous in a neighborhood of $x = a$, except possibly at a;*

3. *f and g admit asymptotic expansions*

$$f(x) \sim f(a) + \sum_{m=0}^{\infty} a_m (x-a)^{m+\alpha} ,\qquad(4.22)$$

and

$$g(x) \sim \sum_{m=0}^{\infty} b_m(x-a)^{m+\beta-1} , \tag{4.23}$$

with $\alpha > 0$ and $Re(\beta) > 0$ as $x \to a^+$. Furthermore, the expansion of f can be term-wise differentiated such that

$$f'(x) \sim \sum_{m=0}^{\infty} a_m(m+\alpha)(x-a)^{m+\alpha-1} , \tag{4.24}$$

as $x \to a^+$;

4. *$I(\lambda)$ converges absolutely for sufficiently large λ.*

Then

$$I(\lambda) \sim e^{-\lambda f(a)} \sum_{n=0}^{\infty} \Gamma\left(\frac{n+\beta}{\alpha}\right) \frac{c_n}{\lambda^{(n+\beta)/\alpha}} , \tag{4.25}$$

as $\lambda \to +\infty$.

The coefficients c_n can be expressed in terms of a_n and b_n,

$$c_n = \frac{1}{\alpha a_0^{(n+\beta)/\alpha}} \sum_{m=0}^{n} \frac{b_{n-m}}{m!} d_{m,n} , \tag{4.26}$$

with

$$d_{m,n} = \lim_{x \to 0} \frac{\mathrm{d}^m}{\mathrm{d}x^m} \left(1 + \sum_{j=1}^{\infty} \frac{a_j}{a_0} x^j \right)^{-(n+\beta)/\alpha} . \tag{4.27}$$

This explicit formula for the coefficients c_n was first presented by Wojdylo in [67] and [66]. For the first three coefficients, we find

$$d_{0,n} = 1 , \tag{4.28}$$

$$d_{1,n} = -\frac{n+\beta}{\alpha} \frac{a_1}{a_0} , \tag{4.29}$$

$$d_{2,n} = \frac{n+\beta}{\alpha} \left(\frac{n+\beta+\alpha}{\alpha} \frac{a_1^2}{a_0^2} - 2\frac{a_2}{a_0} \right) . \tag{4.30}$$

We can now use Theorem 4.1 to prove the following theorem for integral (4.19) that we are interested in.

Theorem 4.2. *Consider the integral (4.19) where f satisfies the requirements of Erdélyi's Theorem 4.1, $1 \leq \alpha \leq s$ and $\beta > 0$. Then, there exists a positive integer $M > 0$, such that (4.19) possesses an asymptotic expansion*

$$I(k) \sim \frac{e^{-k^s f(0)}}{\alpha a_0^{\beta/\alpha} k^{s\beta/\alpha}} \left[\sum_{m=0}^{M-1} I_m(k) + \varphi_M(k) \right] , \quad as \ k \to \infty , \tag{4.31}$$

where

$$
I_m(k) = \frac{\mathrm{e}^{-\frac{\mathrm{i}}{2}\pi m}}{k^m} \sum_{n=m}^{\infty} \mathrm{e}^{\frac{\mathrm{i}}{2}\pi n} \frac{\Gamma\left(\frac{n+\beta}{\alpha}\right)}{m!(n-m)!} \frac{d_{m,n}}{a_0^{n/\alpha}} k^{n(1-s/\alpha)} ,
\tag{4.32}
$$

and

$$
\varphi_M(k) = \sum_{n=M}^{\infty} \sum_{m=M}^{n} \frac{\Gamma\left(\frac{n+\beta}{\alpha}\right)}{(k^s a_0)^{n/\alpha}} \frac{(\mathrm{i}k)^{n-m}}{m!(n-m)!} d_{m,n} .
\tag{4.33}
$$

Proof. We start by specifying Erdélyi's Theorem 4.1 to Fourier-type integrals

$$
I(\lambda,k) = \int_0^b \mathrm{d}x \, \mathrm{e}^{-\lambda f(x)} x^{\beta-1} \mathrm{e}^{\mathrm{i}kx} ,
\tag{4.34}
$$

with constant mode k and $b > 0$. Notice that for $\lambda = k^s$, we obtain (4.19). We assume that f satisfies the conditions of Erdélyi's Theorem and consider without loss of generality the lower integration boundary $a = 0$. We use the Taylor series for the exponential in $g(x) = x^{\beta-1}\mathrm{e}^{\mathrm{i}kx}$ in (4.25) and arrive at the asymptotic expansion

$$
I(\lambda,k) \sim \mathrm{e}^{-\lambda f(0)} \sum_{n=0}^{\infty} \Gamma\left(\frac{n+\beta}{\alpha}\right) \frac{c_n(k)}{\lambda^{(n+\beta)/\alpha}} , \quad \text{as } \lambda \to +\infty ,
\tag{4.35}
$$

where the coefficients (4.26) depend on the wave number k

$$
c_n(k) = \frac{1}{\alpha a_0^{(n+\beta)/\alpha}} \sum_{m=0}^{n} \frac{(\mathrm{i}k)^{n-m}}{m!(n-m)!} d_{m,n} .
\tag{4.36}
$$

Since we aim at an asymptotic expansion where also k becomes a large parameter, we now consider the sum over n of those terms in the double sum (4.35) with (4.36) where m is constant. This re-ordering then yields an asymptotic expansion for (4.34) as $\lambda \to \infty$ that is also ordered in decreasing orders of k.

Lemma 4.1. *For $\alpha \geq 1$ and $k > 0$, there exists a positive integer $M > 0$ and a real number λ_0 such that*

$$
I_m(\lambda,k) := \frac{-\mathrm{e}^{\frac{\mathrm{i}}{2}\pi m}}{k^m} \sum_{n=m}^{\infty} \Gamma\left(\frac{n+\beta}{\alpha}\right) \left(\frac{k}{(\lambda a_0)^{1/\alpha}}\right)^n \frac{\mathrm{e}^{\frac{\mathrm{i}}{2}\pi n} d_{m,n}}{m!(n-m)!}
\tag{4.37}
$$

is finite for all $m < M$ and all $\lambda > \lambda_0$.

Proof. Consider

$$
I_0(\lambda,k) = \sum_{n=0}^{\infty} \Gamma\left(\frac{n+\beta}{\alpha}\right) \frac{1}{(\lambda a_0)^{n/\alpha}} \frac{(\mathrm{i}k)^n}{n!} d_{0,n} .
\tag{4.38}
$$

Since $d_{0,n} = 1$ for all n, we estimate

$$
\left| I_0(\lambda,k) \right| = \left| \sum_{n=0}^{\infty} \Gamma\left(\frac{n+\beta}{\alpha}\right) \frac{1}{n!} \left(\frac{\mathrm{i}k}{(\lambda a_0)^{1/\alpha}}\right)^n \right|
\tag{4.39}
$$

$$
\leq \sum_{n=0}^{\lceil 2\alpha-\beta \rceil} \left| \Gamma\left(\frac{n+\beta}{\alpha}\right) \frac{1}{n!} \left(\frac{\mathrm{i}k}{(\lambda a_0)^{1/\alpha}}\right)^n \right|
\tag{4.40}
$$

$$
+ \sum_{n=0}^{\infty} \left| \frac{\Gamma(n+\beta)}{n!} \left(\frac{\mathrm{i}k}{(\lambda a_0)^{1/\alpha}}\right)^n \right| ,
\tag{4.41}
$$

where we used that $\alpha \geq 1$ and that $\Gamma\left(\frac{n+\beta}{\alpha}\right) \leq \Gamma(n+\beta)$ for all $2 \leq \frac{n+\beta}{\alpha}$. Since $\beta > 0$, the first sum is a finite sum of finite terms, thus finite. For the term, we calculate

$$
\sum_{n=0}^{\infty} \left| \frac{\Gamma(n+\beta)}{n!} \left(\frac{\mathrm{i}k}{(\lambda a_0)^{1/\alpha}} \right)^n \right| = \Gamma(\beta) \frac{\Gamma(t)}{\Gamma(t)\Gamma(\beta)} \sum_{n=0}^{\infty} \frac{\Gamma(n+\beta)}{n!} \frac{\Gamma(n+t)}{\Gamma(n+t)} \left(\frac{k}{(\lambda a_0)^{1/\alpha}} \right)^n
$$

$$
= \Gamma(\beta) {}_2F_1 \left(\beta, t; t; \frac{k}{(\lambda a_0)^{1/\alpha}} \right) ,
$$

(4.42)

where we introduced the variable $t > 0$, arbitrary, and ${}_2F_1$ denotes the (generalized) hypergeometric function [1]. For $\lambda > \frac{k^\alpha}{a_0} =: \lambda_0$, (4.42) converges to

$$
\Gamma(\beta) {}_2F_1 \left(\beta, t; t; \frac{k}{(\lambda a_0)^{1/\alpha}} \right) = \Gamma(\beta) \left[1 - \frac{k}{(\lambda a_0)^{1/\alpha}} \right]^{-\beta} ,
$$

(4.43)

implying (4.38) exists for $\lambda > \lambda_0$ and thus (4.37) exists for $M > 0$ and $\lambda > \lambda_0$, proving Lemma 4.2. □

From the definition (4.37) we directly infer

$$
I_m(\lambda, k) = \mathcal{O}\left(\lambda^{-m/\alpha} \right) , \quad \text{as } \lambda \to \infty .
$$

(4.44)

Lemma 4.1 implies that we can partially resum the infinite double sum appearing in (4.35). Together with definition (4.37), we arrive at the asymptotics for (4.34)

$$
I(\lambda, k) \sim \frac{\mathrm{e}^{-\lambda f(0)}}{\alpha(\lambda a_0)^{\beta/\alpha}} \left[\sum_{m=0}^{M-1} I_m(\lambda, k) + \varphi_M(\lambda, k) \right] ,
$$

(4.45)

as $\lambda \to \infty$, where we defined

$$
\varphi_M(\lambda, k) := \sum_{n=M}^{\infty} \sum_{m=M}^{n} \frac{\Gamma\left(\frac{n+\beta}{\alpha}\right)}{(\lambda a_0)^{n/\alpha}} \frac{(\mathrm{i}k)^{n-m}}{m!(n-m)!} d_{m,n} .
$$

(4.46)

Comparing $\varphi_M(\lambda, k) = \mathcal{O}(\lambda^{-M/\alpha})$ with, we find that 4.44, φ_M is asymptotically suppressed compared to the I_m in (4.45), as $k \to \infty$.

We now derive the asymptotics of (4.19) from (4.45). First, we find that for $\lambda = k^s$, where $1 \leq \alpha \leq s$ and $m < M$, the terms (4.37) are

$$
I_m(k^s, k) = \frac{\mathrm{e}^{-\frac{\mathrm{i}}{2}\pi m}}{k^m} \sum_{n=m}^{\infty} \mathrm{e}^{\frac{\mathrm{i}}{2}\pi n} \frac{\Gamma\left(\frac{n+\beta}{\alpha}\right)}{m!(n-m)!} \frac{d_{m,n}}{a_0^{n/\alpha}} k^{n(1-s/\alpha)}
$$

(4.47)

$$
= \frac{k^{-ms/\alpha}}{m! a_0^{m/\alpha}} \sum_{n=0}^{\infty} \mathrm{e}^{\frac{\mathrm{i}}{2}\pi n} \frac{\Gamma\left(\frac{n+m+\beta}{\alpha}\right)}{n!} \frac{d_{m,n+m}}{a_0^{n/\alpha}} k^{n(1-s/\alpha)}
$$

(4.48)

$$
=: I_m(k) .
$$

(4.49)

Due to the constraint $s \geq \alpha$,

$$
I_m(k) = \mathcal{O}\left(k^{-ms/\alpha} \right) .
$$

(4.50)

Next, for $\lambda = k^s$, φ_M in (4.45) becomes

$$
\begin{aligned}
\varphi_M&(k^s, k) \\
&= \sum_{n=0}^{\infty} \sum_{m=0}^{n} \frac{\Gamma\left(\frac{n+M+\beta}{\alpha}\right)}{(k^s a_0)^{(n+M)/\alpha}} \frac{(ik)^{n-m}}{(m+M)!(n-m)!} d_{m+M,n+M} \\
&= \frac{k^{-sM/\alpha}}{a_0^{m/\alpha}} \sum_{n=0}^{\infty} e^{\frac{i}{2}\pi n} \frac{k^{n(1-s/\alpha)}}{a_0^{n/\alpha}} \sum_{m=0}^{n} e^{-\frac{i}{2}\pi m} \frac{\Gamma\left(\frac{n+M+\beta}{\alpha}\right) d_{m+M,n+M}}{(m+M)!(n-m)!} k^{-m} \\
&=: \varphi_M(k) \,,
\end{aligned}
\tag{4.51}
$$

which is of order $\mathcal{O}\left(k^{-sM/\alpha}\right)$. Due to (4.50), φ_M is asymptotically suppressed compared to the I_m as $k \to \infty$. We thus conclude, that there exists a positive integer $M > 0$, such that the integral (4.19), which is for $\lambda = k^s$ equivalent to (4.34), satisfies the asymptotic expansion (4.31). $\qquad\square$

4.3 MULTIDIMENSIONAL INTEGRALS

In this section, we consider integrals in $\mathbb{R}^N$, $N > 1$ of the form

$$
P(k) = \int_D e^{-|k|^s f(x)} g(x) e^{ik \cdot x} dx \,, \quad s \geq 2 \,,
\tag{4.52}
$$

where $k \in \mathbb{R}^N$ and $D \subset \mathbb{R}^N$ is a possibly unbounded domain. As in the one-dimensional case, we start by considering Laplace integrals

$$
J(\lambda) = \int_D g(x) e^{-\lambda f(x)} dx \,,
\tag{4.53}
$$

where $\lambda > 0$ is a large positive parameter. We summarize Laplace's method for multidimensional integrals as presented by Wong [68]. For a proof, we refer to the same reference.

Theorem 4.3 (Laplace's Method)**.** *For the integral (4.53) we assume that*

1. *$f, g \in C^{\infty}(D)$;*

2. *$J(\lambda)$ converges absolutely for all sufficiently large λ;*

3. *f has a global minimum at and only at $x_0 \in D$ such that*

$$
\rho(\varepsilon) = \inf_{D \setminus B_\varepsilon(x_0)} \{f(x) - f(x_0)\} > 0
\tag{4.54}
$$

   for all $\varepsilon > 0$, where $B_\varepsilon(x_0)$ is the open ball with radius ε around x_0; and that

4. *the Hessian matrix of f in x_0*

$$
A = \left(\frac{\partial^2 f(x)}{\partial x_i \partial x_j} \right)\Bigg|_{x=x_0}
\tag{4.55}
$$

   is positive definite.

Then, the integral has an the asymptotic expansion

$$J(\lambda) \sim e^{-\lambda f(x_0)} \sum_{n=0}^{\infty} \frac{c_n}{\lambda^{N/2+n}} , \qquad (4.56)$$

as $\lambda \to \infty$. The coefficients c_n are given by

$$c_n = \sum_{|\alpha|=2n} \delta(\alpha) \left(\frac{2}{\mu} \right)^{(\alpha+1)/2} \Gamma\left(\frac{\alpha+1}{2} \right) \frac{D^{\alpha} G(0)}{\alpha!} , \qquad (4.57)$$

where $\alpha = (\alpha_1, \alpha_2, \dots, \alpha_N)$ is a multi-index, $\mu = (\mu_1, \mu_2, \dots, \mu_N) \in \mathbb{R}^N$ is the collection of the eigenvalues of the Hessian matrix A from (4.55), and

$$\delta(\alpha) = \begin{cases} 1, & \text{all } \alpha_i \text{ even} \\ 0, & \text{else} \end{cases} . \qquad (4.58)$$

The function $G : D_0 \to \mathbb{R}^N$, where $D_0 \subset D$, is given by (4.64) below.

Note that condition 3 implies that f has its essential infimum in D at and only at the point x_0. If x_0 is an interior point, this will in turn imply that x_0 is a critical point of f, i.e., $\nabla f(x)|_{x=x_0} = 0$. Condition 4 is equivalent to the statement that all eigenvalues of A are positive.

We now make use of Theorem 4.3 to prove the following theorem for the asymptotics of the integral (4.52).

Theorem 4.4. *Consider the integral (4.52) where f and g satisfy the conditions of Theorem 4.3, $x_0 = 0$ and $g(0) \neq 0$. Then, the asymptotics of (4.52) is given by*

$$P(k) \sim g(0) e^{-|k|^s f(0)} \sqrt{\frac{(2\pi)^N}{|k|^{sN} \det A}} \exp\left(-\frac{k^{\mathsf{T}} A^{-1} k}{2|k|^s} \right) , \quad \text{as } |k| \to \infty . \qquad (4.59)$$

Our strategy is very similar to our proof in one dimension. We first consider Fourier-Laplace type integrals with two distinct coefficients and then perform a resummation of terms. To this end, we need an expression for the function G, that appears in the coefficients (4.57). This can be derived from Morse's Lemma. We summarize Wong's presentation of Morse's Lemma [68].

Lemma 4.2 (Morse's Lemma). *Let f be a real-valued C^{∞}-function in a neighborhood of the non-degenerate critical point x_0, with the Hessian matrix*

$$A = \left(\frac{\partial^2 f}{\partial x_i \partial x_j} \right) \Bigg|_{x=x_0} \qquad (4.60)$$

being positive definite. Then there exist neighborhoods U, V of the points $y = 0$, $x = x_0$ and a diffeomorphism $h : U \to V$ of class C^{∞} such that

$$(f \circ h)(y) = f(x_0) + \sum_{j=1}^{N} \mu_j y_j^2 , \qquad (4.61)$$

where the μ_j are the eigenvalues of A. Furthermore, the Jacobian of the transformation satisfies

$$\frac{\partial(x_1, \dots, x_N)}{\partial(y_1, \dots, y_N)} \Bigg|_{y=0} = 1 . \qquad (4.62)$$

When λ in (4.53) becomes very large, the integrand outside a small neighborhood of x_0 is is exponentially suppressed compared to the peak value. With this consideration and applying a diffeomorphism h from Morse's Lemma, the asymptotics of (4.53) is given by

$$J(\lambda) \sim \int_U e^{-\lambda \sum_{j=1}^N \mu_j y_j^2} g(h(y)) \det h'(y) dy , \quad \text{as } \lambda \to \infty , \tag{4.63}$$

where U is the transformed integration domain. This transformation defines the function G (4.57),

$$G(y) = g(h(y)) \det h'(y) , \tag{4.64}$$

where

$$h'_{ij}(y) := \left(\frac{\partial h_i(y)}{\partial y_j} \right) \tag{4.65}$$

denotes the Jacobian of the diffeomorphism, with $h'_0 := h'(y = 0)$, at the critical point.

Proof of Theorem 4.4. We now specify Laplace's method, Theorem 4.3, to Fourier-type integrals with constant wave vector $k \in \mathbb{R}^N$,

$$J(\lambda, k) := \int_D e^{-\lambda f(x)} g(x) e^{ik \cdot x} dx , \tag{4.66}$$

for large parameters λ and $|k| \neq 0$. Note that for $\lambda = k^s$, this integral is equivalent to (4.52). According to Theorem 4.3, the asymptotics of 4.66 as $\lambda \to \infty$ is given by

$$J(\lambda, k) \sim e^{-\lambda f(0)} \sum_{n=0}^\infty \frac{c_n(k)}{\lambda^{N/2+n}} . \tag{4.67}$$

The coefficients $c_n(k)$ depend on the orientation and the absolute value of the wave vector k,

$$c_n(k) = \sum_{|\alpha|=2n} \delta(\alpha) \left(\frac{2}{\mu} \right)^{(\alpha+1)/2} \Gamma\left(\frac{\alpha+1}{2} \right) \frac{D^\alpha G(k,0)}{\alpha!} , \tag{4.68}$$

where G is according to (4.64) given by

$$G(k,y) = g(h(y)) e^{ik \cdot h(y)} \det h'(y) . \tag{4.69}$$

Since our ultimate goal is to arrive at an asymptotic series where also $|k|$ becomes very large, we determine the leading $|k|$ behavior of the coefficients $c_n(k)$.

Lemma 4.3. *The coefficients c_n in (4.68) with G as in (4.69) acquire the expansion*

$$c_n(k) = g(0) e^{i\pi n} k^{2n} \sum_{|\alpha|=2n} \frac{\delta(\alpha)}{\alpha!} \left(\frac{2}{\mu} \right)^{\frac{\alpha+1}{2}} \Gamma\left(\frac{\alpha+1}{2} \right) \prod_{j=1}^N \left(\frac{\partial}{\partial y_j} \hat{k} \cdot h(y) \right)^{\alpha_j} \Bigg|_{y=0} \tag{4.70}$$

$$+ \varphi_n(k) ,$$

with $\hat{k} := k/|k|$, where $\varphi_n(k)$ is asymptotically suppressed as $|k| \to \infty$.

Note that the eigenvalues μ_i of the Hessian, the scalar function f and the vector valued function h do not depend on $|k|$, but may depend on the direction of k.

Proof. We first determine the leading $|k|$ behavior of the terms $D^\alpha G(k, 0)$. Recalling that $h(0) = x_0 = 0$ and $\det h'_0 = 1$, we find

$$
\begin{aligned}
D^\alpha G(k, 0) &= \sum_{\rho+\sigma=\alpha} \binom{\alpha}{\rho} \left(D^\rho e^{ik \cdot h(y)} \right) \left(D^\sigma g(y) \det h'(y) \right) \Big|_{y=0} \\
&= g(h(y)) \det h'(y) D^\alpha e^{ik \cdot h(y)} \big|_{y=0} + \phi_\alpha(k) \\
&= g(0) D^\alpha e^{ik \cdot h(y)} \big|_{y=0} + \phi_\alpha(k) \,,
\end{aligned}
\tag{4.71}
$$

as $|k| \to \infty$, where ρ and σ are multi-indices and

$$
\phi_\alpha(k) := \sum_{\rho+\sigma=\alpha, \rho \neq \alpha} \binom{\alpha}{\rho} \left(D^\rho e^{ik \cdot h(y)} \right) \left(D^\sigma g(y) \det h'(y) \right) \Big|_{y=0} ,
\tag{4.72}
$$

contains those terms from (4.71), where not all derivatives act on the exponential. In the first step of (4.71), we applied Leibniz's rule (4.18). Since derivatives acting on $e^{ik \cdot h(y)}$ generate higher orders of $|k|$, $\phi_\alpha = \mathcal{O}(|k|^{2n-1})$ is asymptotically suppressed compared to $D^\alpha e^{ik \cdot h(y)} \big|_{y=0} = \mathcal{O}(|k|^{2n})$, as $|k| \to \infty$.

Applying a single differential operator to the exponential function, we find

$$
\begin{aligned}
\frac{\partial e^{ik \cdot h(y)}}{\partial y_i} &= \sum_{j=1}^N \frac{\partial e^{ik \cdot h(y)}}{\partial h_j} \frac{\partial h_j(y)}{\partial y_i} \\
&= i e^{ik \cdot h(y)} \frac{\partial}{\partial y_i} k \cdot h(y) \\
&= i|k| e^{ik \cdot h(y)} \frac{\partial}{\partial y_i} \hat{k} \cdot h(y) \,,
\end{aligned}
\tag{4.73}
$$

where $\hat{k} := k/|k|$ denotes the unit vector pointing in the direction of k. Applying $|\alpha|$ differential operators, we infer from (4.71)

$$
\begin{aligned}
D^\alpha G(k, 0) &= g(0) \, D^\alpha e^{ik \cdot h(y)} \big|_{y=0} + \phi_\alpha(k) \\
&= g(0) \, (i|k|)^{|\alpha|} \prod_{j=1}^N \left(\frac{\partial}{\partial y_j} \hat{k} \cdot h(y) \right)^{\alpha_j} \Bigg|_{y=0} + \phi_\alpha(k) \,.
\end{aligned}
\tag{4.74}
$$

Using this result in (4.68), we can write the c_n as

$$
\begin{aligned}
c_n(k) &= g(0) e^{i\pi n} |k|^{2n} \sum_{|\alpha|=2n} \frac{\delta(\alpha)}{\alpha!} \left(\frac{2}{\mu} \right)^{\frac{\alpha+1}{2}} \Gamma\left(\frac{\alpha+1}{2} \right) \prod_{j=1}^N \left(\frac{\partial}{\partial y_j} \hat{k} \cdot h(y) \right)^{\alpha_j} \Bigg|_{y=0} \\
&\quad + \varphi_n(k) \,.
\end{aligned}
\tag{4.75}
$$

The remainder

$$
\varphi_n(k) = \sum_{|\alpha|=2n} \delta(\alpha) \left(\frac{2}{\mu} \right)^{(\alpha+1)/2} \Gamma\left(\frac{\alpha+1}{2} \right) \frac{\phi_\alpha(k)}{\alpha!} \,,
\tag{4.76}
$$

is $\mathcal{O}(|k|^{2n-1})$ as $k \to \infty$ and therefore asymptotically suppressed. $\qquad \square$

We insert (4.75) into the asymptotic series (4.67) to get the asymptotics as $\lambda \to \infty$,

$$
J(\lambda, k) \sim \frac{e^{-\lambda f(0)}}{\lambda^{N/2}} \times
$$

$$
\left[\sum_{n=0}^{\infty} \left\{ g(0) \sum_{|\alpha|=2n} \frac{\delta(\alpha)}{\alpha!} \left(\frac{-|k|^2}{\lambda} \right)^n \left(\frac{2}{\mu} \right)^{\frac{\alpha+1}{2}} \Gamma\left(\frac{\alpha+1}{2} \right) \prod_{j=1}^{N} \left(\frac{\partial}{\partial y_j} \hat{k} \cdot h(y) \right)^{\alpha_j} \Bigg|_{y=0} \right. \right.
$$

$$
\left. \left. + \frac{\varphi_n(k)}{\lambda^n} \right\} \right] .
$$

(4.77)

We simplify the double sum with our result (B.13) from Appendix B.2 and note that by construction $\varphi_0(k) = 0$, to arrive at

$$
J(\lambda, k) \sim \frac{e^{-\lambda f(0)}}{\lambda^{N/2}} \left[g(0) \sqrt{\frac{(2\pi)^N}{\det A}} \exp\left(-\frac{|k|^2}{2\lambda} \hat{k}^\mathsf{T} A^{-1} \hat{k} \right) + \sum_{n=1}^{\infty} \frac{\varphi_n(k)}{\lambda^n} \right] , \qquad (4.78)
$$

as $\lambda \to \infty$.

We now consider $\lambda = |k|^s$. Since $\varphi_n(k) = \mathcal{O}\left(|k|^{2n-1} \right)$,

$$
\frac{\varphi_n(k)}{|k|^{sn}} = \mathcal{O}\left(|k|^{n(2-s)-1} \right) = \mathcal{O}\left(|k|^{-1} \right) , \qquad (4.79)
$$

for all $s \geq 2$, as $|k| \to \infty$. Furthermore,

$$
\sum_{n=1}^{\infty} \frac{\varphi_n(k)}{|k|^{sn}} = \mathcal{O}\left(|k|^{1-s} \right) = o\left(|k|^{2-s} \right) ,
$$

$$
\exp\left(-\frac{|k|^2}{2|k|^s} \hat{k}^\mathsf{T} A^{-1} \hat{k} \right) = \mathcal{O}\left(|k|^{2-s} \right) , \qquad (4.80)
$$

$$
\Rightarrow \sum_{n=1}^{\infty} \frac{\varphi_n(k)}{|k|^{sn}} = o\left(\exp\left(-\frac{|k|^2}{2|k|^s} \hat{k}^\mathsf{T} A^{-1} \hat{k} \right) \right)
$$

as $|k| \to \infty$. We therefore conclude, that (4.78) holds for $J(|k|^s, k)$ as $k \to \infty$, such that (4.78) is equivalent to (4.59), proving the theorem. $\qquad \square$

4.4 EXTENSION TO INFINITE INTEGRATION DOMAINS

In the previous sections, we have derived the asymptotics of integrals of the type

$$
P(k) = \int_{\mathbb{R}^N} e^{-|k|^s f(x)} g(x) e^{ik \cdot x} \mathrm{d}x \qquad (4.81)
$$

as $k \to \infty$ when the integral is absolutely convergent. We demanded this as condition 4 in one dimension and condition 2 in N dimensions. In this section, we show for the general multidimensional case, that we can relax this assumption.

Theorem 4.5. *We consider the integral 4.52, satisfying the conditions of Theorem 4.3 with $x_0 = 0$, but instead of condition 2, f and g satisfy*

2'. $f \in L_2(\mathbb{R}^N)$ *and* $g \in L^\infty(\mathbb{R}^N)$, $g(0) \neq 0$; *and*

3b. the infimum

$$\sigma(\varepsilon) = \inf_{x \in \mathbb{R}^N \setminus B_\varepsilon(0)} \{|f(0)| - |f(x)|\} > 0 \tag{4.82}$$

for all $\varepsilon > 0$.

Then, the asymptotic expansion (4.59) of Theorem 4.4 holds, as $|k| \to \infty$.

Proof. Without loss of generality, it is sufficient to assume $g(x) = 1$, since the expansion (4.59) from Theorem 4.4 depends only on the value of g at the critical point. For $k \neq 0$, we consider the integral

$$\begin{aligned}
\tilde{P}(k) &:= \int_{\mathbb{R}^N} \left[e^{-|k|^s f(x)} - 1 + |k|^s f(x) \right] e^{ikx} dx \\
&= P(k) - (2\pi)^N \delta_D(k) + |k|^s \hat{f}(k) \\
&= P(k) + |k|^s \hat{f}(k) ,
\end{aligned} \tag{4.83}$$

where $\hat{f}$ denotes the Fourier transform of f. Since the Fourier transform maps L_2 onto itself, $\hat{f} \in L_2$. We further split the integration domain as

$$\tilde{P}(k) = \left(\int_{D_0} + \int_{\mathbb{R}^N \setminus D_0} \right) \left[e^{-|k|^s f(x)} - 1 + |k|^s f(x) \right] e^{ikx} dx =: \tilde{P}_1(k) + \tilde{P}_2(k) , \tag{4.84}$$

where we choose $D_0 \subset \mathbb{R}^N$, a finite, open neighborhood of the origin, such that Morse's Lemma applies.

We now investigate the contributions to $\tilde{P}(k)$ from a neighborhood of the origin and from outside this neighborhood as $|k| \to \infty$. The integral $\tilde{P}_1(k)$ is given by

$$\begin{aligned}
\tilde{P}_1(k) &= \int_{D_0} e^{-|k|^s f(x)} e^{ikx} dx - \int_{D_0} e^{ikx} dx + \int_{D_0} |k|^s f(x) e^{ikx} dx \\
&\leq \int_{D_0} e^{-|k|^s f(x)} e^{ikx} dx + \left(1 + |k|^s |f(0)| \right) |D_0|
\end{aligned} \tag{4.85}$$

Since the second term in the last line of (4.85) is exponentially suppressed compared to the asymptotics (4.59) – recall that $f(0) < 0$ and (4.59) therefore grows exponentially with increasing $|k|^s$ – we conclude that

$$\tilde{P}_1(k) \sim e^{-|k|^s f(0)} \sqrt{\frac{(2\pi)^N}{|k|^{sN} \det A}} \exp\left(-\frac{k^\mathsf{T} A^{-1} k}{2|k|^s} \right) , \tag{4.86}$$

as $|k| \to \infty$.

For $\tilde{P}_2(k)$ we estimate

$$\begin{aligned}
|\tilde{P}_2(k)| &\leq \int_{\mathbb{R}^N \setminus D_0} \left| e^{-|k|^s f(x)} - 1 + |k|^s f(x) \right| dx \\
&= \int_{\mathbb{R}^N \setminus D_0} \left| \sum_{n=2}^\infty \frac{[-|k|^s f(x)]^n}{n!} \right| dx \\
&\leq \sum_{n=2}^\infty \frac{1}{n!} \int_{\mathbb{R}^N \setminus D_0} \left| |k|^s f(x) \right|^n dx
\end{aligned} \tag{4.87}$$

We now choose

$$\varepsilon := \inf \left\{ |x| : x \in \mathbb{R} \setminus D_0 \right\} .$$

(4.88)

By condition 3b there exists a $\sigma(\varepsilon) > 0$ such that

$$|f(x)| \leq |f(0)| - \sigma(\varepsilon), \quad \forall x \in \mathbb{R}^N \setminus D_0 ,$$

(4.89)

With this, we get

$$
\begin{aligned}
|\tilde{P}_2(k)| &\leq \sum_{n=2}^{\infty} \frac{|k|^{sn}}{n!} \int_{\mathbb{R}^N \setminus D_0} |f(x)|^n \, \mathrm{d}x \\
&\leq \sum_{n=2}^{\infty} \frac{|k|^{sn} \left[|f(0)| - \sigma(\varepsilon) \right]^{n-2}}{n!} \int_{\mathbb{R}^N} |f(x)|^2 \, \mathrm{d}x \\
&= \frac{\int_{\mathbb{R}^N} |f(x)|^2 \, \mathrm{d}x}{\left(|f(0)| - \sigma(\varepsilon) \right)^2} \sum_{n=2}^{\infty} \frac{\left[|k|^s \left(|f(0)| - \sigma(\varepsilon) \right) \right]^n}{n!} \\
&= \frac{\int_{\mathbb{R}^N} |f(x)|^2 \, \mathrm{d}x}{\left(|f(0)| - \sigma(\varepsilon) \right)^2} \left[\mathrm{e}^{-|k|^s \left[f(0) + \sigma(\varepsilon) \right]} - 1 + |k|^s f(0) \right]
\end{aligned}
$$

(4.90)

since $f \in L_2$ and therefore $\int_{\mathbb{R}^N} |f(x)|^2 \mathrm{d}x$ finite. This result is exponentially suppressed by a factor $\exp \left[-|k|^s \sigma(\epsilon) \right]$ compared to the asymptotics 4.59. Since $\hat{f} \in L_2$ vanishes at infinity, we conclude

$$
\begin{aligned}
P(k) &= \tilde{P}(k) - |k|^s \hat{f}(k) \\
&\sim \tilde{P}(k) \sim \tilde{P}_1(k) \\
&= \mathrm{e}^{-|k|^s f(0)} \sqrt{\frac{(2\pi)^N}{|k|^{sN} \det A}} \exp \left(-\frac{k^\mathsf{T} A^{-1} k}{2|k|^s} \right) , \quad \text{as } |k| \to \infty ,
\end{aligned}
$$

(4.91)

as claimed. Note that $f(0) < 0$, thus (4.91) increases exponentially for increasing values of $|k|^s$. $\qquad \square$

4.5   SUMMARY AND DISCUSSION

In this chapter, we derived the asymptotics of Laplace-Fourier type integrals, where the large parameter k appears with different powers in the exponential. For integrals in one dimension, we derived a complete asymptotic series by a resummation of Laplace's method from Erdélyi's Theorem. In N dimensions, we derived an expression for the leading term in the asymptotic expansion. In the last section, we showed that our results are also valid when the integral does not converge absolutely, as long as the function f is quadratically integrable and bounded. In order to derive further terms of the asymptotic sequence in N dimensions, one needs to evaluate derivatives of the diffeomorphism h in Morse's Lemma, at the critical point. Since the proof of Morse's Lemma by Milnor gives a construction of the inverse h^{-1}, a derivation of further asymptotic terms should in principle be possible.

Our method in N dimensions provides an efficient way to obtain the leading behaviour for large parameters k. However, one disadvantage of this method is

that the function f needs to be asymptotically quadratic in the neigborhood of the critical point. One way to overcome this shortcoming in certain cases and additionally construct more terms of the asymptotic expansion in N dimensions might be to introduce spherical coordinates and apply the one-dimensional method to the integral over the radial coordinate. Then, for each term in the resulting asymptotic series, the integration over the angular coordinates has to be performed. This strategy was for example used in [31] to extend the one-dimensional Laplace's method to multiple dimensions.

The methods we presented are valid when k^s dominates the Laplace part of the kernel, i.e. the power s needs to be above some critical value. This constraint is the reason why a modification of Laplace's method leads to our results. For smaller values of s, when the oscillation due to the Fourier phase dominates the behaviour of the kernel, another method has to be derived. A starting point to derive such a method might be the saddle-point approximation.

CHARACTERISTICS OF THE INITIAL CORRELATIONS

The initial correlations in the cosmic density and velocity fields are key ingredients to understand cosmic structures today. In kinetic field theory (KFT), the initial density correlations

$$C_{\delta\delta}(\vec{q}) = \int_k P_\delta^{(i)}(k) e^{i\vec{k}\cdot\vec{q}} = \xi_{\delta\delta}(q) \,, \tag{5.1}$$

the initial density-momentum correlations

$$\vec{C}_{\delta p}(\vec{q}) = i \int_k \vec{k} k^2 P_\psi^{(i)}(k) e^{i\vec{k}\cdot\vec{q}} = \vec{\nabla}_q \xi_{\delta\psi}(q) \,, \tag{5.2}$$

and the initial momentum correlations

$$\hat{C}_{pp}(\vec{q}) = \int_k (\vec{k} \otimes \vec{k}) P_\psi^{(i)}(k) e^{i\vec{k}\vec{q}} = -(\vec{\nabla}_q \otimes \vec{\nabla}_q) \xi_{\psi\psi}(q) \tag{5.3}$$

are built-in in the free generating functional, thus they are completely incorporated in the free theory. In this chapter, we analyze the characteristics of the initial correlation functions in the limit of very large and very small scales. Their asymptotic limiting behavior is not only interesting by itself. In KFT, knowing the asymptotics is also important for the numerical evaluation and analytical estimation of the correlation functions at later times – in particular in the strongly non-linear regime. Because we assume that the initial fluctuations are Gaussian, the initial correlation functions are completely determined by the initial density perturbation power spectrum. The features we identify in our analysis apply to a broad class of initial power spectra relevant to cosmological structure formation.

This chapter is organized as follows. In the first section, we motivate the introduction of a smoothing scale. In the second section, we derive an asymptotic expansion for small scales $q \to 0$ and in the third section the asymptotics for large scales $q \to \infty$. In the final section, we present the exact analytical solution to the initial correlation functions for a type of hot dark matter with an initial power spectrum $P_\delta^{(i)}(k) \propto k\, e^{-k/k_s}$, where k_s defines the smoothing scale in Fourier space.

5.1 MOTIVATION OF A SMALL-SCALE SMOOTHING

Since KFT operates in the N-particle phase space, there is fundamentally no need to introduce a smoothing scale. However, there are several resons why we nevertheless might want to introduce a smoothing scale for non-exponentially cut-off power spectra, like the CDM power spectrum in [4]. First, calculations become significantly simpler because the resulting asymptotic series for the initial correlation functions (5.1)–(5.3) are power series. Considering initial power spectra that are not exponentially cut-off results in asymptotic series that involve logarithms, which in turn need to be handled differently in later calculations. Second, from a physical perspective it is unlikely that the initial power spectrum, even for cold dark matter, behaves asymptotically like a rational function up to arbitrarily large wave numbers.

The primordial power spectrum, set after inflation, was a simple power law proportional to k^{n_s} with $n_s \lesssim 1$ and a very small amplitude[1]. The way how these perturbations grow strongly depends on the dominant energy component in the universe. During the radiation dominated era, perturbations with wavelength smaller than the particle horizon stop growing because of the so called *Meszaros effect*, while large-scale perturbations grow without mode coupling. This results in a power spectrum that at large scales (small k) is still proportional to k^{n_s}, while at small scales (large k) it asymptotically behaves like $\sim k^{n_s-4}$ [4].

When dark matter consists of particles and is not completely cold, random thermal motions additionally wash out fluctuations below a free-streaming scale that corresponds to the typical comoving distance that a particle travels in the age of the universe [28]. This scale is inversely proportional to the dark matter particle mass m_X. The product of the comoving critical density and the cubed comoving free-streaming scale then defines a mass scale for cosmological structures. Hot dark matter with $m_X \sim 30$ eV has a free-streaming length of the order of a galaxy cluster, warm dark matter with $m_X \sim 2$ keV has a free-streaming length that corresponds to the halo of a dwarf galaxy, while for CDM, $m_X \sim 100$ GeV, the free-streaming length corresponds to the scale of the Earth [28]. Thus, when dark matter consists of particles, thermally or non-thermally produced, some kind of cutoff compared to the $\sim k^{n_s-4}$ tail has to be imprinted in the linear power spectrum [28, 69]. Since this cutoff is physically related to m_X, all of our later results that depend on the cutoff scale contain information about the mass of hypothetical dark matter particles. The linear power spectra of hypothetical non-cold dark matter typically possess steeper power laws, are exponentially damped, and/or assume oscillating behaviour in the high-k regime. A general framework to parametrize the linear power spectra of non-cold dark matter at small scales was recently put forward in [45].

For any initial power spectrum that is not exponentially cut-off, we introduce a smoothing scale k_s in Fourier space by applying an exponential UV regulator to the initial density power spectrum

$$P_\delta^{(i)}(k) \to P_\delta^{(i)}(k)\, \mathrm{e}^{-k/k_s} \,, \tag{5.4}$$

such that the moments σ_n^2 of the initial velocity potential power spectrum $P_\psi^{(i)}(k) = k^{-4} P_\delta^{(i)}(k)$,

$$\sigma_n^2 := \int_k k^{2n} P_\psi^{(i)}(k) = \frac{1}{2\pi^2} \int_0^\infty \mathrm{d}k\, k^{2n-2} P_\delta^{(i)}(k) < \infty \,, \tag{5.5}$$

are finite.

Note that in the Lagrangian picture, a smoothing scale needs to be introduced to define a smooth displacement field [18]. The smoothing in KFT is physically very different to the smoothing in the Lagrangian picture: in KFT, the smoothing occurs in the initial correlation functions and not in the initial density or velocity (displacement) fields. In an individual realisation, particles are still allowed to cross at arbitrarily small distances at initial times.

Throughout this work, the initial power spectra that we consider either naturally possess tails that fall off at least exponentially, or they are smoothed according to (5.4), unless stated otherwise.

---

1 The exponent might change with k, but such a change has not been observed.

5.2 SMALL-SCALE ASYMPTOTICS

In this section, we derive the asymptotics of the correlation functions $C_{\delta\delta}$, $\vec{C}_{\delta p}$ and $\hat{C}_{pp}$, (5.1)-(5.3), for small scales, i.e. as $q \to 0$. To this end, we make use of the following theorem from Erdélyi on the integration of asymptotic expansions [25]. A proof of the theorem can be found in the same reference.

Theorem 5.1 (Integration of Asymptotic Expansions). *Let* $\{\varphi_n\}_{n\in\mathbb{N}}$ *be an asymptotic sequence and* $a < q < b$. *For the integral*

$$I(q) := \int_a^b f(k)W(k,q)\mathrm{d}k \,, \tag{5.6}$$

we assume that

1. *the function*

   $$W(k,q) \sim \sum_{n=0}^{N} a_n(k)\varphi_n(q) + o\left(\varphi_N(q)\right) \tag{5.7}$$

   as $q \to q_0$ *uniformly in* q;

2. $W(k,q)$ *is a measurable function of* k *for each fixed* q;

3. $a_n(k)$ *is a measurable function of* k *for each fixed* n; *and*

4. $f(k)$ *is an integrable function of* k *for which each of the integrals*

   $$A_n = \int_a^b f(k)a_n(k)\mathrm{d}k \tag{5.8}$$

   exists.

Then, also the integral (5.6) exists for each q *in some neighborhood of* q_0, *and*

$$I(q) \sim \sum_{n=0}^{N} A_n\varphi_n(q) + o\left(\varphi_N(q)\right) \,. \tag{5.9}$$

In order to apply Theorem 5.1 we first note that the integrals (5.1)-(5.3) are absolutely convergent because we introduced an exponential cutoff and because $n_s > 0$. Starting with $C_{\delta\delta}$, we introduce spherical coordinates, perform the integral over the angles and arrive at

$$C_{\delta\delta}(q) = \frac{1}{2\pi^2} \int_0^\infty \mathrm{d}k \, k^2 P_\delta^{(\mathrm{i})}(k)j_0(kq) \,, \tag{5.10}$$

where j_n denotes the spherical Bessel function of the first kind of order n. This integral expression is of the same type as (5.6) in Theorem 5.1. The conditions for Theorem 5.1 are fulfilled in (5.10), where $a = q_0 = 0$, $b \to \infty$, $W(k,q) = j_0(kq)$ and $f(k) = k^2 P_\delta^{(\mathrm{i})}(k)$, because

1. $j_0(x)$ possesses a convergent Taylor series at $x = 0$ such that

   $$j_0(kq) = \sum_{n=0}^{\infty}(-1)^n \frac{k^{2n}}{(2n+1)!}q^{2n} \,, \tag{5.11}$$

   where we choose $\varphi_n(q) = q^{2n}$;

2. $j_0(kq)$ is a measurable function of k for each fixed q;

3. $(-1)^n \frac{k^{2n}}{(2n+1)!}$ is a measurable function of k for each fixed n; and

4. $k^2 P_\delta^{(i)}(k)$ is an integrable function of k for which each of the integrals

$$A_n = \int_a^b k^2 P_\delta^{(i)}(k)(-1)^n \frac{k^{2n}}{(2n+1)!} dk = \frac{(-1)^n}{(2n+1)!} \sigma_{2+n}^2 , \tag{5.12}$$

exist due to the exponential cutoff in $P_\delta^{(i)}$ and because $n_s > 0$.

We thus arrive at the asymptotic expansion

$$C_{\delta\delta}(q) \sim \frac{1}{2\pi^2} \sum_{n=0}^{\infty} (-1)^n \frac{\sigma_{2+n}^2}{(2n+1)!} q^{2n} , \quad \text{as } q \to 0 . \tag{5.13}$$

We apply the same procedure to compute the asymptotic expansion of $\vec{C}_{\delta p}$ as $q \to 0$,

$$\vec{C}_{\delta p}(q) = \vec{\nabla}_q \int_k k^{-2} P_\delta^{(i)}(k) e^{i\vec{k}\vec{q}} \tag{5.14}$$

$$= \frac{\vec{\nabla}_q}{2\pi^2} \int_0^\infty dk \, P_\delta^{(i)}(k) \frac{\sin(kq)}{kq} \tag{5.15}$$

$$\sim \frac{\vec{\nabla}_q}{2\pi^2} \sum_{n=0}^{\infty} (-1)^n \frac{q^{2n}}{(2n+1)!} \int_0^\infty dk \, k^{2n} P_\delta^{(i)}(k) \tag{5.16}$$

$$= \frac{1}{2\pi^2} \frac{\vec{q}}{q} \sum_{n=1}^{\infty} (-1)^n \frac{2n \, q^{2n-1}}{(2n+1)!} \int_0^\infty dk \, k^{2n} P_\delta^{(i)}(k) \tag{5.17}$$

$$= -\frac{\vec{q}}{2\pi^2} \sum_{n=0}^{\infty} (-1)^n \frac{\sigma_{2+n}^2}{(2n+3)(2n+1)!} q^{2n} . \tag{5.18}$$

For the asymptotics of the initial momentum-momentum correlation matrix, we first rewrite $\hat{C}_{pp}$ as in (3.126),

$$\hat{C}_{pp}(\vec{q}) = -\vec{\nabla}_q \otimes \vec{\nabla}_q \int_k P_\psi^{(i)}(k) e^{i\vec{k}\cdot\vec{q}} \tag{5.19}$$

$$= -\frac{\vec{q} \otimes \vec{q}}{q^2} \left(\xi_\psi''(q) - \frac{\xi_\psi'(q)}{q} \right) - \mathbb{I}_3 \frac{\xi_\psi'(q)}{q} \tag{5.20}$$

$$=: -\frac{\vec{q} \otimes \vec{q}}{q^2} a_2(q) - \mathbb{I}_3 a_1(q) , \tag{5.21}$$

with the functions

$$a_1(q) := \frac{\xi_\psi'(q)}{q} = -\frac{1}{2\pi^2} \int_0^\infty dk \, P_\delta^{(i)}(k) \frac{j_1(kq)}{kq} , \tag{5.22}$$

$$a_2(q) := \xi''(q) - \frac{\xi_\psi'(q)}{q} = \frac{1}{2\pi^2} \int_0^\infty dk \, P_\delta^{(i)}(k) j_2(kq) . \tag{5.23}$$

We arrive at the asymptotics of a_1 by applying Theorem 5.1,

$$a_1(q) = -\frac{1}{2\pi^2} \int_0^\infty dk P_\delta^{(i)}(k) \frac{j_1(kq)}{kq}$$

$$\sim -\frac{1}{2\pi^2} \int_0^\infty dk P_\delta^{(i)}(k) \sum_{n=0}^{\infty} \frac{(-1)^n (2+2n)}{(3+2n)!} (kq)^{2n} \tag{5.24}$$

$$= \frac{1}{2\pi^2} \sum_{n=0}^{\infty} \frac{(-1)^{n+1}}{(2n+3)(2n+1)!} \sigma_{1+n}^2 q^{2n} ,$$

as $q \to 0$, where we used the Taylor series of $j_1(x)$,

$$j_1(x) = x \sum_{n=0}^{\infty} \frac{(-1)^n (2+2n)}{(3+2n)!} x^{2n} . \tag{5.25}$$

We compute the asymptotic expansion of a_2 by exploiting $a_2(q) = q a_1'(q)$ and finally arrive at

$$a_1(q) \sim \sum_{n=0}^{\infty} \frac{(-1)^{n+1} \sigma_{n+1}^2}{(3+2n)(1+2n)!} q^{2n} , \quad \text{as } q \to 0 , \tag{5.26}$$

$$a_2(q) \sim \sum_{n=1}^{\infty} \frac{(-1)^{n+1} 2n \, \sigma_{n+1}^2}{(3+2n)(1+2n)!} q^{2n} , \quad \text{as } q \to 0 . \tag{5.27}$$

To make further calculations more compact, we define the coefficients

$$a_n := \frac{(-1)^{n+1} \sigma_{n+1}^2}{(3+2n)(1+2n)!} , \tag{5.28}$$

such that the asymptotic expansions of a_1 and a_2 are now given by

$$a_1(q) \sim \sum_{n=0}^{\infty} a_n q^{2n} , \quad \text{as } q \to 0 , \tag{5.29}$$

$$a_2(q) \sim \sum_{n=1}^{\infty} 2n \, a_n q^{2n} , \quad \text{as } q \to 0 . \tag{5.30}$$

The convergence radius of the asymptotic series (5.29) and (5.30) is given by $q = \frac{1}{k_s}$ when an exponential smoothing according to (5.4) is chosen. This can be seen from the following consideration. Recall that we chose an exponential regularization for the initial power spectrum, then we can write (5.22) as

$$a_1(q) = -\frac{1}{2\pi^2} \int_0^{\infty} P_{\delta,\mathrm{nr}}^{(i)}(k) e^{-k/k_s} \left(\frac{e^{ikq} - e^{-ikq}}{2i(kq)^3} - \frac{e^{ikq} + e^{-ikq}}{2(kq)^2} \right) \frac{j_1(kq)}{kq} , \tag{5.31}$$

where $P_{\delta,\mathrm{nr}}^{(i)}$ now denotes the un-regularized initial power spectrum, which for cold dark matter has a power law tail. Furthermore, we wrote the trigonometric representation of $j_1(x) = x^{-2} \sin x - x^{-1} \cos x$ in terms of complex exponentials. When we now consider $q = \pm iy$ with $y \geq \frac{1}{k_s}$, then the integral (5.31) is not exponentially regularized any more and might even diverge. Although we only consider positive values of q, this possible divergence in the complex plane indicates the finite convergence radius of the series (5.29) and (5.30) that we derived for a_1 and a_2. The same argument holds for the series (5.13) and (5.18), which also have a finite radius of convergence $q = \frac{1}{k_s}$. Note that for a stronger regularization kernel, like for example a Gaussian, these series might actually be convergent for all finite k_s for all values of q.

Note that it is also possible to derive the asymptotic expansions of the initial correlation functions without smoothing, i.e. when the initial density perturbation power spectrum has a power law tail. Depending on the power, this leads to an asymptotic expansion that either involves logarithms or a sum of two power series. In this work, we restrict our analysis to power spectra with exponential cutoff.

5.3   LARGE-SCALE ASYMPOTICS

In KFT, when we want to compute density correlation functions, for example via the factors of the generating functional (3.124), we have to numerically evaluate integrals that contain the initial correlation functions in the integration kernel. From a numerical perspective these integrals are typically difficult to compute, as they (i) are rapidly oscillating and (ii) have to be performed over infinite integration domains. In order to implement these integrals numerically, we need to know the degree to which they converge and how they can numerically be regularized. Thus, we need to know the behavior of the integration kernel for large arguments.

Since we consider only the effect of initial momentum correlations in this work, we restrict our analysis to the large-scale asymptotics of $\hat{C}_{pp}$. To this end, we apply the asymptotic expansion techniques for Hankel transforms presented in [68]. We start by stating the necessary theorems from [68], and refer for proofs of these theorems to the same reference.

We consider the Hankel transform of the function f,

$$H_\nu(q) = \int_0^\infty \mathrm{d}k\, f(k) J_\nu(kq)\,, \tag{5.32}$$

where J_ν denotes the Bessel function of first kind of order ν.

Theorem 5.2. *In (5.32), we assume that*

1. *f is m times continuously differentiable in $(0,\infty)$, m being a non-negative integer;*

2. *f has an asymptotic expansion*

$$f(k) \sim \sum_{n=0}^\infty c_n k^{\lambda_n - 1}, \quad \text{as } k \to 0\,, \tag{5.33}$$

   where $\mathrm{Re}(\lambda_0 + \nu) > 0$, $\mathrm{Re}\,\lambda_{n+1} > \mathrm{Re}\,\lambda_n$ for $n = 0,1,2,\dots$ and this asymptotic expansion can be differentiated m times; and

3. *each of the integrals*

$$\int_1^\infty f^{(j)}(k) k^{-1/2} \mathrm{e}^{\mathrm{i}k\cdot q}\mathrm{d}k, \quad j = 0,1,\dots,m, \tag{5.34}$$

   converges uniformly for all sufficiently large q, where $f^{(j)}$ denotes the j-th derivative of f.

Let N be the smallest non-negative integer such that

$$\mathrm{Re}\,\lambda_N > m\,, \tag{5.35}$$

and define $f_N(k)$ by

$$f(k) = \sum_{n=0}^{N-1} c_n k^{\lambda_n - 1} + f_N(k)\,. \tag{5.36}$$

Then the Hankel transform (5.32) satisfies

$$H_\nu(q) = \sum_{n=0}^{N-1} c_n \frac{\Gamma\left(\frac{1}{2}\nu + \frac{1}{2}\lambda_n\right) 2^{\lambda_n - 1}}{\Gamma\left(\frac{1}{2}\nu - \frac{1}{2}\lambda_n + 1\right)} q^{-\lambda_n} + E_N(q)\,, \tag{5.37}$$

where

$$E_N(q) = \left(-\frac{1}{q}\right)^m \int_0^\infty f_{N,m}(q) J_{\nu+m}(kq) \ , \tag{5.38}$$

and the functions $f_{N,j}(k)$, $j = 0, 1, \ldots, m$ are defined recursively by $f_{N,0}(k) = f_N(k)$ and

$$f_{N,j+1}(k) = f'_{N,j}(k) - \frac{(\nu+j+1)}{k} f_{N,j}(k) \ . \tag{5.39}$$

The following corollary from [68] provides a sufficient condition such that the expansion in Theorem 5.2 is asymptotic.

Corollary 5.1. *To show that the expansion in Theorem 5.2 is asymptotic, it is enough to prove that*

$$E_N(q) = o\left(q^{-m}\right), \quad \text{as } q \to \infty \ , \tag{5.40}$$

or equivalently

$$\lim_{q\to\infty} \int_0^\infty dk \, f_{N,m}(k) J_{\nu+m}(kq) = 0 \ . \tag{5.41}$$

Finally, an estimate for the remainder E_N in Theorem 5.2 is given by the following theorem from [68].

Theorem 5.3. *Assume that conditions 1 and 2 hold, and replace condition 3 by*

3'. Each of the integrals

$$\int_1^\infty dk \, f^{(j)}(k) k^{-1/2} e^{ikq} \ , \tag{5.42}$$

where $j = 0, 1, \ldots, m$, converges uniformly for all sufficiently large q, and

$$\int_1^\infty dk \, |f^{(j)}(k)| k^{j-m} < \infty \ , \tag{5.43}$$

for each $j = 0, 1, \ldots, m$.

Choose N again as in Theorem 5.2. (i) If $\mathrm{Re}\, \lambda_{N-1} < m$, then

$$|E_N(q)| \le \frac{A_{\nu+m}}{q^m} \int_0^\infty dk \, |f_{N,m}(k)| \ . \tag{5.44}$$

(ii) If $\mathrm{Re}\, \lambda_{N-1} = m$, then

$$|E_N(q)| \le \frac{B_{\nu+m}}{q^{m+1/2}} \int_0^\infty dk \, k^{-1/2} |f_{N,m}(k)| \ . \tag{5.45}$$

The coefficients in (5.44) and (5.45) are given by

$$A_\alpha = \sup_{0 \le k \le \infty} |J_\alpha(k)| \quad \text{and} \quad B_\alpha = \sup_{0 \le k \le \infty} |k^{1/2} J_\alpha(k)| \ . \tag{5.46}$$

We now apply these theorems, to derive the asymptotics of a_1 and a_2 as $q \to \infty$. We start by expressing the integrals (5.22) and (5.23) as Hankel transforms,

$$a_1(q) = -\frac{1}{2\pi^2}\sqrt{\frac{\pi}{2q}}\int_0^\infty dk \frac{P_\delta^{(i)}(k)}{qk\sqrt{k}} J_{3/2}(kq) , \tag{5.47}$$

$$a_2(q) = \frac{1}{2\pi^2}\sqrt{\frac{\pi}{2q}}\int_0^\infty dk \frac{P_\delta^{(i)}(k)}{\sqrt{k}} J_{5/2}(kq) , \tag{5.48}$$

using the relation

$$j_\nu(x) = \sqrt{\frac{\pi}{2x}} J_{\nu+1/2}(x) . \tag{5.49}$$

For the initial density perturbation power spectrum, we assume that

1. $P_\delta^{(i)}$ can be continuously differentiated at least three times ($m = 3$ in Theorem 5.2) in $k \in (0, \infty)$, which is safe to assume due to its regularity; and that

2. $P_\delta^{(i)}$ has an asymptotic expansion of the form

$$P_\delta^{(i)}(k) \sim \sum_{n=0}^\infty P_n k^{n_s+n}, \quad \text{as } k \to 0^+ , \tag{5.50}$$

that can be differentiated at least three times.

Note that the reason for demanding $m = 3$ is of practical nature: it allows us to calculate the first three terms in the asymptotic expansion.

With these assumptions, the kernel functions in (5.47) and (5.48) satisfy the first two requirements of Theorems 5.2 and 5.3. The first three exponents λ_n for both cases are shown in Table 5.1. Note that the remaining requirements related to integrability are fulfilled because of the smoothing.

	ν	λ_0	λ_1	λ_2	N (for $\frac{1}{2} < n_s < \frac{3}{2}$)
$a_1(q)$	$3/2$	$n_s - 1/2$	$n_s + 1/2$	$n_s + 3/2$	3
$a_2(q)$	$5/2$	$n_s + 1/2$	$n_s + 3/2$	$n_s + 5/2$	2

Table 5.1: Parameters for the asymptotic expansion (5.37) of the functions $a_1(q)$ and $a_2(q)$, respectively. Recall that N is given by condition (5.35) with $m = 3$. For a_1, we assumed the existence of a $\lambda_3 \geq \lambda_2 + 1$.

In accordance with our requirement (5.50), we write the initial density perturbation power spectrum,

$$P_\delta^{(i)}(k) = P_0 k^{n_s} + P_1 k^{n_s+1} + P_2 k^{n_s+2} + P_3(k) , \tag{5.51}$$

where P_0, P_1 and P_2 are real-valued coefficients. Combining (5.51) with (5.36) then yields the following expressions for the kernel functions (5.47) and (5.48),

$$a_1 : \quad \frac{P_\delta^{(i)}(k)}{qk\sqrt{k}} = \frac{P_0}{q}k^{(n_s-1/2)-1} + \frac{P_1}{q}k^{(n_s+1/2)-1} + \frac{P_2}{q}k^{(n_s+3/2)-1} + \frac{P_3(k)}{qk\sqrt{k}} , \tag{5.52}$$

$$a_2 : \quad \frac{P_\delta^{(i)}(k)}{\sqrt{k}} = P_0 k^{(n_s+1/2)-1} + P_1 k^{(n_s+3/2)-1} + P_2 k^{(n_s+5/2)-1} + \frac{P_3(k)}{\sqrt{k}} . \tag{5.53}$$

With (5.37) from Theorem 5.2, we arrive for a_1 at the expansion

$$
a_1(q) = -\frac{1}{2\pi^2}\sqrt{\frac{\pi}{2q}}\frac{P_0}{q}\frac{\Gamma\left(\frac{3}{4}+\frac{n_s}{2}-\frac{1}{4}\right)2^{n_s-3/2}}{\Gamma\left(\frac{3}{4}-\frac{n_s}{2}+\frac{1}{4}+1\right)}q^{-n_s+1/2}
$$

$$
-\frac{1}{2\pi^2}\sqrt{\frac{\pi}{2q}}\frac{P_1}{q}\frac{\Gamma\left(\frac{3}{4}+\frac{n_s}{2}+\frac{1}{4}\right)2^{n_s-1/2}}{\Gamma\left(\frac{3}{4}-\frac{n_s}{2}-\frac{1}{4}+1\right)}q^{-n_s-1/2}
$$

$$
-\frac{1}{2\pi^2}\sqrt{\frac{\pi}{2q}}\frac{P_2}{q}\frac{\Gamma\left(\frac{3}{4}+\frac{n_s}{2}+\frac{3}{4}\right)2^{n_s+1/2}}{\Gamma\left(\frac{3}{4}-\frac{n_s}{2}-\frac{3}{4}+1\right)}q^{-n_s-3/2}
$$

$$
+ E_{3,1}(q) \tag{5.54}
$$

$$
= -\frac{P_0}{2\pi^2}\frac{\sqrt{\pi}}{2^{2-n_s}}\frac{\Gamma\left(\frac{1}{2}+\frac{n_s}{2}\right)}{\Gamma\left(2-\frac{n_s}{2}\right)}q^{-n_s-1}
$$

$$
-\frac{P_1}{2\pi^2}\frac{\sqrt{\pi}}{2^{1-n_s}}\frac{\Gamma\left(1+\frac{n_s}{2}\right)}{\Gamma\left(\frac{3}{2}-\frac{n_s}{2}\right)}q^{-n_s-2}
$$

$$
-\frac{P_2}{2\pi^2}\frac{\sqrt{\pi}}{2^{-n_s}}\frac{\Gamma\left(\frac{3}{2}+\frac{n_s}{2}\right)}{\Gamma\left(1-\frac{n_s}{2}\right)}q^{-n_s-3}
$$

$$
+ E_{3,1}(q) \ .
$$

This expansion is an asymptotic expansion for $\frac{1}{2}<n_s<\frac{3}{2}$ with $E_{3,1}(q)\leq O(q^{-4.5})$, because $m=3$ and $\lambda_2 = n_s+3/2$ in Theorem 5.3. Equivalently, we arrive for a_2 at the asymptotics

$$
a_2(q) = \frac{1}{2\pi^2}\sqrt{\frac{\pi}{2q}}P_0\frac{\Gamma\left(\frac{5}{4}+\frac{n_s}{2}+\frac{1}{4}\right)2^{n_s-1/2}}{\Gamma\left(\frac{5}{4}-\frac{n_s}{2}-\frac{1}{4}+1\right)}q^{-n_s-1/2}
$$

$$
+\frac{1}{2\pi^2}\sqrt{\frac{\pi}{2q}}P_1\frac{\Gamma\left(\frac{5}{4}+\frac{n_s}{2}+\frac{3}{4}\right)2^{n_s-3/2}}{\Gamma\left(\frac{5}{4}-\frac{n_s}{2}-\frac{3}{4}+1\right)}q^{-n_s-3/2}
$$

$$
+ E_{2,2}(q) \tag{5.55}
$$

$$
= \frac{P_0}{2\pi^2}\frac{\sqrt{\pi}}{2^{1-n_s}}\frac{\Gamma\left(\frac{3}{2}+\frac{n_s}{2}\right)}{\Gamma\left(2-\frac{n_s}{2}\right)}q^{-n_s-1}
$$

$$
+\frac{P_1}{2\pi^2}\frac{\sqrt{\pi}}{2^{-n_s}}\frac{\Gamma\left(2+\frac{n_s}{2}\right)}{\Gamma\left(\frac{3}{2}-\frac{n_s}{2}\right)}q^{-n_s-2}
$$

$$
+ E_{2,2}(q).
$$

For $n_s\approx 1$, these expressions for the asymptotics become

$$
a_1(q) = -\frac{P_0}{2\pi^2}q^{-2} - \frac{\pi}{2}\frac{P_1}{2\pi^2}q^{-3} - 2\frac{P_2}{2\pi^2}q^{-4} + O(q^{-4.5}) \ , \tag{5.56}
$$

$$
a_2(q) = 2\frac{P_0}{2\pi^2}q^{-2} + \frac{3\pi}{2}\frac{P_1}{2\pi^2}q^{-3} + O(q^{-3.5}) \ . \tag{5.57}
$$

In Figure 5.1, we show the functions $-a_1$ (purple solid), a_2 (green solid) and $\frac{\sigma_1^2}{3} + a_1$ (blue solid) together with the corresponding first-order asymptotics (dashed lines) for small and large scales, derived from an initial cold dark matter power spectrum from [4] with smoothing at large scales ($k_s = 10$ Mpc^{-1}h, left) and small scales ($k_s = 1000$ Mpc^{-1}h, right). The asymptotics coincides in all cases excellently with the limiting behavior of the functions. Note that for the smaller smoothing wave number (left picture), the amplitudes of $\frac{\sigma_1^2}{3} + a_1(q)$ and $a_2(q)$ for small values of q is smaller than in the right picture, while the large-scale behavior is the same. Furthermore, the small-scale asymptotics in the left picture is valid for a wider range of q. This reflects the larger convergence radius k_s^{-1} of the asymptotic series compared to the right picture.
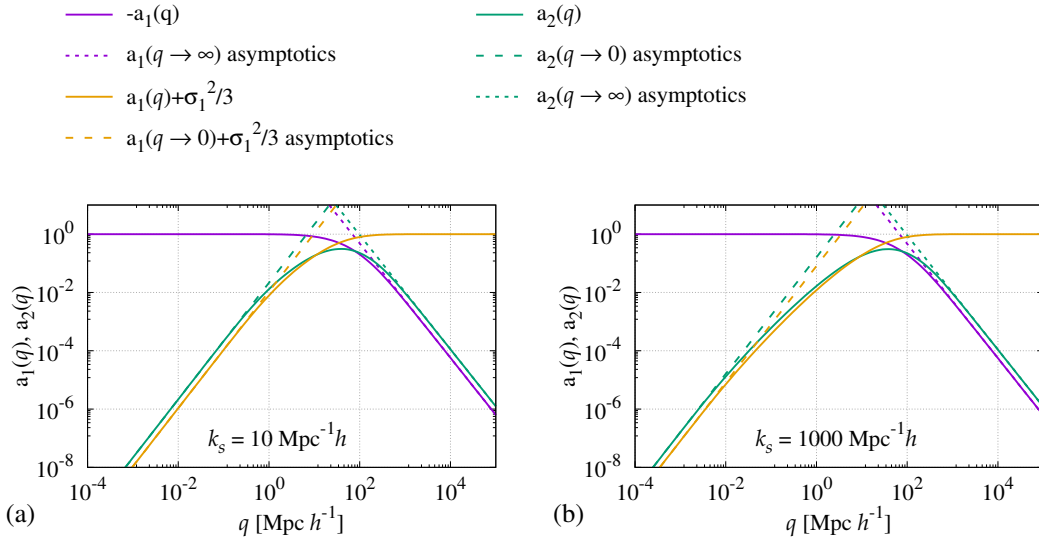
Figure 5.1: The functions $-a_1(q)$ (purple lines), $\frac{\sigma_1^2}{3} + a_1(q)$ (golden lines), and $a_2(q)$ (green lines) normalized to $\frac{\sigma_1^2}{3} = -a_1(0)$ for the CDM power spectrum from [4], with $n_s = 0.96$ and two different smoothing scales. Dashed lines show the asymptotics q^2 for small scales (5.29) and (5.30), and the q^{-n_s-1} asymptotics for large scales (5.54) and (5.55). The cosmological parameters used are shown in Table E.1.

5.4 AN ANALYTICAL TEST CASE

In some special cases, the initial correlation matrices can be computed analytically. Such analytical expressions are helpful in gaining a qualitative understanding of the initial correlations. Furthermore, they are very useful in testing numerical algorithms, as numerical uncertainties are minimized compared to fit functions or data.

In this section, we consider initial power spectra

$$P_\delta^{(i)}(k) = A\, k\, e^{-k/k_s}\, , \tag{5.58}$$

that correspond to an analytically tractable test case with $n_s = 1$ and an exponential cutoff. Recall that the initial power spectra of the velocity potential and of the density correlations are given by

$$k^4 P_\psi(k) = P_\delta^{(i)}(k) \,, \tag{5.59}$$

where $A > 0$ is an amplitude and $k_s > 0$ a fixed smoothing scale.

For the initial density correlations, we plug (5.58) in (5.1). Carrying out the integral, we arrive at

$$
\begin{aligned}
C_{\delta\delta}(q) &= \frac{A}{2\pi^2} \int_0^\infty \mathrm{d}k\, k^3 \mathrm{e}^{-k/k_s} \frac{\sin(kq)}{kq} \\
&= \frac{A}{\pi^2} \frac{\frac{3}{k_s^2} - q^2}{\left(\frac{1}{k_s^2} + q^2\right)^3} \,.
\end{aligned}
\tag{5.60}
$$

Similarly, we compute the initial momentum-density correlations (5.2),

$$
\begin{aligned}
\vec{C}_{\delta p}(q) &= \frac{A}{2\pi^2} \vec{\nabla}_q \int_0^\infty \mathrm{d}k\, k \mathrm{e}^{-k/k_s} \frac{\sin(kq)}{kq} \\
&= \frac{A}{2\pi^2} \vec{\nabla}_q \frac{1}{\frac{1}{k_s^2} + q^2} \\
&= -\vec{q}\, \frac{A}{\pi^2} \frac{1}{\left(\frac{1}{k_s^2} + q^2\right)^2} \,.
\end{aligned}
\tag{5.61}
$$

In order to obtain $\hat{C}_{pp}$, we first compute a_1 by plugging (5.58) into (5.10),

$$
\begin{aligned}
a_1(q) &= -\frac{A}{2\pi^2} \frac{1}{q} \int_0^\infty \mathrm{d}k\, \mathrm{e}^{-k/k_s} j_1(kq) \\
&= -\frac{A}{2\pi^2} \frac{1}{q} \int_0^\infty \mathrm{d}k\, \mathrm{e}^{-k/k_s} \left(\frac{\sin(kq)}{(kq)^2} - \frac{\cos(kq)}{kq} \right) \\
&= -\frac{A}{2\pi^2} \frac{1}{q^2} \left[\int_0^\infty \mathrm{d}x\, \mathrm{e}^{-x/(qk_s)} \left(\frac{\sin(x)}{x^2} - \frac{1}{x} \right) + \int_0^\infty \mathrm{d}x\, \mathrm{e}^{-x/(qk_s)} \left(\frac{1}{x} - \frac{\cos(x)}{x} \right) \right] \,.
\end{aligned}
\tag{5.62}
$$

We performed the last step in order to apply the following integral solutions from [36],

$$\int_0^\infty \mathrm{d}x\, \mathrm{e}^{-x/t} \left(\frac{\sin(x)}{x^2} - \frac{1}{x} \right) = -\frac{1}{2} \ln\left(1 + t^2\right) - \frac{\arctan(t)}{t} + 1 \,, \tag{5.63}$$

$$\int_0^\infty \mathrm{d}x\, \mathrm{e}^{-x/t} \left(\frac{1}{x} - \frac{\cos(x)}{x} \right) = \frac{1}{2} \ln\left(1 + t^2\right) \,. \tag{5.64}$$

Using these relations, we arrive at

$$a_1(q) = \frac{A}{2\pi^2} \frac{1}{q^2} \left(\frac{\arctan(k_s q)}{k_s q} - 1 \right) \,, \tag{5.65}$$

and, with $a_2(q) = qa_1'(q)$,

$$a_2(q) = \frac{A}{2\pi^2}\left[\frac{3}{q^2}\left(1 - \frac{\arctan(k_sq)}{k_sq}\right) - \frac{k_s^2}{1 + k_s^2q^2}\right] . \tag{5.66}$$

In Figure 5.2 we show an example of these functions for $A = 2\pi^2$ and $k_s = 1$ Mpc^{-1}h. Qualitatively, they behave similar to the CDM functions shown in Figure 5.1, which makes them excellent test functions for numerical routines.
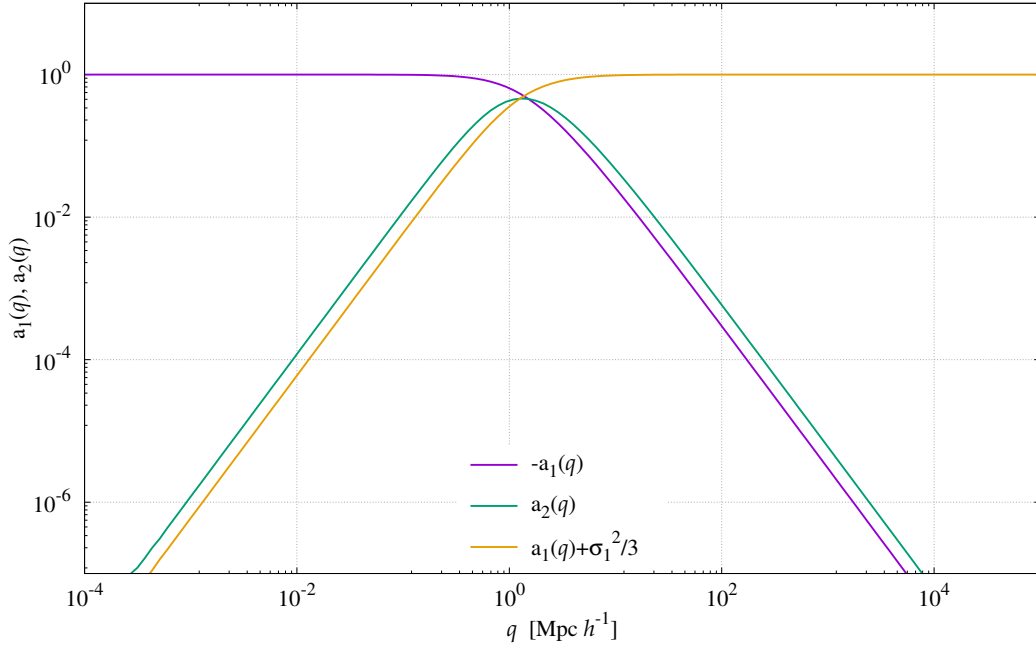
Figure 5.2: The functions $-a_1(q)$ (purple line) from (5.65), $\frac{\sigma_1^2}{3} + a_1(q)$ (golden line), and $a_2(q)$ (green line) from (5.66) normalized to $\frac{\sigma_1^2}{3} = -a_1(0)$ for the analytically tractable power spectrum $P_\delta^{(i)}(k) = k\,e^{-k/k_s}$. These functions behave qualitatively very similar to the CDM functions, shown in Figure 5.1. The parameters used are shown in Table E.1.

Finally, we compute the asymptotic series for small and large q, respectively. We first note the series expansion for the inverse tangent, for real arguments,

$$\arctan(x) = \begin{cases} \displaystyle\sum_{n=0}^{\infty}\frac{(-1)^n x^{1+2n}}{1+2n} & \text{for } |x| < 1 , \\[2ex] \pm\dfrac{\pi}{4} & \text{for } x = \pm 1 , \\[2ex] \dfrac{\pi}{2} - \displaystyle\sum_{n=0}^{\infty}\frac{(-1)^n x^{-1-2n}}{1+2n} & \text{for } |x| > 1 . \end{cases} \tag{5.67}$$

For a_1 we thus arrive at the series expression

$$
a_1(q) = -\frac{Ak_s^2}{2\pi}
\begin{cases}
\displaystyle\sum_{n=0}^{\infty} \frac{(-1)^n}{2n+3}(k_s q)^{2n} & \text{for } |k_s q| < 1 \,, \\[3ex]
\displaystyle 1 \mp \frac{\pi}{4} & \text{for } k_s q = \pm 1 \,, \\[3ex]
\displaystyle \frac{1}{(k_s q)^2} - \frac{\pi}{2}\frac{1}{(k_s q)^3} + \frac{1}{(k_s q)^4}\sum_{n=0}^{\infty}\frac{(-1)^n}{1+2n}(k_s q)^{-2n} & \text{for } |k_s q| > 1 \,.
\end{cases}
\tag{5.68}
$$

Comparing the series for small scales to our results (5.29) for the asymptotics as $q \to 0$, the expansion coefficients are given by

$$
a_n = -\frac{Ak_s^2}{2\pi^2}\frac{(-1)^n k_s^{2n}}{2n+3} \,.
\tag{5.69}
$$

Identifying this with (5.28), we can read off the moments of the initial velocity potential power spectrum,

$$
\sigma_{n+1}^2 = \frac{A}{2\pi^2}k_s^{2n+2}(2n+1)! \,.
\tag{5.70}
$$

Note that (5.68) implies that the convergence radius of the small q power series expansion is set by the smoothing scale k_s^{-1}. Furthermore, let us note that the ratio of two successive moments of the initial velocity potential power spectrum is quadratic in the smoothing wave number

$$
\frac{\sigma_{n+1}^2}{\sigma_n^2} = k_s^2 2n(2n+1) \,.
\tag{5.71}
$$

This property will be relevant for our analysis of the free power spectrum in the next chapter.

5.5 SUMMARY AND DISCUSSION

In this chapter, we derived the asymptotic expansions of the initial density-density $C_{\delta\delta}$, density-momentum $\vec{C}_{\delta p}$ and momentum-momentum $\hat{C}_{pp}$ correlation functions of the cosmic fluid. In the first section, we derived the asymptotic series for small scales. These are power series of even powers of q, where the series coefficients depend on the moments σ_n^2 of the initial velocity potential power spectrum. These expansions are valid for a broad class of initial density perturbation power spectra, provided the σ_n^2 exist. To this end, we introduced an exponential cutoff in the initial power spectrum with smoothing scale k_s in Fourier space. Depending on the nature of dark matter, this cutoff may be physical. In particle models of dark matter, k_s is related to the dark matter particle mass m_X and therefore – for thermally produced dark matter – to their temperature. In the next chapter, when we derive the asymptotics of the free power spectrum at small scales, the physical relevance of this cutoff scale for cosmic structure formation becomes clear, because σ_2^2 determines the mass and time scale of stream crossing.

In general, it is also possible to derive an asymptotic series for the initial correlation functions from power spectra with power law tails. Such an expansion contains either logarithmic terms, when the power law tail is an integer, or otherwise consists of a sum of more than one power series [68]. This case will be studied in later work.

In the second section, we derived the asymptotics of the momentum correlation function $\hat{C}_{pp}$ for large scales. The lowest-order terms for $a_1(q)$ and $a_2(q)$ are both proportional to q^{-1-n_s}. This large-scale behavior is important when implementing numerical codes for the evaluation of correlation functions in KFT, since it determines the convergence rate of the integrals. Since we consider only initial momentum-momentum correlations in this work, we restricted our analysis of the large-scale limit to $\hat{C}_{pp}$. In practice, both the asymptotics for large scales as well as the asymptotics for small scales turned out to be highly relevant for the numerical evaluation of density correlation functions in KFT. In the next two chapters, we demonstrate the relevance of the small-scale asymptotics for numerical implementations of the correlation functions.

In the last section, we derived the analytic solutions to the initial correlation functions for a type of hot dark matter. These behave qualitatively similar to the correlation functions for smoothed CDM. Therefore, these analytical expressions can be used to test numerical integration routines with asymptotically safe functions.

SMALL-SCALE ASYMPTOTICS OF THE FREE POWER SPECTRUM

In this chapter, we study the small-scale properties of the free power spectrum in KFT,

$$\mathcal{P}(k,t) = e^{-\frac{\sigma_1^2}{3}k^2 g_{qp}^2(t,0)} \int d^3q \; \left(e^{g_{qp}^2(t,0)\vec{k}^\intercal \hat{C}_{pp}(\vec{q})\vec{k}} - 1 \right) e^{i\vec{k}\cdot\vec{q}} \;, \tag{6.1}$$

with the initial momentum-momentum correlation matrix

$$
\begin{aligned}
\hat{C}_{pp}(\vec{q}) &= \int_k \left(\vec{k} \otimes \vec{k} \right) P_\psi^{(i)}(k) e^{i\vec{k}\cdot\vec{q}} \\
&= -\frac{\vec{q}\otimes\vec{q}}{q^2} a_2(q) - \mathbb{I}_3 a_1(q) \;.
\end{aligned}
\tag{6.2}
$$

Equation (6.1) was derived by assuming (i) straight particle trajectories, (ii) a curl-free initial velocity field with a velocity potential ψ, (iii) an initial Gaussian random field, and (iv) considering only the initial momentum-momentum correlations. The free power spectrum in KFT is equivalent to the non-linear Zel'dovich power spectrum when we choose the Zel'dovich propagator $g_{qp}^Z(t,0) = D_+(t) - D_+(t^{(i)})$. It is also the unperturbed zeroth-order power spectrum in KFT, thus the starting point to calculate the non-linear power spectrum from KFT perturbation theory or mean-field approaches, when no further initial correlations are considered. As in the previous chapter on the initial correlation functions, we consider smoothed initial power spectra (5.4).

This chapter consists of three parts. In the first part, we present our technical results. Our main result is the derivation of the first-order asymptotics $\mathcal{P} \sim k^{-3}$ for $k \to \infty$ where the exponent is independent of the initial steepness of the power spectrum. Furthermore, we derive the expressions for the coefficients of the whole asymptotic series of the free power spectrum and of the time-evolved free density-density correlation function $\xi_{\delta\delta}(k,t)$ in real space. In the second part, we discuss the implications for cosmic structure formation in view of the numerically observed universal halo density profiles, the time evolution of small-scale perturbations and the implications for the interpretation of the exponential damping prefactor in (6.1). Furthermore, we derive the characteristic redshift-, length- and mass scales when stream crossing at small scales occurs and show how these scales depend on the smoothing of the initial dark matter spectrum and the values of the cosmological parameters. In the final part, we summarize and discuss the conclusions that can be drawn from these results.

6.1 DERIVATION OF THE SMALL-SCALE ASYMPTOTICS

In this section, we first derive the first-order asymptotics by applying our Theorem 4.4 for N-dimensional Fourier-Laplace type integrals. We then derive an expression of the whole asymptotic series by applying our Theorem 4.2 to the one-dimensional integral of the radial coordinate. Finally, we derive an expression for the asymptotics of the time-evolved free density correlation function $\xi_{\delta\delta}$ in real space.

6.1.1 *First-order Asymptotics*

We start by aligning the wave vector $\vec{k}$ with the z-axis and denote the cosine of the angle enclosed by $\vec{k}$ and $\vec{q}$ by

$$\mu := \frac{\vec{k} \cdot \vec{q}}{kq} \,. \tag{6.3}$$

Next, we denote the function appearing in the exponential of the integration kernel (6.1) by

$$
\begin{aligned}
f_\mu(\vec{q}) &:= g_{qp}^2(t,0) \left[\mu^2 a_2(q) + a_1(q) \right] \\
&= -g_{qp}^2(t,0) \int_{k'} k_z'^2 P_\psi(k') e^{i\vec{k}' \cdot \vec{q}} \,,
\end{aligned}
\tag{6.4}
$$

such that we can write the free power spectrum as

$$\mathcal{P}(k,t) = e^{-\frac{\sigma_1^2}{3} k^2 g_{qp}^2(t,0)} \int \mathrm{d}^3 q \left(e^{-k^2 f_\mu(\vec{q})} - 1 \right) e^{i\vec{k} \cdot \vec{q}} \,. \tag{6.5}$$

We apply our Theorems 4.4 and 4.5 to compute the asymptotics of this expression in the limit $k \to \infty$. In order to apply these theorems, we first have to show that

1. $|f_\mu|$ and $-f_\mu$ both have an isolated global maximum at $\vec{q} = 0$;

2. f_μ is quadratically integrable in $\mathbb{R}^3$; and

3. the Hessian matrix A of f_μ at the origin exists and is positive definite.

Then, Theorem 4.5 allows us to drop the 1 in the integration kernel and to apply Theorem 4.4, yielding the asymptotics

$$\mathcal{P}(k,t) \sim e^{-\frac{\sigma_1^2}{3} k^2 g_{qp}^2(t,0) - k^2 f_\mu(0)} \sqrt{\frac{(2\pi)^3}{k^6 \det A}} \exp \left(-\frac{1}{2} A_{zz}^{-1} \right) \,, \quad \text{as } k \to \infty \,, \tag{6.6}$$

where A_{zz}^{-1} is the zz-component of the inverse of the Hessian A.

Requirement 1 is satisfied, because f_μ has an isolated global minimum at the origin,

$$
\begin{aligned}
|f_\mu(\vec{q})| &\leq g_{qp}^2(t,0) \int_{k'} \left| k_z'^2 P_\psi(k') e^{i\vec{k}' \cdot \vec{q}} \right| \\
&\leq g_{qp}^2(t,0) \int_{k'} k_z'^2 P_\psi(k') \\
&= g_{qp}^2(t,0) \frac{\sigma_1^2}{3} \\
&= -f_\mu(0) \,,
\end{aligned}
\tag{6.7}
$$

and $|f_\mu(\vec{q})| = -f_\mu(0)$ if and only if $q = 0$ because $P_\psi(k') \geq 0 \; \forall k' \in \mathbb{R}^3$.

In order to prove requirement 2, it is sufficient to show that there exist constants $C > 0$ and $\epsilon > 0$ such that

$$|f_\mu(\vec{q})| \leq C \left(1 + q \right)^{-3/2 - \epsilon} \,, \quad \forall \vec{q} \in \mathbb{R}^3 \,. \tag{6.8}$$

In (5.56) and (5.57), we have shown that there are $A, B > 0$ such that

$$a_2(q) \sim \frac{A}{q^{n_s+1}} \quad \text{and} \quad a_1(q) \sim -\frac{B}{q^{n_s+1}} \,, \quad \text{as } q \to \infty \,. \tag{6.9}$$

Furthermore, f_μ is bounded, which proves that f_μ is quadratically integrable in $\mathbb{R}^3$ for $n_s > 1/2$.

We now compute the Hessian A at the origin,

$$\begin{aligned}
A = \left. \frac{\partial^2 f(q)}{\partial q_i \partial q_j} \right|_{q=0} &= g_{qp}^2(t,0) \int_{k'} k_z'^2 k_i' k_j' P_\psi(k') e^{i\vec{k}'\cdot\vec{q}} \bigg|_{q=0} \\
&= g_{qp}^2(t,0) \int_{k'} k_z'^2 k_i' k_j' P_\psi(k') \\
&= g_{qp}^2(t,0) \frac{\sigma_2^2}{15} \left(\delta_{ij} + 2\delta_{iz}\delta_{jz} \right) \,,
\end{aligned} \tag{6.10}$$

where we used the definition of the moments σ_n^2 (5.5) of the initial velocity potential power spectrum and

$$\int_{k'} k_z'^4 P_\psi(k) = \frac{1}{4\pi^2} \int_{-1}^{1} d\mu \, \mu^4 \int_0^\infty dk \, k^2 P_\delta^{(i)}(k) = \frac{1}{5}\sigma_2^2 \,, \tag{6.11}$$

$$\int_{k'} k_z'^2 k_{x/y}'^2 P_\psi(k) = \frac{1}{8\pi^2} \int_{-1}^{1} d\mu \, \mu^2(1-\mu^2) \int_0^\infty dk \, k^2 P_\delta^{(i)}(k) = \frac{1}{15}\sigma_2^2 \,. \tag{6.12}$$

Since A is diagonal with only positive entries, A is positive definite and has the determinant

$$\det A = 3 \left(\frac{g_{qp}^2(t,0)\sigma_2^2}{15} \right)^3 > 0 \quad \forall g_{qp}^2(t,0) \neq 0 \,, \tag{6.13}$$

which proves the last requirement 3. The inverse of A is

$$A^{-1} = \frac{15}{g_{qp}^2(t,0)\sigma_2^2} \left[\delta_{ij} - \frac{2}{3}\delta_{iz}\delta_{jz} \right] \,. \tag{6.14}$$

We denote the linearly evolved second moment of the initial velocity potential field by

$$\tau_2^2(t) := g_{qp}^2(t,0)\sigma_2^2 \,, \tag{6.15}$$

and plug our results for $f(0)$ from (6.7), $\det A$ from (6.13) and A^{-1} from (6.14) into (6.6), arriving at the asymptotics

$$\mathcal{P}(k,t) \sim \frac{3(4\pi)^{3/2}}{k^3} \left(\frac{5}{2\tau_2^2(t)} \right)^{3/2} \exp\left(-\frac{5}{2\tau_2^2(t)} \right) \,, \tag{6.16}$$

as $k \to \infty$. This result proves that the free power spectrum always asymptotically falls off like k^{-3}. This result is remarkably independent on the slope of the initial power spectrum. The only condition is the existence of a finite value for the moment σ_2^2.

6.1.2   *Full Asymptotic Series*

Since our method for Fourier-Laplace type integrals in N dimensions, just as the standard Laplace method in N-dimensions, does not provide a straight-forward way to calculate the terms of the asymptotic series beyond the first term, we make use of another strategy. As shown in [31], asymptotic series expansions for N-dimensional Laplace integrals can be obtained without any smoothness conditions on the involved functions, as long as their asymptotic expansions near the critical minimum exist. Then, the complete expansion series is obtained by first transforming the integrand to spherical coordinates. Afterwards, the one-dimensional Laplace method is applied to the integral over the radial coordinate. Finally, the integration over the angles for each term in the asymptotic expansion has to be performed.

We make use of the same strategy to obtain an asymptotic series for $\mathcal{P}$. First, we transform to spherical coordinates and apply Theorem 4.2 for Laplace-Fourier type integrals in one dimension to the q integral. This yields an asymptotic series for which the integral over $\mu = \cos\theta$ can be performed term-wise.

We introduce radial coordinates (q, ϕ, μ), where $\vec{k} \neq 0$ is aligned with the z-axis. Since the integration kernel is independent of the angle ϕ, we perform this integral immediately and arrive at

$$\mathcal{P}(k,t) \sim 2\pi e^{-\frac{\sigma_1^2}{3} k^2 g_{qp}^2(t,0)} \int_{-1}^{1} d\mu \int_{0}^{Q} dq\, q^2 e^{-k^2 f_\mu(q)} e^{ikq\mu} \,, \tag{6.17}$$

as $k \to \infty$, where we applied our Theorem 4.5 to drop the 1 in the kernel, and $Q > 0$ is arbitrary. We now define

$$I_\mu(k^2, k\mu) := \int_{0}^{Q} dq\, q^2 e^{-k^2 f_\mu(q)} e^{ikq\mu} \,, \tag{6.18}$$

in close analogy to (4.35), where we replaced $k \to k\mu$ and $\lambda \to k^2$. Note that the meaning of f_μ changed compared to (6.4) in the last section. In the present context, we consider $\mu \in [-1, 1]$ as a fixed parameter such that $f_\mu(q) : \mathbb{R}^+ \to D \subset \mathbb{R}$. We apply the intermediate result (4.45), with $s = 2$, $\alpha = 2$ and $\beta = 3$, and obtain the asymptotic expansion

$$I_\mu(k^2, k\mu) \sim \frac{e^{-k^2 f_\mu(0)}}{2a_0^{3/2}(\mu) k^3} \left[\sum_{m=0}^{M-1} \frac{I_m(\mu)}{k^{2m}} + \varphi_M(k^2, k\mu) \right], \tag{6.19}$$

as $k \to \infty$, with the functions $_m$ from (4.37),

$$I_m(\mu) := k^{2m} I_{2m}(k^2, k\mu)$$
$$= \frac{-e^{\frac{i}{2}\pi m}}{\mu^m} \sum_{n=m}^{\infty} \Gamma\left(\frac{n+3}{2}\right) \left(\frac{\mu}{\sqrt{a_0(\mu)}}\right)^n \frac{e^{\frac{i}{2}\pi n} d_{m,n}(\mu)}{m!(n-m)!} \,. \tag{6.20}$$

The coefficients $d_{m,n}(\mu)$ are given in (4.27),

$$d_{m,n}(\mu) = \lim_{x \to 0^+} \frac{d^m}{dx^m} \left(1 + \sum_{j=1}^{\infty} \frac{a_j(\mu)}{a_0(\mu)} x^j\right)^{-\frac{n+3}{2}} . \tag{6.21}$$

Using the asymptotic expansions of the functions $a_1(q)$ and $a_2(q)$, f_μ acquires an asymptotic expansion of the form

$$f_\mu(q) \sim f_\mu(0) + \sum_{m=0}^{\infty} a_m(\mu) q^{2+m}, \quad \text{as } q \to 0^+, \tag{6.22}$$

where the coefficients $a_m(\mu)$ vanish for odd indices m, and

$$f_\mu(0) = -\frac{\sigma_1^2}{3} g_{qp}^2(t,0) = -\frac{\tau_1^2(t)}{3}. \tag{6.23}$$

Combining (6.17)–(6.19) yields the asymptotic series

$$\mathcal{P}(k,t) \sim \sum_{m=0}^{M-1} \mathcal{P}^{(m)}(t) k^{-2m-3}, \tag{6.24}$$

with the time-dependent coefficients

$$\mathcal{P}^{(m)}(t) := 8 \cdot 3^{3/2} \pi \left(\frac{5}{2\tau_2^2(t)}\right)^{3/2} \int_{-1}^{1} d\mu \, \frac{I_m(\mu)}{(2\mu^2+1)^{3/2}}. \tag{6.25}$$

In order to demonstrate that this procedure yields the correct result, we re-derive the result for the first-order asymptotics,

$$\mathcal{P}^{(0)}(t) = 3(4\pi)^{3/2} \left(\frac{5}{2\tau_2^2(t)}\right)^{3/2} \exp\left(-\frac{5}{2\tau_2^2(t)}\right), \tag{6.26}$$

which is equal to (6.16). For the second coefficient in the asymptotic series, we arrive at

$$\mathcal{P}^{(1)}(t) = \frac{2\pi^{3/2}}{7} \frac{\sigma_3^2}{\sigma_2^2} \left(\frac{5}{2\tau_2^2(t)}\right)^{5/2} \exp\left(-\frac{5}{2\tau_2^2(t)}\right) \times \\ \left[123 - 132 \left(\frac{5}{2\tau_2^2(t)}\right) + 20 \left(\frac{5}{2\tau_2^2(t)}\right)^2\right]. \tag{6.27}$$

The derivation of expressions (6.26) and (6.27) is shown in Appendix C.1.

6.1.3 *Asymptotics in Real Space*

We now have closer look at the small-scale behavior of the time-evolved free density correlation function $\xi_{\delta\delta}$ in real space. The free density fluctuation correlation function is related to the free power spectrum (6.1) by a Fourier transform,

$$\xi_{\delta\delta}(q) = \frac{1}{2\pi^2} \int_0^\infty dk \, \mathcal{P}(k) k^2 \frac{\sin(kq)}{kq} \\ = \frac{(iq)^{-1}}{4\pi^2} \int_0^\infty dk \, \mathcal{P}(k) k \left(e^{ikq} - e^{-ikq}\right). \tag{6.28}$$

Note that for better readability, we drop the time-dependence of $\xi_{\delta\delta}$ and $\mathcal{P}$ here and in the following.

In order to derive the asymptotics for small scales, we apply the method to calculate the asymptotic expansion of the Fourier transform near the origin as presented in [68]. This method makes use of the Mellin transform, which is defined in [68] as follows.

Definition 6.1 (Mellin Transform). *The Mellin transform of a locally integrable function f on $(0, \infty)$ is defined by*

$$M[f;s] = \int_0^\infty t^{s-1} f(t) dt ,$$ (6.29)

when the integral converges.

Let us now consider the one-sided Fourier transform of a suitable function f

$$F_f(x) = \int_0^\infty f(t) e^{ixt} dt .$$ (6.30)

An asymptotic expansion of F_f at the origin can be obtained by the following theorem that we took from [68] and slightly adapted in its formulation. For a proof of this theorem, we refer to the same reference.

Theorem 6.1. *Let f be a locally integrable function on $[0, \infty)$ with an asymptotic expansion*

$$f(t) \sim \sum_{s=0}^\infty a_s t^{-s-\alpha} , \quad \text{as } t \to \infty ,$$ (6.31)

where $0 < \alpha \leq 1$.
(i) If $0 < \alpha < 1$, then

$$F_f(x) = e^{-\alpha\pi i/2} \sum_{s=0}^{n-1} (-i)^{s-1} \Gamma(1-s-\alpha) a_s x^{\alpha+s-1} - \sum_{s=1}^{n} c_s (-ix)^{s-1} + R_n(x) ,$$ (6.32)

where the coefficients c_s are given by (6.36).
(ii) If $\alpha = 1$, then

$$F_f(x) = -\log x \sum_{s=0}^{n-1} \frac{a_s}{s!} (ix)^s + \sum_{s=0}^{n-1} \gamma_s^* (-ix)^s + R_n(x) ,$$ (6.33)

where

$$\gamma_s^* = \frac{(-1)^{s+1}}{s!} \left(\gamma - i\frac{\pi}{2} \right) a_s - d_{s+1} ,$$ (6.34)

and the coefficients d_{s+1} are given by (6.37) and $\gamma \approx 0.5772$ denotes the Euler-Mascheroni constant. The remainder in both cases satisfies

$$R_n(x) = (-ix)^n \int_0^\infty f_{n,n}(t) e^{ixt} dt ,$$ (6.35)

with $f_{n,n}(t)$ being defined in (6.39).

The c_s coefficients are given by

$$c_s = \frac{(-1)^s}{(s-1)!} M[f;s] ,$$ (6.36)

where $M[f;s]$ is the Mellin transform of f, or its analytic continuation. The d_s coefficients are given by

$$d_{s+1} = \frac{(-1)^{s+1}}{s!} a_s \sum_{k=1}^{s} \frac{1}{k} - \frac{(-1)^s}{s!} a_s^* ,$$ (6.37)

and a_s^* denotes the value of the limit

$$a_s^* := \lim_{z \to s+1} \left(M\left[f;z\right] + \frac{a_s}{z-s-1} \right) . \tag{6.38}$$

The function $f_{n,n}$ is defined by

$$f_{n,n}(t) := \frac{(-1)^n}{(n-1)!} \int_t^\infty (\tau-t)^{n-1} f_n(\tau) d\tau , \tag{6.39}$$

with

$$f_n(t) = f(t) - \sum_{s=0}^{n-1} a_s t^{-s-\alpha} . \tag{6.40}$$

We start by expressing $\xi_{\delta\delta}$ as the linear combination

$$\xi_{\delta\delta}(q) = \frac{(iq)^{-1}}{4\pi^2} \left[\xi_+(q) - \xi_-(q) \right] \tag{6.41}$$

of the two functions

$$\xi_+(q) := \int_0^\infty dk\, \mathcal{P}(k) k e^{ikq} , \tag{6.42}$$

$$\xi_-(q) := \xi_+(-q) . \tag{6.43}$$

Since $k\mathcal{P}$ is absolutely integrable in $\mathbb{R}$, the one-dimensional Fourier transform exists and the functions ξ_+ and ξ_- are well defined.

Next, we apply Theorem 6.1 to derive the terms of the asymptotic series of (6.42) and (6.43). The terms in the expansion of $\xi_{\delta\delta}$ then follow from the sum of ξ_+ and ξ_-. In the last chapter, we derived the asymptotics (6.24) of $\mathcal{P}$ for large wave numbers. Thus, the kernel $k\mathcal{P}(k)$ in (6.42) has the asymptotics

$$k\mathcal{P}(k) \sim \sum_m^{M-1} \mathcal{P}^{(m)} k^{-2+2m} , \quad \text{as } k \to \infty , \tag{6.44}$$

with the coefficients $\mathcal{P}^{(m)}$ given by (6.25). Comparing (6.44) to (6.31) implies to use $\alpha = 1$ and

$$a_s = \begin{cases} 0 & s \text{ even} , \\ \mathcal{P}^{(\frac{s-1}{2})} & s \text{ odd} , \end{cases} \tag{6.45}$$

in Theorem 6.1. With (6.41)–(6.45) and the coefficients (6.25), the asymptotic expansion of $\xi_{\delta\delta}$ for $q \to 0$ is completely determined. We now compute the first term in this expansion, for which we need the first coefficient (6.26). For the first term in the expansion (6.33) of ξ_+ we arrive at

$$\xi_+(q) = \int_0^\infty dk\, k\mathcal{P}(k) e^{ikq} \sim (iq) \left[-\mathcal{P}^{(0)} \log q - \gamma_1^* \right] , \tag{6.46}$$

as $q \to 0^+$. The coefficient γ^* is given by

$$\gamma_1^* = \left(\gamma - i\frac{\pi}{2} - 1 \right) \mathcal{P}^{(0)} - a_1^* , \tag{6.47}$$

with

$$a_1^* = \lim_{z \to 2} \left(M\left[\mathcal{P}(k)k; z\right] + \frac{\mathcal{P}^{(0)}}{z-2} \right) . \tag{6.48}$$

We calculate the first ξ_- term analogously and arrive at

$$\begin{aligned}
\xi_-(q) &= \int_0^\infty \mathrm{d}k \, k\mathcal{P}(k)\mathrm{e}^{-ikq} \sim (-iq)\left[-\mathcal{P}^{(0)}\log(-q) - \gamma_1^*\right] \\
&= -(iq)\left[-\mathcal{P}^{(0)}\left(\log q + i\pi\right) - \gamma_1^*\right] ,
\end{aligned} \tag{6.49}$$

as $q \to 0^+$. Subtracting (6.42) and (6.41) yields

$$\int_0^\infty \mathrm{d}k \, k\mathcal{P}(k)\left(\mathrm{e}^{ikq} - \mathrm{e}^{-ikq}\right) \sim -2iq\mathcal{P}^{(0)}\left[\log q + \gamma - 1\right] + 2iqa_1^* \tag{6.50}$$

and we finally arrive at the first-order asymptotics

$$\xi_{\delta\delta}(q,t) \sim -\frac{1}{2\pi^2}\left[\mathcal{P}^{(0)}(t)\log q + (\gamma - 1)\,\mathcal{P}^{(0)}(t) - a_1^*(t)\right] , \tag{6.51}$$

as $q \to \infty$, where we re-added the time dependence for clarity. The free density correlation function thus diverges logarithmically for small scales, as expected. The amplitude $\mathcal{P}^{(0)}$ of the tail of the fee power spectrum sets the amplitude of $\xi_{\delta\delta}$ and the q-independent offset $(\gamma - 1)\,\mathcal{P}^{(0)}(t) - a_1^*(t)$.

6.2   IMPLICATIONS FOR COSMIC STRUCTURE FORMATION

In this section, we discuss the implications of our results on the formation of cosmic structures.

6.2.1   *Universality at Small Scales*

In the last section, we proved that the power spectrum for particles on free trajectories with initially correlated momenta always develops a k^{-3} tail. This universal power law evolves independently of the initial slope of the power spectrum at large k values. The value -3 of the exponent is solely determined by the number of spatial dimensions.

To demonstrate the validity of the asymptotic expansion, we show in Figure 6.1 the numerical evaluation of the free power spectrum (6.1) (purple lines), together with the k^{-3} (6.16) (green lines) and the k^{-5} term (6.27) (blue lines) in the asymptotic expansion (6.24), for two different redshifts ($z = 2$ and 10) and two different smoothing scales ($k_s = 10$ and $1000\,h\,\mathrm{Mpc}^{-1}$). We discuss free power spectra at today's redshift $z = 0$ in below in Section 6.2.5. For comparison, we also show the linearly evolved smoothed power spectra (5.4, grey lines),

$$P_\delta^{\mathrm{lin.}}(k) = g_{qp}^2(t)P_\delta^{(i)}(k) . \tag{6.52}$$

For the initial power spectra $P_\delta^{(i)}$, we choose the cold dark matter power spectrum from [4] and multiply it with an exponential regulator with smoothing scale k_s as in (5.4). To relate the propagator to redshift, we choose the Zel'dovich propagator

$g_{qp}(t, 0) = D_+(t) - D_+(t^{(i)})$. For the linear growth function D_+, we use the cosmological parameters shown in Table E.2. The free power spectrum converges in all four examples to the k^{-3} asymptotics. A comparison with the linearly evolved power spectra shows that a huge increase in power occurs at small scales: all formerly exponentially damped power spectra acquire a k^{-3} tail. Moreover, the asymptotic behavior is independent of the first moment of the initial velocity potential σ_1^2, i.e. the initial velocity dispersion. Next, we explain the general meaning of the k^{-5} term, i.e. the second-order asymptotics (6.27) (blue lines in Figure 6.1).
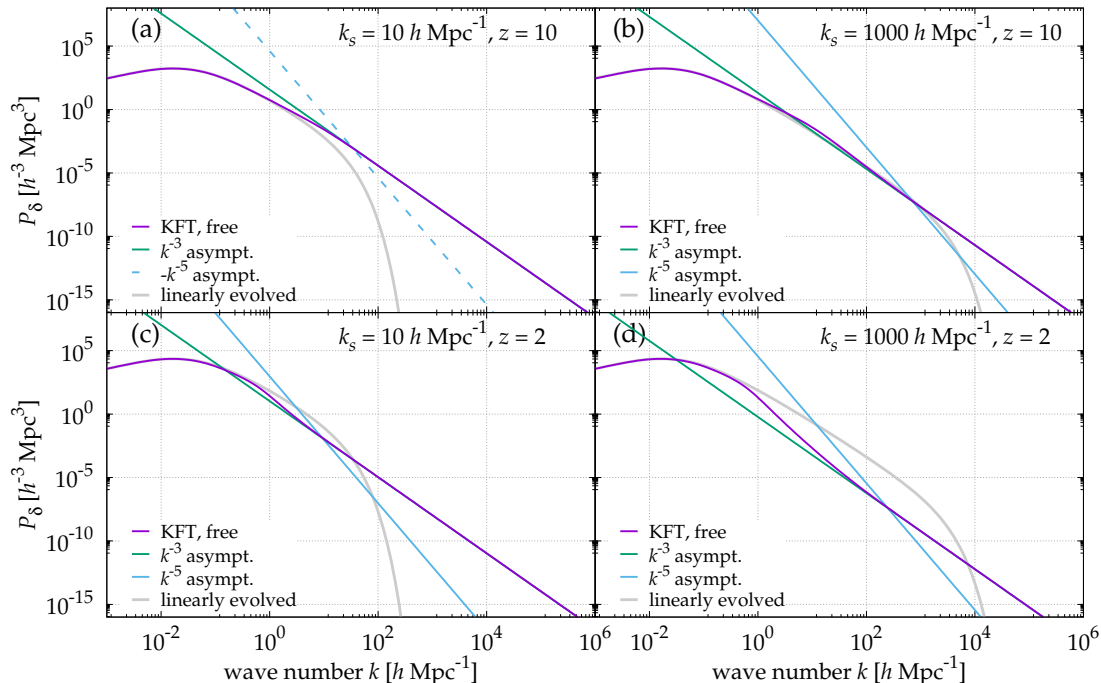
Figure 6.1: At large wave numbers, the k^{-3} asymptotics (6.16) (green lines) is in perfect agreement with the numerical evaluation of the free power spectrum (6.1) (purple lines) for early (top) and late (bottom) times as well as for large (left) and small (right) smoothing scales. The second order of the asymptotic expansion (6.27) (blue lines) predicts the scale of the onset of the k^{-3} behavior at those wave vectors, where the k^{-3} and the k^{-5} asymptotics cross. The blue dashed line in (a) indicates that the k^{-5} asymptotics is negative. The linearly evolved smoothed power spectra (6.52) (grey lines) are drawn for comparison. The cosmological and power spectrum parameters used are shown in Tables E.2 and E.3, respectively.

6.2.2 *Characteristic Self-Similarity Scale*

As can be seen in Figure 6.1, the scale at which the power spectrum converges to the k^{-3} asymptotics is well described by the intersection of the first- and second-order

asymptotics, (6.26) and (6.27). This intersection defines a characteristic time-dependent wave number $k^{\mathrm{char}}(t)$,

$$
\begin{aligned}
k^{\mathrm{char}}(t) &= \sqrt{\left|\left|\frac{\mathcal{P}^{(1)}(t)}{\mathcal{P}^{(0)}(t)}\right|\right|} \\
&= \left\{\frac{1}{84}\frac{\sigma_3^2}{\sigma_2^2}\left(\frac{5}{2\tau_2^2(t)}\right)\left|123 - 132\left(\frac{5}{2\tau_2^2(t)}\right) + 20\left(\frac{5}{2\tau_2^2(t)}\right)^2\right|\right\}^{1/2}, \quad (6.53)
\end{aligned}
$$

above which the free power spectrum attains the universal k^{-3} behavior. However, note that (6.53) vanishes for

$$
\tau_{2,1/2}^2(t) = \frac{5}{123}\left(33 \pm \sqrt{475}\right) \approx 1.34 \pm 0.89 . \tag{6.54}
$$

This implies that there exist neighborhoods of $\tau_{2,1/2}^2(t)$, such that (6.53) does not characterize the wave number above which the free power spectrum attains the k^{-3} behavior. To get better estimates for k^{char} at these points, one could for example compare the first-order asymptotics to higher orders, following the optimal truncation rule 4.5. Another possibility is to consider the monotonic envelope of (6.53). An exploration of the detailed properties of the asymptotics in the vicinity of $\tau_{2,1/2}^2(t)$ will be the subject of future work. For now we consider time scales such that the free power spectrum for wave numbers above the k^{char} from (6.53) is dominantly described by the first-order asymptotics.

In general, for wave numbers above k^{char}, the free power spectrum is scale-free because it turns into a power law. If most of dark matter is organized in halos[1], then the one-halo term determines the small-scale part of the power spectrum as shown in Figure 2.1 of Chapter 2. Since the one-halo part of the power spectrum P_δ^{1h} (2.48) is determined by the density profiles of individual halos and the number density $n(M)$ of halos with a given mass M, i.e. the halo mass function, the self-similarity of the power spectrum supports universal halo profiles that are independent of the halo mass. This is an indication that the universality of halo profiles arises very early in the formation history of protohalos during the first gravitational infall of material. Up to now, it has been unknown why these universal halo profiles emerge, while the general shape of the halo mass function seems to be relatively well understood [69]. However, further work is needed to investigate this proposed scenario, because we related the properties of a two-point function in Fourier space (the power spectrum) to the properties of a conditional density function in real space (the halo profile), where additionally the halo mass function $n(M)$ enters. Furthermore, it is subject to future work to explore whether this universality at small scales fundamentally emerges also when gravitational interactions are taken into account.

6.2.3 *Implications for Numerical Implementations*

The expression for the free power spectrum (6.1) contains the prefactor $\mathrm{e}^{-\frac{\sigma_1^2}{3}k^2 g_{qp}^2(t,0)}$, which may be interpreted as a damping factor. When an asymptotic expansion of

---

1 Reference [69] and references therein suggest that probably more than 80% of dark matter is organized in halos.

the integral (6.1) for small k is performed – which is equivalent to an expansion in the initial momentum correlations – one obtains a linearly evolved power spectrum multiplied by this damping factor,

$$\mathcal{P}(k,t) \sim e^{-\frac{\sigma_1^2}{3}k^2 g_{qp}^2(t,0)} g_{qp}^2(t,0) P_\delta^{(i)}(k) , \quad \text{as } k \to 0^+ . \tag{6.55}$$

A natural question to ask is: What is the meaning of this damping factor? In Figure 6.2, we compare the free power spectra from Figure 6.1 (purple lines) to the linearly evolved damped power spectra (6.55) (golden lines). In these examples, no visible features from the damping are apparent in the free power spectra. Indeed, our analytical result (6.16) shows that for large k the damping is completely canceled in the asymptotics. The free power spectrum is not exponentially cut-off but has a power-law tail with exponent -3. This observation has important consequences for numerical implementations to evaluate free power spectra at large wave numbers. Equation (6.6) shows that when we use a numerical fit for the initial momentum correlation function (6.4), this fit function needs to obey the correct limit (6.23),

$$\lim_{q \to 0} f_\mu(q) = -g_{qp}^2(t,0)\frac{\sigma_1^2}{3} . \tag{6.56}$$

Otherwise, the damping is not correctly compensated for large values of k and the numerical results differ exponentially from the true value. In order for the numerical result to yield values that are in agreement with the first-order asymptotics, any implementation of $f_\mu(q)$ needs to satisfy the correct small-scale behavior (6.22) at least up to the order q^2.

6.2.4 *Time-dependence of the Amplitude*

The time-dependent amplitude of the first-order asymptotics, $\mathcal{P}^{(0)}(t)$ in (6.26), is a function of the product $g_{qp}^2(t,0)\sigma_2^2$. Thus, for straight particle trajectories, $\tau_2^2(t) = g_{qp}^2(t,0)\sigma_2^2$ acts as a (squared) time coordinate that describes the growth of structures at small scales. For small values of σ_2^2, i.e. large smoothing scales of the initial structures in real space, the small-scale structure evolution proceeds more slowly, while large values of σ_2^2 imply a faster evolution of the structures on small scales.

Figure 6.3 (b) shows the asymptotic amplitude $\mathcal{P}^{(0)}$ as a function of $\tau_2^2(t)$, (grey line). Colored crosses mark the asymptotic amplitude of the power spectra shown in panel (a). The grey line shows that $\mathcal{P}^{(0)}$ first rises steeply during the free infall of structures until it reaches a maximum at

$$\tau_2^2(\text{max}) = \frac{5}{3} . \tag{6.57}$$

This maximum indicates stream crossing at small scales because for larger values of $\tau_2^2(t)$ re-expansion of structures sets in, such that the asymptotic amplitude $\mathcal{P}^{(0)}$ starts to decrease and eventually falls of like $(\tau_2^2)^{-3/2}$ for late times. Therefore,

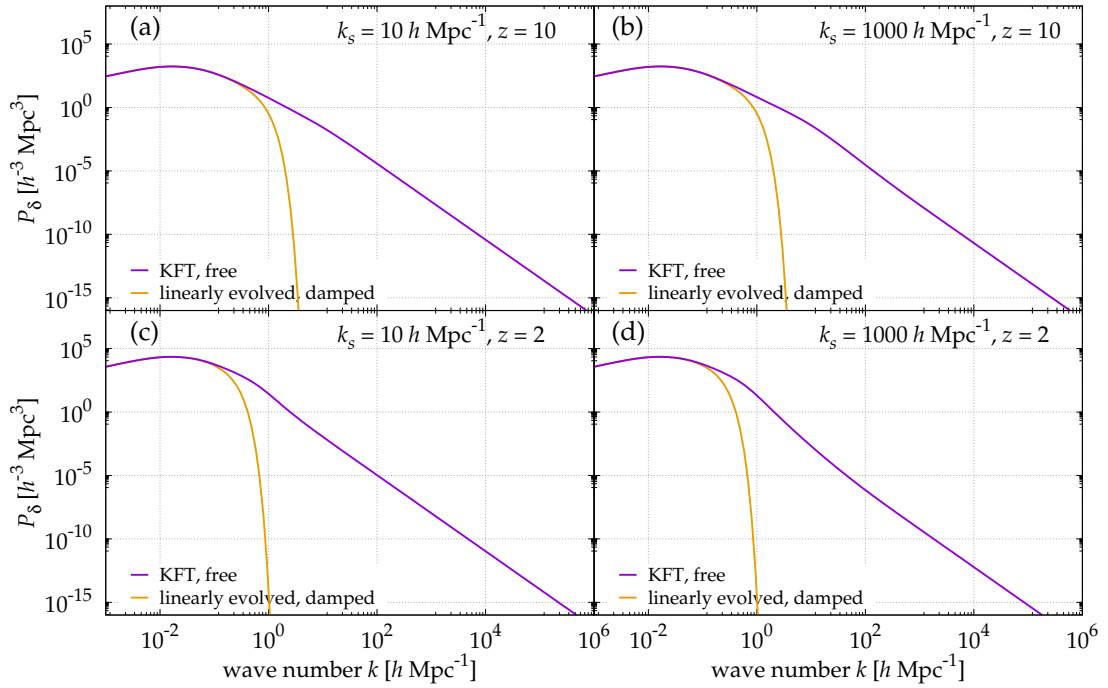$$g_{qp}(\text{max}) = \sqrt{\frac{5}{3\sigma_2^2}} \tag{6.58}$$

Figure 6.2: The free power spectra from Figure 6.1 (purple lines) show no features of the damped linearly evolved power spectra (6.55) (golden lines) at small scales. The effect of the damping term is not visible at all for early (top) and late (bottom) times as well as for large (left) and small (right) smoothing scales. Parameters as in Figure 6.1.

sets the time of small-scale stream crossing in units of the linear growth factor and the amplitude reaches the maximal value

$$\mathcal{P}^{(0)}(\tau_2^2(\mathrm{max})) = 3\left(\frac{6\pi}{\mathrm{e}}\right)^{3/2} \approx 54.78 \ . \tag{6.59}$$

This maximum value is universal for all cosmological models and all initial power spectra. The small-scale regime of the power spectrum will never grow beyond this amplitude when straight particle trajectories and initially correlated momenta are considered. Just the time (6.58), in units of of the linear growth factor, at which this universal amplitude is reached depends on σ_2^2, thus on the smoothing scale.

In Figure 6.3 (a), we show the free dimensionless power spectrum

$$\Delta(k) = \mathcal{P}(k)k^3 \tag{6.60}$$

as a function of $\tau_2^2(t)$ for $k_s = 1000\,h\,\mathrm{Mpc}^{-1}$ at five different redshifts. The dimensionless power spectra shown become constant for large values of k because $\Delta(k) \to \mathcal{P}^{(0)}$ (6.26). Note that the plateaus show that the k^{-3} asymptotics emerges already before stream crossing ($z = 29$ and 25 in Figure 6.3) and persists after the onset of re-expansion ($z = 17$ and 13 in Figure 6.3).

6.2.5 *Non-linear Zel'dovich Power Spectrum at Redshift $z = 0$*

At large scales, the non-linear Zel'dovich power spectrum is known to correspond to the linear power spectrum, which accurately describes the structure on the largest
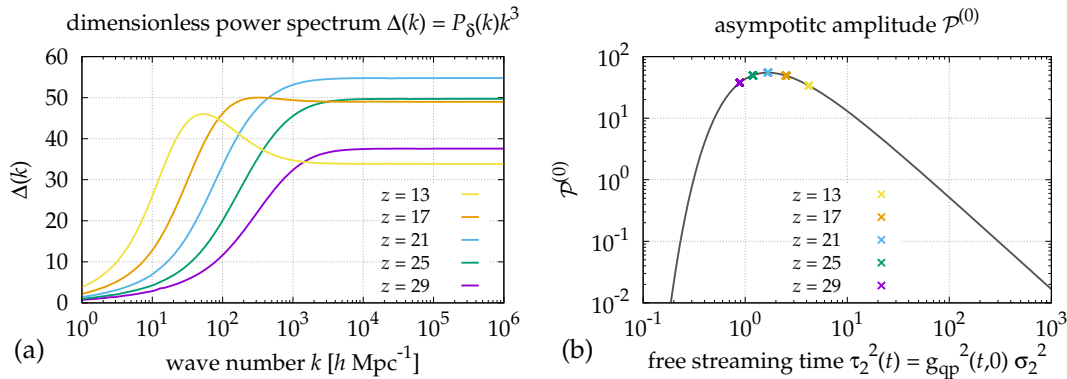
Figure 6.3: (a) The free dimensionless power spectrum (6.60) for a smoothed initial Bardeen power spectrum with $k_s = 1000\ h\ \mathrm{Mpc}^{-1}$ is shown for different redshifts z. The amplitude rises from $z = 29$ and reaches the universal maximum (6.59) at $z = 21$. After the onset of re-expansion, the amplitude goes down while the k^{-3} behavior persists. (b) The amplitude $\mathcal{P}^{(0)}$ of the first-order asymptotics (6.26) as a function of the free streaming time τ_2^2 (6.15) rises until it reaches the maximum value ≈ 54.78 at $\tau_2^2 = 5/3$, when stream crossing occurs. After stream crossing, re-expansion leads to a decay of structures and the amplitude decreases with $(\tau_2^2)^{-3/2}$. Colored points correspond to the asymptotic amplitudes from (a). The cosmological and power spectrum parameters used are shown in Tables E.2 and E.4, respectively.

scales – even today. However, it is also known that the Zel'dovich approximation leads to a re-expansion of structures after stream crossing that goes along with decreasing power at small scales, as can be seen in Figure 6.3. In order to prevent this re-expansion, techniques like for example the adhesion approximation, that makes particles stick together, were developed, e.g. in [65]. Another method to lift the tail of the Zel'dovich power spectrum is to use a so-called truncated Zel'dovich power spectrum, e.g. in [20]. This means that the initial power spectrum is truncated similarly to the action of the regulator that we introduced in (5.4). Thus the initial power spectra are smoothed at appropriate scales. In Figure 6.4, we show how truncation, i.e. smoothing away the small-scale fluctuations, at different scales affects the tail of the Zel'dovich power spectrum at today's redshift $z = 0$. In Figure 6.4 (a), the free power spectra (colored lines) for four different smoothing scales are shown, together with the linearly evolved Bardeen power spectrum (black line). The tail of all four free power spectra stays below the linear Bardeen spectrum. In Figure 6.4 (b) we show the same dimensionless power spectra that all reach plateau values for $k \gtrsim 100\ h\ \mathrm{Mpc}^{-1}$. In Figure 6.4 (c) we show the amplitude $\mathcal{P}^{(0)}$ as a function of τ_2^2 ((6.26), grey line), where the colored crosses indicate the values for four example power spectra at $z = 0$. The truncation at smaller wave numbers leads to smaller values of σ_2^2 causing a slower evolution of the amplitude at small scales. However, since the amplitude is bounded by the maximal value ≈ 54.78 (6.59), there is no truncation scale such that the free Zel'dovich power spectrum reaches the amplitude of the linear cold dark matter power spectrum at small scales today.

We conclude that our results are in agreement with the known fact that the truncated Zel'dovich power spectrum cannot be tuned to yield the amplitude of the linear CDM power spectrum or even the non-linear power spectrum at today's redshift $z = 0$.

Additionally, we derived the value that the amplitude of any truncated Zel'dovich power spectrum can maximally reach at small scales.
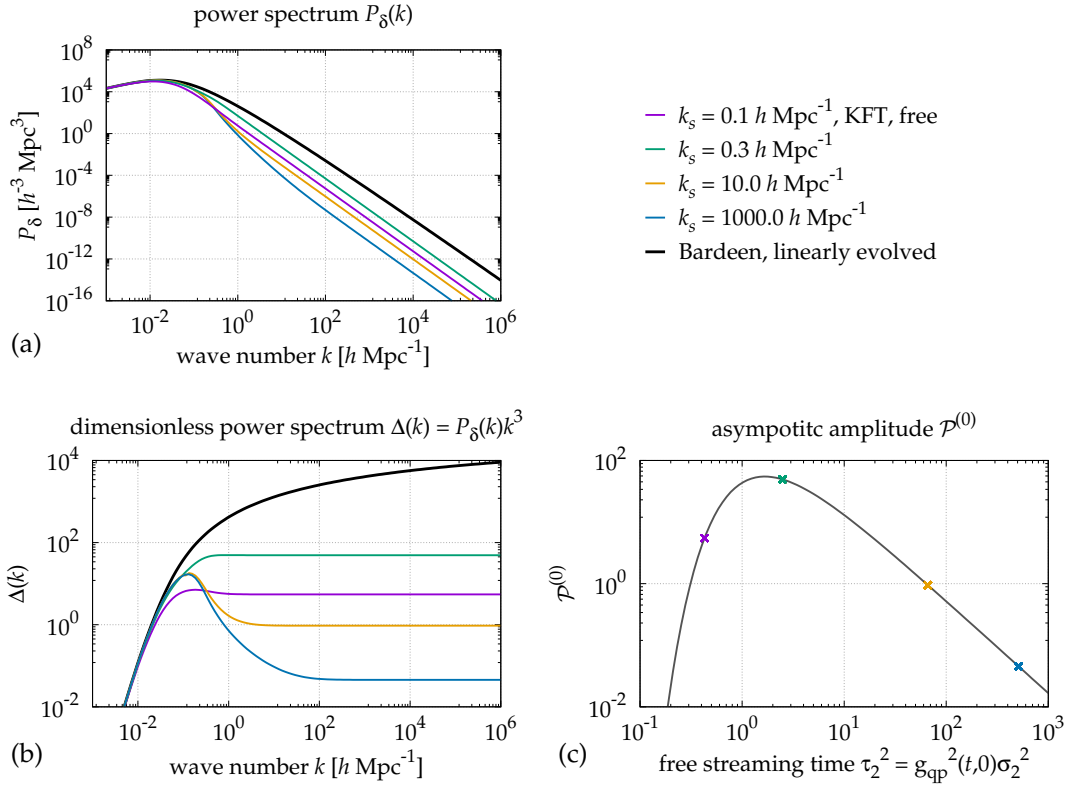

Figure 6.4: The asymptotic amplitude evolves more slowly for smaller smoothing wave numbers. (a) The free power spectra (6.1) (colored lines) for different values of k_s and the linearly evolved Bardeen power spectrum (black line) are shown at today's redshift $z = 0$. The amplitudes at small scales differ by more than three orders of magnitude. (b) The dimensionless power spectra as in (a) are shown. All free power spectra reach different plateau values for $k \gtrsim 100 \, h \, \mathrm{Mpc}^{-1}$. (c) The asymptotic amplitude $\mathcal{P}^{(0)}$ (6.26) (grey line) as a function of the free streaming time τ_2^2 is shown as in Figure 6.3 (b). Colored crosses indicate the plateau values of the dimensionless power spectra in (b). For smaller k_s, the evolution of $\mathcal{P}^{(0)}$ proceeds slower, implying a slower growth of small-scale structures. The cosmological and power spectrum parameters used are shown in Tables E.2 and E.4, respectively.

6.2.6   *Asymptotic Stream Crossing Scales*

The Zel'dovich approximation is considered to be appropriate up to scales when stream crossing occurs[2]. From the asymptotics of the free power spectrum we can derive the redshift-, length- and mass scales of stream crossing. In the following, we denote these scales as the *asymptotic stream crossing scales* and indicate the corresponding variables by the superscript sc. These scales are of particular interest as they characterize the process of the formation of the first dense structures in the universe.

---

2 In one spatial dimension, the Zel'dovich approximation is exact before particles meet.

Asymptotic Stream Crossing Redshift

We already derived the stream crossing time (6.58) at small scales in units of the linear growth factor. The redshift z^{sc} at which small-scale stream crossing occurs thus depends on σ_2^2 and on the cosmological parameters that determine the growth factor $D_+(z)$ as a function of redshift. From (6.57) with $\tau_2^2(t) = g_{qp}^2(t)\sigma_2^2$ and the Zel'dovich propagator $g_{qp}(t,0) = D_+(z(t)) - D_+(z^{(i)})$, the condition for z^{sc} is

$$\frac{3\sigma_2^2\left(D_+(z^{sc}) - D_+(z^{(i)})\right)^2}{5} \overset{!}{=} 1 . \tag{6.61}$$

To demonstrate the dependence of z^{sc} on the cosmological parameters, we show in Figure 6.5 (a) the σ_2^2-dependent asymptotic stream crossing redshift for three different sets of cosmological parameters. In Figure 6.5 (b), we show the linear growth factor as a function of redshift. The faster the linear growth factor rises with decreasing redshift at early times, the earlier small-scale stream crossing occurs. We conclude that the asymptotic stream crossing redshift is sensitive to both the cosmological parameters and the smoothing scale of the initial power spectrum and thus on the dark matter type.
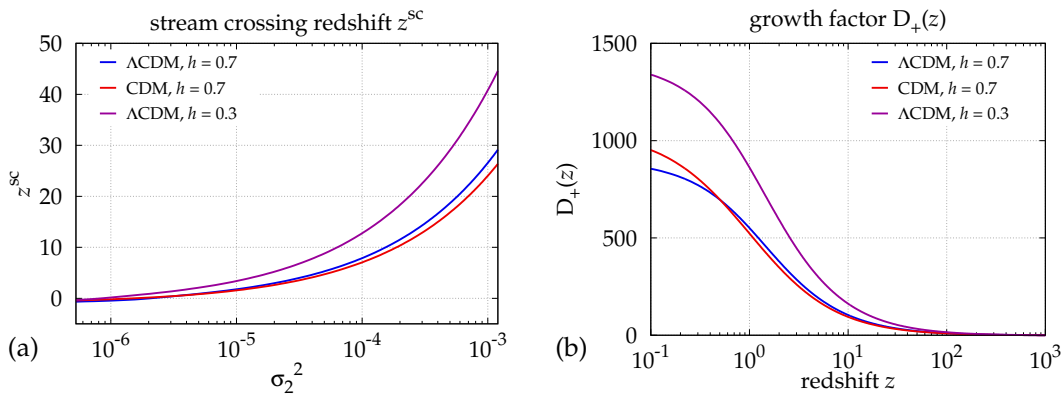
Figure 6.5: (a) The redshift z^{sc} at which small-scale stream crossing occurs is determined by σ_2^2 and the underlying cosmological parameters. It is implicitly given by (6.61). The different colors indicate the different sets of cosmological parameters $(\Omega_{\Lambda 0}, \Omega_{m0}, \Omega_{b0}, h)$, where ΛCDM $= (0.7, 0.3, 0.04)$ ($h = 0.7$ blue lines, $h = 0.3$ purple lines) and CDM $= (0.0, 0.999, 0.001)$ ($h = 0.7$ red lines). The reason for the differences in z^{sc} is the different redshift evolution of the corresponding growth factors $D_+(z)$, which are shown in (b). The cosmological and power spectrum parameters used are shown in Tables E.2 and E.4, respectively.

Asymptotic Stream Crossing Amplitude

We derived the amplitude (6.59) that determines the small-scale behavior of the non-linear Zel'dovich power spectrum at stream crossing. In Figure 6.6 we demonstrate how different smoothing scales ($k_s = 1\ h\ \text{Mpc}^{-1}$ left and $k_s = 1000\ h\ \text{Mpc}^{-1}$ right) influence the relative power of the Zel'dovich power spectrum (purple lines) compared

to the linearly evolved CDM power spectrum (black lines) at small scales. Figure 6.6 (c) and (d) show the ratios

$$\text{ratio} = \frac{\mathcal{P}(k, t^{\text{sc}})}{g_{qp}^2(t^{\text{sc}}, 0) P_\delta^{\text{CDM,(i)}}(k)} \tag{6.62}$$

between the non-linear Zeldovich power spectra and the linearly evolved Bardeen power spectra at small-scale stream crossing, where $P_\delta^{\text{CDM,(i)}}(k)$ denotes the Bardeen power spectrum at initial time, i.e. the non-smoothed CDM spectrum. Since the asymptotic amplitude evolves more slowly for small smoothing wave numbers, z^{sc}, which is implicitly given by (6.61), is smaller in (a) and (c) compared to (b) and (d). This is why for $k_s = 1\ h\ \text{Mpc}^{-1}$ the free power spectrum falls below the linear CDM spectrum, while for $k_s = 1000\ h\ \text{Mpc}^{-1}$ the growth at small scales was faster, such that the free power spectrum has more power on small scales compared to the linear spectrum.
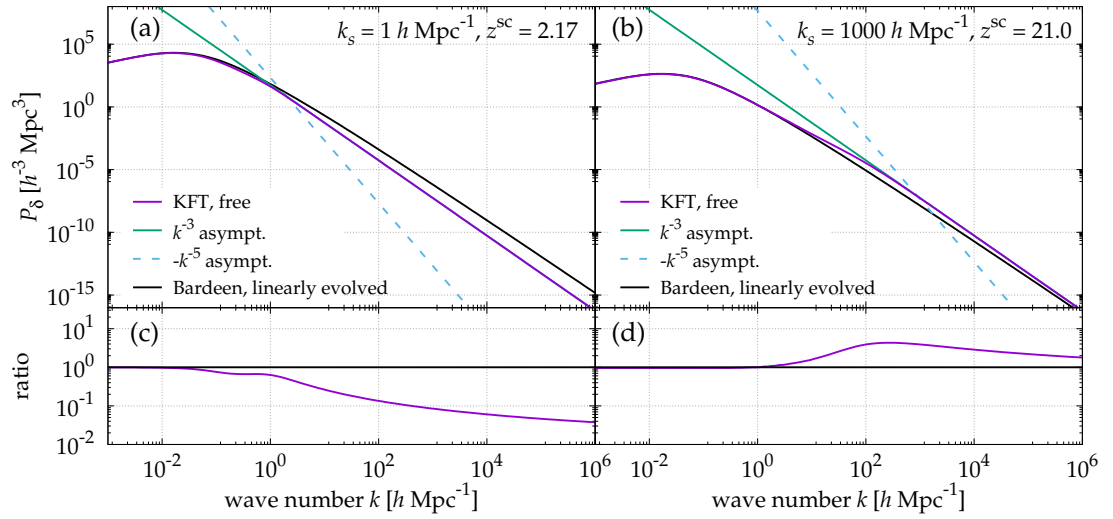
Figure 6.6: The free power spectra (6.1) (purple lines) for the smoothing scales $k_s = 1\ h$ Mpc^{-1} (a) and $k_s = 1000\ h$ Mpc^{-1} (b) are shown at the respective asymptotic stream crossing redshift, together with the k^{-3} asymptotics (6.16) (green lines), the second-order k^{-5} asymptotics (6.27) (blue lines) and the linearly evolved Bardeen power spectrum (black lines). For $k_s = 1\ h$ Mpc^{-1} (a) the free power spectrum falls below the linear power spectrum at small scales. For $k_s = 1000\ h$ Mpc^{-1} (b) the small-scale evolution of the free power spectrum is faster than linear growth. (c) and (d) show the ratios (6.62) between the free and the linear power spectra. The cosmological and power spectrum parameters used are shown in Tables E.2 and E.4, respectively.

Asymptotic Stream Crossing Length Scale

We obtain the characteristic wave number k^{sc} above which the power spectrum attains the k^{-3} tail at small-scale stream crossing from (6.53) and (6.57),

$$k^{\text{sc}} = \sqrt{\frac{15}{28} \frac{\sigma_3^2}{\sigma_2^2}}. \tag{6.63}$$

We convert this wave number into the asymptotic stream crossing length scale

$$R^{\mathrm{sc}} = \frac{2\pi}{k^{\mathrm{sc}}} \, . \tag{6.64}$$

Note that k^{sc} and R^{sc} depend only on the ratio of the second and the third moments of the initial velocity potential power spectrum. They depend neither on the cosmological parameters nor on the amplitude of the initial power spectrum.

From the asymptotic stream crossing length scale, we next derive a mass scale.

Asymptotic Stream Crossing Mass Scale

From the asymptotic stream crossing length scale, we deduce a mass scale

$$
\begin{aligned}
M^{\mathrm{sc}} = \rho_{\mathrm{cr}0} \Omega_{\mathrm{m}0} \left(\frac{k^{\mathrm{sc}}}{2\pi} \right)^{-3} &\approx 1.16 \times 10^{13} M_{\odot} \left(\frac{k^{\mathrm{sc}}}{\mathrm{Mpc}^{-1}h} \right)^{-3} \\
&\approx 2.96 \times 10^{13} M_{\odot} \left(\sqrt{\frac{\sigma_3^2}{\sigma_2^2}} \mathrm{Mpc}\, h^{-1} \right)^{-3} .
\end{aligned}
\tag{6.65}
$$

Thus, the asymptotic stream crossing mass scale M^{sc} depends on the matter density today and on the shape of the initial power spectrum, via the ratio of the second and third moments σ_3^2 and σ_2^2, but not on its amplitude. Note that the explicit dependence on the stream crossing redshift cancels because the matter density scales like a^{-3}, i.e. inversely with the proper volume.

To demonstrate the sensitivity of k^{sc} and M^{sc} to the shape of the initial power spectrum, we show them in Figure 6.7 as a function of σ_2^2 for two different types of initial power spectra. The blue lines are for smoothed Bardeen initial power spectra. The golden lines show the results for non-cold dark matter type (nCDM-type) initial power spectra that have power law tails instead of an exponential smoothing. In this example, we characterize the initial power spectra of the nCDM-type by the transfer function

$$\frac{P_\delta^{\mathrm{nCDM,(i)}}(k)}{P_\delta^{\mathrm{CDM,(i)}}(k)} = T^2(k) = \left[1 + (\alpha k)^\beta \right]^{2\gamma} , \tag{6.66}$$

relative to the initial CDM power spectrum $P_\delta^{\mathrm{CDM,(i)}}(k)$, for which we choose the Bardeen spectrum. In [45], it has been shown that the power spectra of many types of nCDM can be characterized by such a transfer function. Without specifying our example to a specific dark matter model, we used the exemplary parameter values $\alpha = 1.0$, $\beta = 2.0$ and varied $\gamma \in [-20.0, -0.02]$.

Figure 6.7 shows that the initial nCDM-type power spectra lead to different asymptotic stream crossing wave numbers and mass scales compared to the initially smoothed CDM power spectra. This is a direct consequence of the different shapes, which demonstrates the sensitivity of the stream crossing length- and mass scales to the shape of the initial power spectrum.

The asymptotic stream crossing length scale might be related to a scale in physical space below which structures attain self-similar profiles, while the asymptotic stream crossing mass scale might be related to the mass of bound structures such as halos.

It will be the subject of future work to explore to which degree these scales are actually imprinted in cosmic structures, for example by comparisons with N-body simulations. If these scales can be related to any observables, these observables might serve as a probe for σ_3^2/σ_2^2, which in turn gives constraints on the shape of linear power spectrum and therefore on the models assumed for dark matter. Furthermore, it will also be interesting to explore in the framework of KFT whether these scales remain fundamental when higher orders of the gravitational interaction are taken into account.
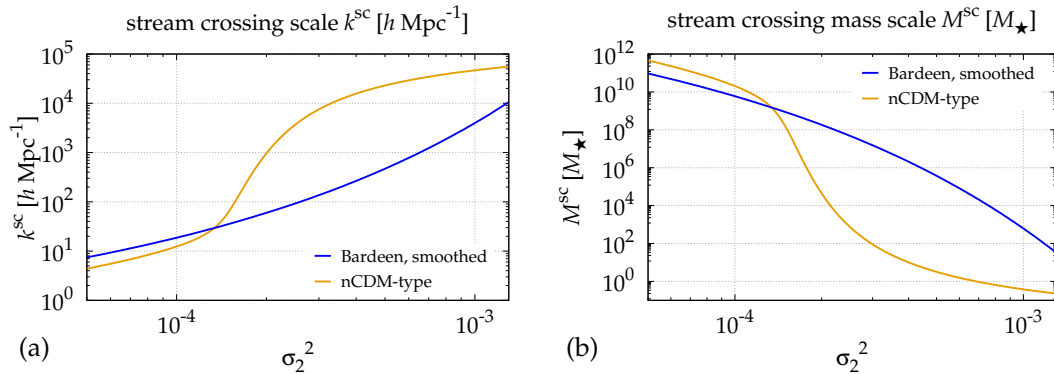

Figure 6.7: The stream crossing wave number k^{sc} (6.63), shown in (a), and mass scale M^{sc} (6.65) in units of solar mass, shown in (b), are sensitive to the shape of the initial power spectrum. We show the σ_2^2-dependent values obtained from initially smoothed Bardeen power spectra (blue lines) and for non-dark matter type (nCDM-type) power spectra (golden lines). The latter are related to the Bardeen power spectrum by the transfer function (6.66). Both k^{sc} and M^{sc} are sensitive to the shape of the initial power spectrum because they are functions of σ_3^2/σ_2^2. The cosmological and power spectrum parameters used are shown in Tables E.2 and E.5, respectively.

6.3 SUMMARY AND DISCUSSION

In the first part of this Chapter, we first derived the first-order asymptotics of the free power spectrum $\mathcal{P}$ (6.1) in KFT. By applying our Theorem 4.4 for N-dimensional Fourier-Laplace type integrals, we proved that the free power spectrum always develops a k^{-3} tail, independently of the slope of the initial power spectrum. This small-scale behavior was suggested in [58] for the non-linear Zel'dovich power spectrum. Independently of our work, the k^{-3} asymptotics was recently derived in the framework of Lagrangian perturbation theory in [18], finding the same amplitude that we derive here.

By applying our Theorem 4.2, we then derived an expression for the coefficients of the whole asymptotic series of $\mathcal{P}$ in orders of k^{-3-2m} and evaluated the second term of this series that describes the k^{-5} behavior. In the final section of the first part, we derived the asymptotic expansion of the time-evolved free density-density correlation function $\xi_{\delta\delta}$. We proved that $\xi_{\delta\delta}$ diverges logarithmically, as expected, and calculated explicitly the expression for the leading-order term.

In the second part of this chapter, we discussed the relevance of these results for cosmic structure formation in more detail. First, we demonstrated the validity of our

asymptotic expansion by comparing our analytical results to numerical evaluations of the free power spectrum for different initial smoothing scales and at different redshifts.

In the examples that we have shown, the intersection of the first- and second-order asymptotics indicated the wave number above which the free power spectrum is well described by the k^{-3} asymptotics. On the one hand, this suggests that the optimal truncation rule might hold for our asymptotic expansion, such that incorporating higher-order terms of the asymptotic series and truncating before the smallest term might lead to the best possible approximation. On the other hand, we have shown that the second-order asymptotics changes the sign twice, i.e. the coefficient has two zeros. It will be subject of future work to analyze the properties of the asymptotic series in more detail and more specifically for times at which the second coefficient changes sign. Nevertheless, for the examples that we have shown, the intersection of the first- and second-order asymptotics describes the characteristic wave number k^{char} above which the power spectrum assumed the k^{-3} power law, thus scale-free behavior. We suggested that k^{char} might be related to a scale in real space below which dark matter forms self-similar structures. In future work, this can be explored by comparing this scale to results from N-body simulations. However, even when this scale is imprinted in simulations of collisionless dark matter, in the real universe baryonic matter is supposed to have a strong impact on structure formation on small scales. The integration of baryons is currently studied in the framework of Resummed KFT [32, 33]. Another important next step will be to check whether this k^{-3} behavior that we proved for free trajectories, persists also when more gravitational interactions are included, for example via perturbation or mean-field theory. Additionally, we only took initial momentum-momentum correlations into account, neglecting initial density-density and initial density-momentum correlations. At large scales, it has been shown that this is a valid approach. At small scales, however, this assumption also has to be checked more thoroughly in future work.

We then discussed the implications of the exponential damping factor in front of the integral (6.1) for the numerical implementation of codes to evaluate the free power spectrum. We argued that it is crucial for the evaluation at large wave numbers that the small-scale behavior of the initial density correlation function is implemented asymptotically correctly up to order q^2. The results will otherwise diverge exponentially.

Next, we showed that the time evolution of the amplitude of the k^{-3} asymptotics depends only on the product $g_{qp}^2(t,0)\sigma_2^2$, showing that the evolution of the small-scale structure proceeds more slowly when the initial power spectrum has a smaller smoothing wave number. At early times, the amplitude rises steeply, indicating the convergence of particle streams due to their initially correlated momenta. The asymptotics then reaches a universal maximum value ≈ 54.78 when $g_{qp}^2(t,0)\sigma_2^2 = 5/3$. This maximal value of the amplitude marks small-scale stream crossing, where particle trajectories cross and the particles subsequently move apart. This leads to the re-expansion of the small-scale structures that is known to occur in the Zel'dovich approximation and that goes along with the decreasing amplitude at small scales. Our analytical result quantifies the time evolution of the small-scale amplitude for the non-linear Zel'dovich power spectrum with any truncation. Furthermore, we quantified the maximal amplitude that these power spectra eventually reach at small

scales and the time when this maximum is reached, i.e. when small-scale stream crossing occurs.

In the last section, we derived several scales that we associate to small-scale stream crossing and showed how these scales depend on the cosmological parameters and the shape of the initial power spectrum. First, we demonstrated that the asymptotic redshift scale is determined by σ_2^2 and the cosmological parameters. The faster the linear growth factor rises with decreasing redshift at early times, the higher the redshift of small-scale stream crossing. Similarly, higher values of σ_2^2 also imply higher asymptotic stream crossing redshifts. Next, we derived the asymptotic stream crossing wave number and the asymptotic stream crossing length scale from the intersection point of the first- and second-order asymptotics at small-scale stream crossing. This length scale is determined by the ratio σ_3^2/σ_2^2 and thus independent of the cosmological parameters and the amplitude of the initial power spectrum. We did not yet explore whether this scale is indeed imprinted in the cosmic structures formed. Nevertheless, since this scale indicates the wave number above which the free power spectrum attains the k^{-3} behavior, it also determines the physical scale up to which (probably self-similar) structures formed up to the time when stream crossing happens. This is especially interesting for cold dark matter, where σ_2^2 is very large such that stream crossing occurs early. Consequently, the formation of small structures occurs very rapidly and the small-scale amplitude of the free power spectrum at the time of stream crossing experienced a much stronger relative growth than the linearly growing large-scale structures. The asymptotic stream crossing length scale then marks a lower limit below which non-linear structures certainly have formed. Converting the asymptotic stream crossing length scale to a mass scale, this might then set a scale for the mass of non-linear structures that have formed. Furthermore, we demonstrated that these scales depend on the model for dark matter. For initial power spectra with the same values for the moments σ_2^2, different scales emerge when the moments σ_3^2 are different, i.e. when they have similar initial cutoff scales but the steepness of the tails varies. It will be interesting to explore in future work whether these scales that we derived for free trajectories remain evident when more gravitational interactions are included. Since in one dimension, the Zel'dovich approximation is exact before stream crossing, we propose that the scales we derived for three dimensions are also reflected in the early formation of structures in the presence of full gravitational interactions. This can be tested by comparing our results to cosmological N-body simulations. Furthermore, if these scales are then also imprinted in cosmic structures at late times and related to any observables, then these observables are probes for the dark matter type. With this, we lay the foundation for future work to explore the possible imprint of these scales in observables and to derive the precise relations for specific dark matter candidates.

FACTORS OF THE GENERATING FUNCTIONAL

In kinetic field theory (KFT), the factors

$$I_{21}(\vec{J}_{p_1}, \vec{J}_{p_2}, \vec{J}_{q_1}) := \int_q e^{-\vec{J}_{p_1}^\mathsf{T} \hat{C}_{pp}(\vec{q}) \vec{J}_{p_2} + i\vec{J}_{q_1} \cdot \vec{q}} \tag{7.1}$$

are the fundamental building blocks of the free generating functional (3.111) when we consider only initial momentum-momentum correlations C_{pp}. In Section 3.5 of Chapter 3, we reviewed how the free density correlation functions can be expressed in terms of a convolution of these factors (see (3.123)).

When the factorization was originally introduced, it was hoped that it facilitates the numerical evaluation of higher order density correlation functions. The idea was to evaluate the factors (7.1) for a wide range of arguments and store them in a table such that subsequent convolutions could be computed more efficiently. Thus, a fast evaluation of these numerical factors is important to calculate the free density correlation functions to higher orders. Besides, the factorization is used as a basis for ongoing research on the foundations and possible new formulations of KFT, where the individual asymptotic behavior of the factor I_{21} plays a crucial role.

Up to now, it was not possible to successfully implement an algorithm for the numerical evaluation of these factors for general orientations of the involved vectors $\vec{J}_{p_1}$, $\vec{J}_{p_2}$ and $\vec{J}_{q_1}$. This lack of success has several reasons. First, the error made in [9] with regard to the integration kernel that we now resolved in 3.5 led to a wrong implementation of the factors in earlier work [15]. Second, these integrals are in the representation (7.1) numerically not convergent. This is because the initial momentum correlation matrix,

$$\begin{aligned} \hat{C}_{pp}(\vec{q}) &= \int_k (\vec{k} \otimes \vec{k}) P_\psi^{(i)}(k) e^{i\vec{k}\cdot\vec{q}} \\ &= -\vec{q} \otimes \vec{q} \, \frac{a_2(q)}{q^2} - \mathbb{I}_3 a_1(q) \,, \end{aligned} \tag{7.2}$$

with the initial velocity potential power spectrum $P_\psi^{(i)}(k) = k^{-4} P_\delta^{(i)}(k)$ and the functions $a_1(q)$ and $a_2(q)$ as in (5.22) and (5.23), has a tail that falls off like q^{-n_s-1} for large q as shown in Section 5.3 of Chapter 5. Thus, the integration kernel in (7.1) has to be appropriately regularized at large scales for any numerical implementation. In the first section of this chapter, we present such a regularization. A third challenging aspect for the numerical implementation of these factors is the rapid oscillation of the kernel, especially for large absolute values of the vectors involved. In the previous chapter we discussed a related issue for the numerical implementation of the free power spectrum. When the initial momentum-momentum correlation function is not implemented correctly, the result of the numerical integration deviates exponentially from the true value. In the second section of this chapter, we derive the asymptotics of the factors for large absolute values and arbitrary orientations of the vectors in the argument.

7.1 REGULARIZATION AT LARGE SCALES

In this section, we show how the kernel of each factor (7.1) can be regularized to yield numerically well convergent integrals.

In [9, 15], the factors (7.1) were regularized by adding a Dirac delta distribution yielding the *generalized power spectra*

$$\mathcal{P}_{21}(\vec{J}_{p_1}, \vec{J}_{p_2}, \vec{J}_{q_1}) := \int_q \left(e^{-\vec{J}_{p_1}^\top \hat{C}_{pp}(\vec{q}) \vec{J}_{p_2}} - 1 \right) e^{i\vec{J}_{q_1} \cdot \vec{q}} \, , \tag{7.3}$$

such that the factors are

$$I_{21}(\vec{J}_{p_1}, \vec{J}_{p_2}, \vec{J}_{q_1}) = (2\pi)^3 \delta_D\left(\vec{J}_{q_1}\right) + \mathcal{P}_{21}(\vec{J}_{p_1}, \vec{J}_{p_2}, \vec{J}_{q_1}) \, . \tag{7.4}$$

The integration kernel in (7.3), without the oscillating factor, now falls off like q^{-n_s-1}. Since $n_s \lesssim 1$, we wish to increase the steepness of the kernel for better convergence. To go one step further in the regularization, we first note that

$$\int_q \vec{J}_{p_1}^\top \hat{C}_{pp}(\vec{q}) \vec{J}_{p_2} e^{i\vec{J}_{q_1} \cdot \vec{q}} = \int_q \int_k \left(\vec{J}_{p_1} \cdot \vec{k} \right) \left(\vec{J}_{p_2} \cdot \vec{k} \right) P_\psi^{(i)}(k) e^{i\left(\vec{J}_{q_1} + \vec{k} \right) \cdot \vec{q}} \tag{7.5}$$

$$= \frac{(\vec{J}_{p_1} \cdot \vec{J}_{q_1})(\vec{J}_{p_2} \cdot \vec{J}_{q_1})}{J_{q_1}^4} P_\delta^{(i)}(J_{q_1}) \, , \tag{7.6}$$

where we used (7.2). Thus, we can regularize the generalized power spectra (7.3) by adding a zero by adding and subtracting (7.6), and arrive at

$$\begin{aligned}
\mathcal{P}_{21}(\vec{J}_{p_1}, \vec{J}_{p_2}, \vec{J}_{q_1}) = {} & \frac{(\vec{J}_{p_1} \cdot \vec{J}_{q_1})(\vec{J}_{p_2} \cdot \vec{J}_{q_1})}{J_{q_1}^4} P_\delta^{(i)}(J_{q_1}) \\
& + \int_q \left(e^{-\vec{J}_{p_1}^\top \hat{C}_{pp}(\vec{q}) \vec{J}_{p_2}} - 1 + \vec{J}_{p_1}^\top \hat{C}_{pp}(\vec{q}) \vec{J}_{p_2} \right) e^{i\vec{J}_{q_1} \cdot \vec{q}} \, .
\end{aligned} \tag{7.7}$$

The integration kernel in (7.7) now falls of with q^{-n_s-3}, which greatly improves the numerical speed of convergence. We finally arrive at the numerically better tractable expression for the factors (7.1),

$$\begin{aligned}
I_{21}(\vec{J}_{p_1}, \vec{J}_{p_2}, \vec{J}_{q_1}) = {} & (2\pi)^3 \delta_D\left(\vec{J}_{q_1}\right) + \frac{(\vec{J}_{p_1} \cdot \vec{J}_{q_1})(\vec{J}_{p_2} \cdot \vec{J}_{q_1})}{J_{q_1}^4} P_\delta^{(i)}(J_{q_1}) \\
& + \int_q \left(e^{-\vec{J}_{p_1}^\top \hat{C}_{pp}(\vec{q}) \vec{J}_{p_2}} - 1 + \vec{J}_{p_1}^\top \hat{C}_{pp}(\vec{q}) \vec{J}_{p_2} \right) e^{i\vec{J}_{q_1} \cdot \vec{q}} \, .
\end{aligned} \tag{7.8}$$

7.2 SMALL-SCALE ASYMPTOTICS

In this section, we derive the asymptotics of the factors I_{21} for the limit $|J_{p_1} J_{p_2}| \to \infty$, where possibly also $|J_{q_1}| \to \infty$, provided $\lim \frac{|J_{p_1} J_{p_2}|}{J_{q_1}^2} \neq 0$. To this end, we apply our method for N-dimensional Laplace-Fourier type integrals that we derived in Chapter 4.

We start by choosing the orientation of the coordinate frame such that the vectors $\vec{J}_{p_1}$ are $\vec{J}_{p_2}$ located in the x, z-plane. Thus, the we can represent these vectors as follows

$$\vec{J}_{p_1} = J_{p_1} \begin{pmatrix} \sin\theta' \\ 0 \\ \cos\theta' \end{pmatrix} \quad \text{and} \quad \vec{J}_{p_2} = J_{p_2} \begin{pmatrix} -\sin\theta' \\ 0 \\ \cos\theta' \end{pmatrix} , \tag{7.9}$$

where the angle between $\vec{J}_{p_1}$ and $\vec{J}_{p_2}$ is $2\theta'$. In Figure 7.1 we show a sketch of the orientation of these vectors. Next, we define $\tilde{\mu} := \cos\theta'$ and write the exponent in the integrand of (7.1) with (7.2) as

$$-\vec{J}_{p_1}\hat{C}_{pp}(\vec{q})\vec{J}_{p_2} = -J_{p_1}J_{p_2}\left[\left(q_x^2 - (q_x^2 + q_z^2)\tilde{\mu}^2\right)\frac{a_2(q)}{q^2} + \left(1 - 2\tilde{\mu}^2\right)a_1(q)\right] . \tag{7.10}$$

We now define the function

$$f_{\tilde{\mu}}(\vec{q}) := \left(q_x^2 - (q_x^2 + q_z^2)\tilde{\mu}^2\right)\frac{a_2(q)}{q^2} + \left(1 - 2\tilde{\mu}^2\right)a_1(q) \tag{7.11}$$

and write

$$I_{21}(\vec{J}_{p_1}, \vec{J}_{p_2}, \vec{J}_{q_1}) = \int_q e^{-J_{p1}J_{p2}f_{\tilde{\mu}}(\vec{q}) + i\vec{J}_{q_1}\cdot\vec{q}} . \tag{7.12}$$

This integral has the same structure as the integral (4.66) in our proof of Theorem 4.4 if we set $\lambda = J_{p_1}J_{p_2}$ and $\vec{k} = \vec{J}_{q_1}$. The difference to (4.66) is that we need to find the location(s) of critical point(s) that contribute to the asymptotics expansion (4.78), i.e. the minima of $f_{\tilde{\mu}}$. When the critical point is located at the origin, (7.12) has an asymptotic expansion of the form (4.78).
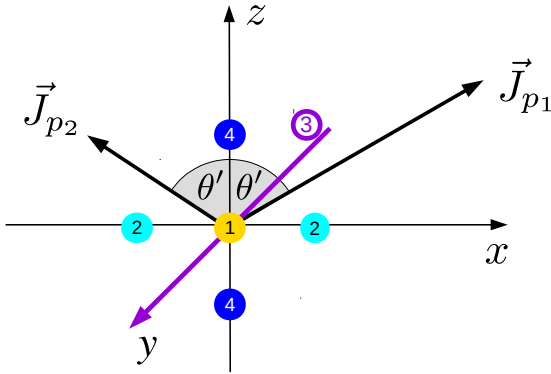
Figure 7.1: The vectors $\vec{J}_{p_1}$ and $\vec{J}_{p_2}$ are turned in the x, z-plane. Both vectors enclose the angle θ' with the z-axis. The location of the critical points are marked with colors and numbers. (1, yellow) is located at the origin. The pair (2, light blue) is located on the x-axis. (3, purple) is critical on the whole y-axis. (4, dark blue) marks the pair of critical points on the z-axis.

7.2.1   *Critical Points*

To identify the local minima of $f_{\tilde{\mu}}$, we first calculate the gradient

$$
\vec{\nabla} f_{\tilde{\mu}}(\vec{q}) = \frac{\vec{q}}{q} \left[\left(q_x^2 - \tilde{\mu}^2(q_x^2 + q_z^2) \right) \left(\frac{a_2'(q)}{q^2} - 2\frac{a_2(q)}{q^3} \right) + (1 - 2\tilde{\mu}^2)\frac{a_2(q)}{q} \right]
$$
$$
+ \begin{pmatrix} 2q_x(1 - \tilde{\mu}^2) \\ 0 \\ -2q_z\tilde{\mu}^2 \end{pmatrix} \frac{a_2(q)}{q^2} \, ,
\tag{7.13}
$$

where we used the relation $a_2(q) = q \cdot a_1'(q)$. By setting the gradient to zero, i.e. $\vec{\nabla} f_{\tilde{\mu}}(q) = 0$, we identify four types of critical points, as derived in Appendix D.1. One critical point is located at the origin and there are pairs of critical points located on the x-axis, on the y-axis, and on the z-axis, respectively. In Appendix D.2, we calculate the Hessian matrix $A = (\vec{\nabla} \otimes \vec{\nabla}) f_{\tilde{\mu}}(q)$ at these critical points. Let us note that, due to our choice of coordinates, the Hessian matrices at the critical points are all diagonal. The signs of the diagonal elements, i.e. the eigenvalues, indicate whether the critical point is a minimum that contributes to the asymptotic approximation of I_{21}. The location of the critical points is sketched in Figure 7.1. In the following, we summarize the properties we find for each critical point.

1. $\vec{q} = (0,0,0)$: For $0 \leq \tilde{\mu}^2 < 1/4$, this critical point is a minimum, since in this case all eigenvalues of the Hessian (D.17),

$$
A^{(0)} = \lim_{q \to 0} \vec{\nabla} \otimes \vec{\nabla} f_{\tilde{\mu}}(\vec{q}) = \frac{\sigma_2^2}{15} \begin{pmatrix} 3 - 4\tilde{\mu}^2 & 0 & 0 \\ 0 & 1 - 2\tilde{\mu}^2 & 0 \\ 0 & 0 & 1 - 4\tilde{\mu}^2 \end{pmatrix} ,
\tag{7.14}
$$

are positive. This critical point is shown in Figure 7.1 as the golden point (1).

2. $\vec{q} = (\pm q_x, 0, 0)$: These two critical points are located on the x-axis, where the location $q_x = q_x(\tilde{\mu})$ is implicitly given by (D.9),

$$
(1 - 2\tilde{\mu}^2)\frac{a_2(q_x)}{q_x} = -(1 - \tilde{\mu}^2)a_2'(q_x) \, .
\tag{7.15}
$$

These critical points are not minima, because the last eigenvalue of the Hessian (D.20),

$$
A^{(x)} = \begin{pmatrix} (1 - \tilde{\mu}^2)a_2''(q_x) + (2 - 3\tilde{\mu}^2)\frac{a_2'(q_x)}{q_x} & 0 & 0 \\ 0 & 2(\tilde{\mu}^2 - 1)\frac{a_2(q_x)}{q_x^2} & 0 \\ 0 & 0 & -2\frac{a_2(q_x)}{q_x^2} \end{pmatrix} , \tag{7.16}
$$

is always negative, given that $a_2(q) > 0$ for all $q > 0$. These critical points are shown in Figure 7.1 as the two light blue points (2).

3. $\vec{q} = (0, \pm q_y, 0)$: For $\tilde{\mu}^2 = 1/2$, all points that are located on the y-axis are critical points of saddle-point type with the Hessian (D.22),

$$A^{(y)} = \frac{a_2(q_y)}{q_y^2} \begin{pmatrix} 1 & 0 & 0 \\ 0 & 0 & 0 \\ 0 & 0 & -1 \end{pmatrix} . \tag{7.17}$$

These critical points are indicated in Figure 7.1 by the purple colored y-axis (3).

4. $\vec{q} = (0, 0, \pm q_z)$: Two critical points are located on the z-axis, where the location $\pm q_z(\tilde{\mu})$ is implicitly given by (D.8),

$$(1 - 2\tilde{\mu}^2)\frac{a_2(q_z)}{q_z} = \tilde{\mu}^2 a_2'(q_z) . \tag{7.18}$$

The Hessian is given by (D.25),

$$A^{(z)} = \begin{pmatrix} 2\frac{a_2(q_z)}{q_z^2} & 0 & 0 \\ 0 & 2\tilde{\mu}^2\frac{a_2(q_z)}{q_z^2} & 0 \\ 0 & 0 & -\tilde{\mu}^2 a_2''(q_z) + (1 - 3\tilde{\mu}^2)\frac{a_2'(q_z)}{q_z} \end{pmatrix} . \tag{7.19}$$

For $\tilde{\mu}^2 \neq 0$, the first two eigenvalues are always positive. When the last eigenvalue is positive, then these two critical points are also minima. These critical points are shown in Figure 7.1 as the two dark blue points (4).

From these results we conclude that for $\tilde{\mu}^2 < 1/4$ the critical point at the origin is the only minimum that contributes to the asymptotics of (7.1). For $\tilde{\mu}^2 > 1/4$, the two critical points located on the z-axis are the contributing minima as can be seen by the eigenvalues shown in Figure 7.3. For $\tilde{\mu}^2 = 1/4$, the critical point at the origin coincides with the critical points on the z-axis with one vanishing eigenvalue. Thus, this critical point is degenerate. The case $\tilde{\mu}^2 = 1/4$ is not captured by our asymptotic method and will be analyzed in future work.

In Figure 7.2, we show the function $f_{\tilde{\mu}}$ (7.11) in the x, z-plane which we derived from a smoothed Bardeen power spectrum for four different values of $\tilde{\mu}^2$. Dark colors indicate smaller values. For $\tilde{\mu}^2 = 0$ (Figure 7.2 (a)) and $\tilde{\mu}^2 = 1/4$ (Figure 7.2 (b)) $f_{\tilde{\mu}}$ has a minimum at the origin. For larger values $\tilde{\mu}^2 = 3/8$ (Figure 7.2 (c)) and $\tilde{\mu}^2 = 5/8$ (Figure 7.2 (d)), $f_{\tilde{\mu}}$ has two minima located on the z-axis, in agreement with our analysis. Note that the minimum for $\tilde{\mu}^2 = 1/4$ (Figure 7.2 (b)) appears elongated along the z-axis, which indicates that this minimum branches out for larger values of $\tilde{\mu}^2$.

In Figure 7.3, we show the eigenvalues of the Hessian at the critical minima as a function of $\tilde{\mu}^2$ which parameterizes the relative orientation of the vectors $\vec{J}_{p_1}$ and $\vec{J}_{p_2}$. In Figure 7.4 we show the location of the critical point q_z that is implicitly given by (7.18) as a function of $\tilde{\mu}^2$. For $\tilde{\mu}^2 < 1/4$, the critical minimum of $f_{\tilde{\mu}}$ is located at the origin, while for $\tilde{\mu}^2 > 1/4$, two critical minima are located at $(0, 0, \pm q_z)$. The inset is a zoom into the transition region $0.2 \leq \tilde{\mu}^2 \leq 0.3$ and shows that q_z increases very steeply for $\tilde{\mu}^2$ slightly above $1/4$.

Now that we have derived the minima of $f_{\tilde{\mu}}$ that contribute to the asymptotics of the factors as well as the corresponding Hessian matrices as a function of the orientation of the two vectors $\vec{J}_{p_1}$ and $\vec{J}_{p_2}$, we derive the asymptotics in the next sections.
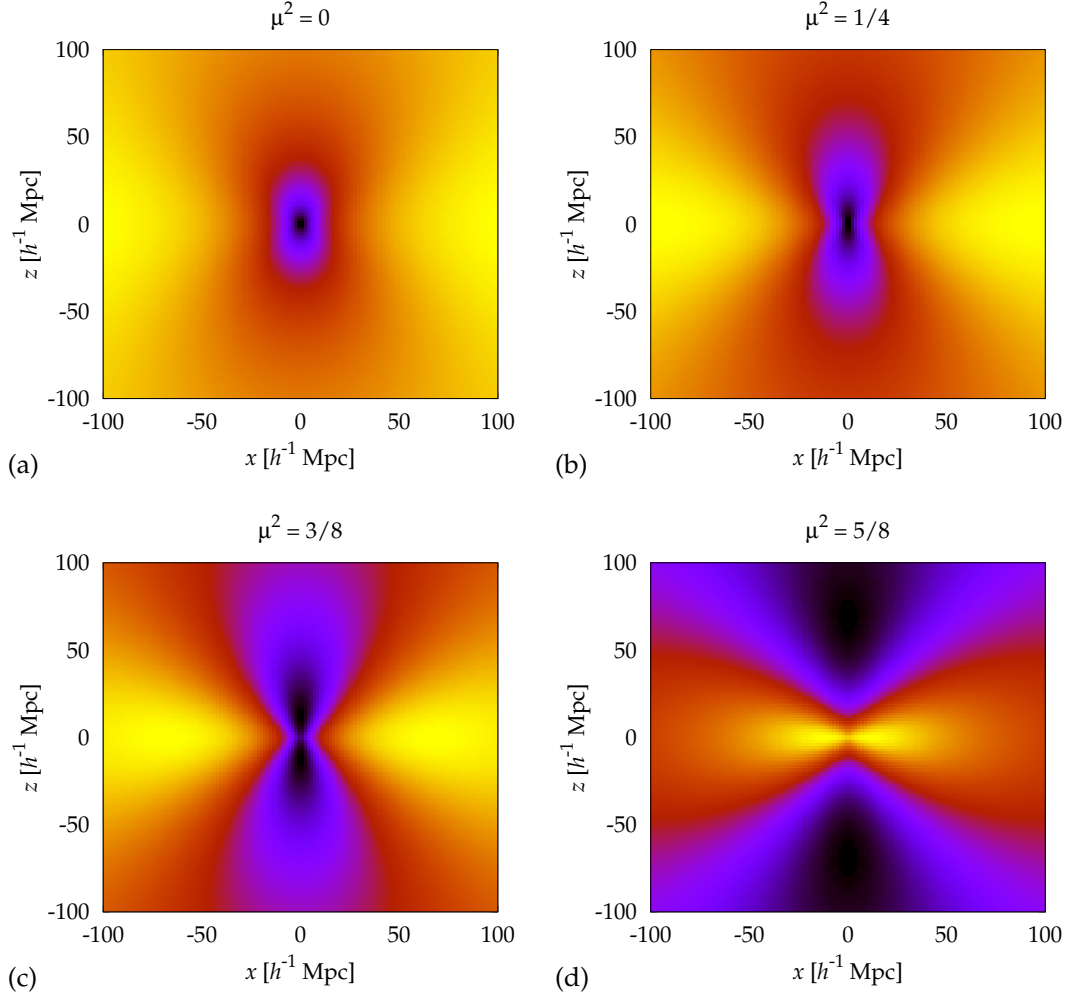
Figure 7.2: The function $f_{\tilde{\mu}}$ (7.11) in the x, z-plane for four different values of $\tilde{\mu}^2$. Dark colors indicate lower values. For $\tilde{\mu}^2 = 0$ (a) and $\tilde{\mu}^2 = 1/4$ (b), $f_{\tilde{\mu}}$ has a minimum at the origin. For larger values $\tilde{\mu}^2 = 3/8$ (c) and $\tilde{\mu}^2 = 5/8$ (d), $f_{\tilde{\mu}}$ has two minima, located at the z-axis. The minimum for $\tilde{\mu}^2 = 1/4$ in (b) appears elongated along the z-axis, which indicates that this minimum branches out for larger values of $\tilde{\mu}^2$. The cosmological and power spectrum parameters are shown in Tables E.2 and E.6, respectively.

7.2.2 *Asymptotics for $\tilde{\mu}^2 < 1/4$:*

For $\tilde{\mu}^2 < 1/4$ the only minimum of $f_{\tilde{\mu}}$ is located at the origin with the value

$$f_{\tilde{\mu}}(0) = -(1 - 2\tilde{\mu}^2)\frac{\sigma_1^2}{3} \tag{7.20}$$

and the Hessian $A = A^{(0)}$ given by (7.14). The asymptotics of (7.1) is given by (4.78) with $\lambda = J_{p1}J_{p2}$ and $\vec{k} = \vec{J}_{q_1}$ and we arrive at

$$
\begin{aligned}
I_{21}\left(\vec{J}_{p_1}, \vec{J}_{p_2}, \vec{J}_{q_1}\right) &= \int_q \exp\left(-\vec{J}_{p_1}\hat{C}_{pp}(\vec{q})\vec{J}_{p_2} + i\vec{J}_{q_1} \cdot \vec{q}\right) \\
&\sim (2\pi)^{3/2}\frac{e^{-J_{p_1}J_{p_2}f_{\tilde{\mu}}(0)}}{\sqrt{\det A}}e^{-\frac{\vec{J}_{q_1}^{\mathsf{T}}A^{-1}\vec{J}_{q_1}}{2J_{p_1}J_{p_2}}},
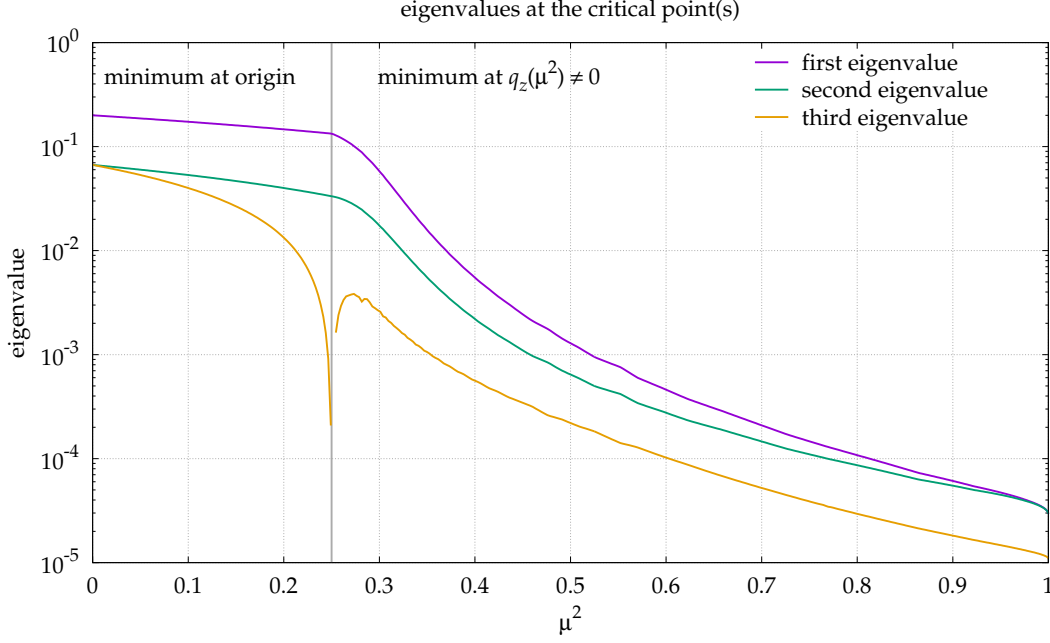\end{aligned}
\tag{7.21}
$$

Figure 7.3: The eigenvalues of the Hessian of $f_{\tilde{\mu}}$ at the critical minimum. For $\tilde{\mu}^2 < 1/4$, the critical minimum is located at the origin and the eigenvalues are the diagonal elements of (7.14). For $\tilde{\mu}^2 > 1/4$, two critical minima are located at $(0, 0, \pm q_z)$, where q_z is implicitly given by (7.18) and the eigenvalues are the diagonal elements of (7.19). In Figure 7.4, q_z is shown as a function of $\tilde{\mu}^2$. At $\tilde{\mu}^2 = 1/4$, the third eigenvalue is zero, indicating a degenerate critical point at the origin. We used the parameters as in Figure 7.2.

as $|J_{p_1} J_{p_2}| \to \infty$, where possibly also $|J_{q_1}| \to \infty$, provided $\lim \frac{|J_{p_1} J_{p_2}|}{J_{q_1}^2} \neq 0$. Using (7.20) and (7.14) yields

$$
I_{21}\left(\vec{J}_{p_1}, \vec{J}_{p_2}, \vec{J}_{q_1}\right) \sim \left(2\pi \frac{15}{J_{p_1} J_{p_2} \sigma_2^2}\right)^{3/2} \frac{\exp\left(J_{p_1} J_{p_2} \frac{\sigma_1^2}{3}(1 - 2\tilde{\mu}^2)\right)}{\sqrt{(3 - 4\tilde{\mu}^2)(1 - 2\tilde{\mu}^2)(1 - 4\tilde{\mu}^2)}}
$$
$$
\times \exp\left(-\frac{15}{2\sigma_2^2 J_{p_1} J_{p_2}}\left(\frac{J_{q_1,x}^2}{3 - 4\tilde{\mu}^2} + \frac{J_{q_1,y}^2}{1 - 2\tilde{\mu}^2} + \frac{J_{q_1,z}^2}{1 - 4\tilde{\mu}^2}\right)\right), \tag{7.22}
$$

as $|J_{p_1} J_{p_2}| \to \infty$, where possibly also $|J_{q_1}| \to \infty$, provided $\lim \frac{|J_{p_1} J_{p_2}|}{J_{q_1}^2} \neq 0$.

7.2.3 *Asymptotics for $\tilde{\mu}^2 > 1/4$:*

For $\tilde{\mu}^2 > \frac{1}{4}$ we found that the two minima located at $(0, 0, \pm q_z)$, where $q_z(\tilde{\mu})$ is implicitly given by (7.18), contribute to the asymptotics of 7.1. If q_z is not infinitesimally small, we consider the two contributions

$$
I_{21}\left(\vec{J}_{p_1}, \vec{J}_{p_2}, \vec{J}_{q_1}\right) \sim \left(\int_{\Omega^-} + \int_{\Omega^+}\right) e^{-\vec{J}_{p_1}^{\top} \hat{C}_{pp}(\vec{q}) \vec{J}_{p_2} + i\vec{J}_{q_1} \cdot \vec{q}}, \tag{7.23}
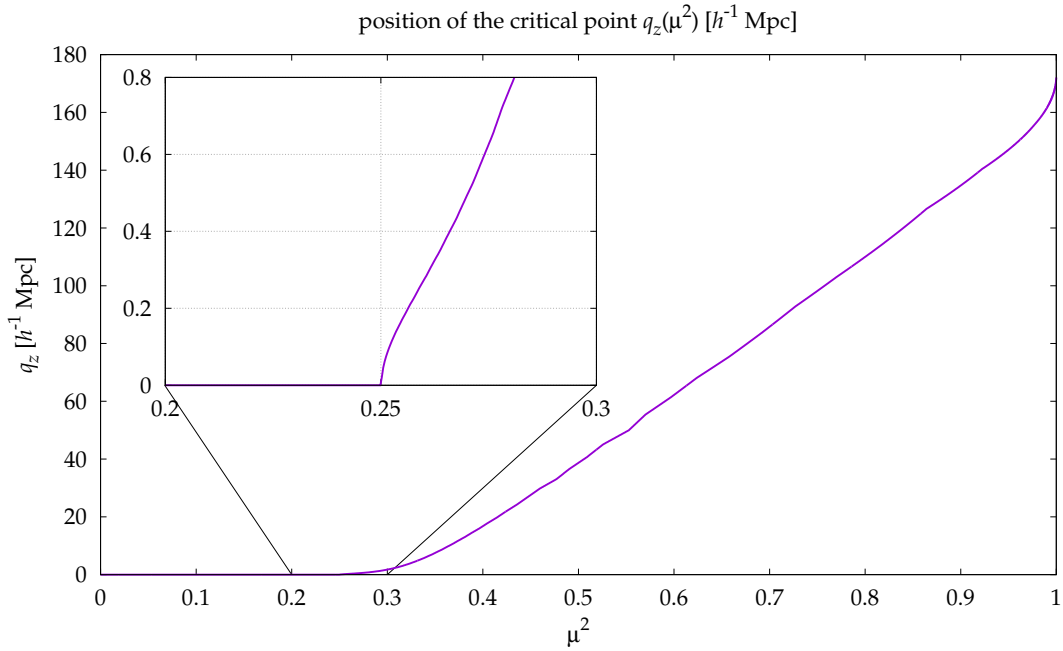$$

Figure 7.4: The location of the critical minima of $f_{\tilde{\mu}}$ as a function of $\tilde{\mu}^2$ is shown. For $\tilde{\mu}^2 < 1/4$, the critical minimum of $f_{\tilde{\mu}}$ is located at the origin, while for $\tilde{\mu}^2 > 1/4$, two critical minima are located at $(0,0,\pm q_z)$. The zoom into the transition region $0.2 \leq \tilde{\mu}^2 \leq 0.3$ shows that q_z increases very steep for $\tilde{\mu}^2$ slightly above $1/4$. We used the parameters as in Figures 7.2 and 7.2.

where $\Omega^\pm$ denote small, non-overlapping neigborhoods of the minima at $(0,0,\pm q_z)$, and $\Omega^- \cap \Omega^+ = \varnothing$.[1] We define $\vec{q}_z := (0,0,q_z)$ and shift the coordinate frame $\vec{q} \to \pm\vec{q}_z$ of both integrals, such that the respective critical point is located at the origin

$$I_{21}\left(\vec{J}_{p_1}, \vec{J}_{p_2}, \vec{J}_{q_1}\right) \sim \int_{\Omega^-} e^{-\vec{J}_{p_1}\hat{C}_{pp}(\vec{q})\vec{J}_{p_2} + i\vec{J}_{q_1}\cdot\vec{q}} + \int_{\Omega^+} e^{-\vec{J}_{p_1}\hat{C}_{pp}(\vec{q})\vec{J}_{p_2} + i\vec{J}_{q_1}\cdot\vec{q}}$$

$$= \int_{\Omega^0} e^{-\vec{J}_{p_1}\hat{C}_{pp}(\vec{q}+\vec{q}_z)\vec{J}_{p_2} + i\vec{J}_{q_1}\cdot(\vec{q}+\vec{q}_z)} + \int_{\Omega^0} e^{-\vec{J}_{p_1}\hat{C}_{pp}(\vec{q}-\vec{q}_z)\vec{J}_{p_2} + i\vec{J}_{q_1}\cdot(\vec{q}-\vec{q}_z)} ,$$

$$(7.24)$$

as $|J_{p_1}J_{p_2}| \to \infty$, where possibly also $|J_{q_1}| \to \infty$, provided $\lim \frac{|J_{p_1}J_{p_2}|}{J_{q_1}^2} \neq 0$. Here, $\Omega_\pm \to \Omega_0$ is a neighborhood of the origin because of the coordinate shift. The asymptotics of (7.24) is given by (4.78) with $\lambda = J_{p1}J_{p2}$, $\vec{k} = \vec{J}_{q_1}$ and $g(0) = e^{\pm i\vec{J}_{q_1}\cdot\vec{q}_z}$,

$$I_{21}\left(\vec{J}_{p_1}, \vec{J}_{p_2}, \vec{J}_{q_1}\right) \sim (2\pi)^{3/2}\frac{e^{-J_{p_1}J_{p_2}f_{\tilde{\mu}}(q_z)}}{\sqrt{\det A(q_z)}}e^{-\frac{\vec{J}_{q_1}^\top A^{-1}(q_z)\vec{J}_{q_1}}{2J_{p_1}J_{p_2}}}\left(e^{i\vec{J}_{q_1}\cdot\vec{q}_z} + e^{-i\vec{J}_{q_1}\cdot\vec{q}_z}\right) \quad (7.25)$$

$$= 2\cos\left(\vec{J}_{q_1}\cdot\vec{q}_z\right)(2\pi)^{3/2}\frac{e^{-J_{p_1}J_{p_2}f_{\tilde{\mu}}(q_z)}}{\sqrt{\det A(q_z)}}e^{-\frac{\vec{J}_{q_1}^\top A^{-1}(q_z)\vec{J}_{q_1}}{2J_{p_1}J_{p_2}}} , \quad (7.26)$$

as $|J_{p_1}J_{p_2}| \to \infty$, where possibly also $|J_{q_1}| \to \infty$, provided $\lim \frac{|J_{p_1}J_{p_2}|}{J_{q_1}^2} \neq 0$, where

$$f_{\tilde{\mu}}(q_z^\pm) = -\tilde{\mu}^2 a_2(q_z) - (1 - 2\tilde{\mu}^2)a_1(q_z) , \quad (7.27)$$

---

1 In the book *Asymptotic Expansions of Integrals*, Bleistein and Handelsman discuss the case of two nearby saddle-points. [12]

$q_z(\tilde{\mu})$ is implicitly given by (7.18), and the Hessian $A = A^{(z)}$ is given by (7.19).

7.3 SUMMARY AND DISCUSSION

In this chapter, we derived several aspects of the factors of the free generating functional, relevant for their numerical implementation, analytical considerations and future developments of KFT.

In the first part, we showed how the integrand can be regularized, without introducing any approximation, such that numerical integrations of the factors converge faster.

In the second part, we derived the asymptotics of the factors for large values of $|J_{p_1}J_{p_2}|$ and possibly large values of $|J_{q_1}|$, provided $\lim \frac{|J_{p_1}J_{p_2}|}{J_{q_1}^2} \neq 0$. We showed that the asymptotics depends on the locations q_z of the critical minima of $f_{\tilde{\mu}}$. These locations are parameterized by the angle that the vectors $\vec{J}_{p_1}$ and $\vec{J}_{p_2}$ enclose. When this angle is larger than $2\pi/3$, the single critical minimum that contributes to the asymptotics is located at the origin. For angles smaller than $2\pi/3$, the two contributing minima are located symmetrically along the axis that cuts the angle of those vectors in halves. In both cases, the asymptotics involves an exponential factor that depends on the value of $f_{\tilde{\mu}}$ at the critical points. This has the important consequence for numerical implementations, that any numerical deviation of $f_{\tilde{\mu}}$ from the true value leads to exponentially deviating results when $|J_{p_1}J_{p_2}|$ becomes larger. Furthermore, since the asymptotics depends on the eigenvalues of the Hessian at the critical points, we advice that for any numerical implementation that aims at the evaluation of the factors at large values of $|J_{p_1}J_{p_2}|$, the function $f_{\tilde{\mu}}$ should be implemented as precisely as possible up to second order in the vicinity of the critical points. Moreover, we suggest for $\tilde{\mu}^2 > 1/4$ to split the integration domain and center the two domains on the critical points, respectively. Note that these numerical considerations are similar to our conclusions for the free power spectrum in the previous chapter. First tests for $\tilde{\mu}^2 < 1/4$ (not shown in this work) showed that the analytical prediction for the asymptotics agree with the numerical results.

When the vectors $\vec{J}_{p_1}$ and $\vec{J}_{p_2}$ enclose an angle of exactly $2\pi/3$, the single minimum at the origin is degenerate and the Hessian matrix A is not positive definite. Since our asymptotic method in N dimensions is built upon Morse's Lemma, it requires A to be positive definite, thus we cannot apply this method in this case. We propose that the application of the splitting lemma, as explained below, will enable us to derive the asymptotics for this relative orientation of $\vec{J}_{p_1}$ and $\vec{J}_{p_2}$. These factors are particularly interesting as they appear in the free bispectrum when the wave vectors are equilateral.

Recent and ongoing work in our group by BSc student Tara Butler [16] and MSc student Christian Sorgenfrei is dedicated to the numerical implementation of the factors and we are looking forward to compare our analytical asymptotics to the upcoming numerical results.

As already mentioned, the free moments of the density field can be expressed as convolutions of the factors that we discussed here. With this work, we hope to facilitate the numerical implementation of the factors such that higher order moments can be calculated. However, the main limitation of our result with respect to the

implementation of convolutions of the factors concerns the restriction $\lim \frac{|J_{p_1}J_{p_2}|}{J_{q_1}^2} \neq 0$, for the following reason. When the free moments are calculated, the convolution has to be performed by integrating over those vectors that are contained in the oscillating phase, while the two vectors $\vec{J}_{p_1}$ and $\vec{J}_{p_2}$ are fixed. Thus, when performing the integral, the factors need to be evaluated at values of $|\vec{J}_{q_1}|$ that are large compared to $|J_{p_1}J_{p_2}|$, which is not covered by our asymptotic expansion. It is subject to future work to explore asymptotic methods – likely based on the saddle-point approximation – that deal with this limit.

When we are interested in the small-scale asymptotics of the free moments of order l of the density field, we could follow another strategy. Instead of deriving the asymptotics from a convolution of the factors, one could think of deriving the asymptotics directly from the free generating functional (3.120) prior to factorization. For large absolute values of the $\mathbf{L}_p$ one would then like to apply our Theorem for N-dimensional Fourier-Laplace type integrals to the $3(l-1)$-dimensional integration over the particle separations $\vec{q}_{j1}$ for $1 < j \leq l$. However, as shown by Ricardo Waibel in his ongoing MSc work, the $3(l-1) \times 3(l-1)$-dimensional Hessian of the function $\mathbf{L}_p^\intercal C_{pp}(\mathbf{q})\mathbf{L}_p$ appearing in the exponent of the integrand (3.120) is in general not positive definite for $l > 2$, i.e. for three-point correlations and higher orders. Moreover, it was shown that the rank of the Hessian for $l \geq 4$ never exceeds 6. We thus cannot straightforwardly apply our asymptotic method for N-dimensional Fourier-Laplace type integrals for moments of order ≥ 3.

In ongoing work with Ricardo Waibel we are working on a way to deal with these non-vanishing co-ranks of the Hessian. The idea is to apply the splitting lemma [54] to find a coordinate transform in the neighborhoods of the critical points such that the function in the exponent splits into a quadratic part with Hessian A and an independent higher-order part h, $\mathbf{L}_p^\intercal C_{pp}(\mathbf{q})\mathbf{L}_p \to (y_1, \cdots, y_j)A(y_1, \cdots, y_j)^\intercal + h(y_{j+1}, \cdots, y_{3(l-1)})$. Then, we can apply our existing method to the j-dimensional integral over the quadratic part and deal with the remaining $[3(l-1) - j]$-dimensional part separately. Thus, we hope to extend the results of this work in the future to formally derive the asymptotics of free density moments of arbitrary order. These are relevant to test the evolution of non-Gaussianities, to improve the implementations of perturbation theory and mean field theory in KFT, and also to test the k^{-3} asymptotics that we derived in the previous chapter for the free power spectrum when gravitational interactions beyond the Zel'dovich approximation are taken into account.

CONCLUSIONS AND OUTLOOK

In this work, we analytically investigated cosmic structure formation in collisionless dark matter in the limit of small scales within the framework of Kinetic Field Theory (KFT).

Our main result is the derivation of the universal k^{-3} asymptotics of the free density fluctuation power spectrum. This asymptotic behavior emerges independently of the steepness of the initial power spectrum, provided its second moment σ_2^2 exists. In this case, the k^{-3} asymptotics emerges substantially earlier than dark-matter streams cross.

Our result therefore suggests that for dark matter types with initially steeply decreasing power spectra, linearly evolved power spectra poorly describe the actual power spectrum at scales smaller than the cutoff scale, even at early times.

Furthermore, we calculated the time-dependent characteristic wave number above which the power spectrum converges to the k^{-3} behavior. This characteristic wave number might be related to a scale in real space, below which dark matter forms self-similar structures. It is subject to future work to explore this possibility and the connection to the observed universal halo profiles by comparisons to numerical simulation and further analytical considerations. For the latter, we will consider the time evolved momentum-density correlation functions that have been firstly derived in [42]. These give information about the velocity dispersion on different scales, while the small-scale asymptotics can be calculated similarly to the free power spectrum which will be done systematically in future work.

In this work, we also derived several scales that are associated to small-scale stream crossing. If cosmic structure formation before shell crossing is well described by the Zel'dovich approximation, these scales might not only be imprinted in the structures at the small-scale stream crossing redshift of dark matter, but also influence the growth of later structures. In this case, cosmic observables could be linked to these scales which in turn are directly linked to the properties of dark matter. Consequently, these observables then serve as probes for dark matter particle candidates. The small-scale stream crossing redshift of dark matter might even mark a cosmic distance promising to search for dark matter annihilation signals [19, 26, 61] as the densities at these scale factors where higher and the initial slopes of halo cores presumably steeper, as suggested by simulations [48].

With the successful implementation of a numerical code, guided by our knowledge about the asymptotics, we are now able to calculate the free power spectrum for a wide range of cosmological parameters, dark matter models and redshifts. This code will be published in the near future to enable a larger community to calculate non-linear Zel'dovich power spectra for various dark matter models at arbitrary scales and a wide range of redshifts. A next step will be to evaluate the free power spectrum for specific non-cold dark matter models and compare these spectra to results from simulations. This is particularly interesting, because a growing number of simulation results in warm dark matter cosmologies is available enabling quantitative comparisons by some range of parameters (see e.g. [21, 43, 62]).

To arrive at these results, we derived novel asymptotic methods for rapidly oscillating integrals with two large parameters. While we successfully applied these methods to integrals appearing in KFT, they may also find applications in other research fields. Compared to our method in one dimension, the method for N-dimensional integrals in its current form is more restrictive in its assumptions on the behavior of the kernel function. Moreover, the N-dimensional method does not provide a straightforward way to derive terms beyond the first order asymptotics. In order to derive the asymptotic series for the free power spectrum, we therefore applied the one-dimensional method to the integral over the radial coordinate. It will be subject to future work to explore if this strategy can be formally generalized for our N-dimensional method.

In this work, we investigated the free power spectrum for particles on straight trajectories when only Gaussian initial momentum-momentum correlations are taken into account. It is subject to future work to explore if these results change when additionally initial density-density and momentum-density correlations are considered. Furthermore, it will be interesting to find out if the k^{-3} asymptotics remains valid when interactions beyond the Zel'dovich approximation are taken into account. Since KFT remains valid beyond shell crossing, this is the perfect framework for such a future study.

In order to evaluate the terms in the perturbation series in future work, we need to evaluate free density moments of high order. These moments are also important in other aspects. Firstly, they probe the early formation of non-Gaussianities. And secondly, 2n-point correlation functions are in general necessary to determine the likelihood of a cosmological model from measured n-point correlation functions. With the factorized generating functional, we have in principle a representation of the free density moments that can be implemented straightforwardly from an algorithmic point of view. However, the implementation of the factors of the generating functional for general alignments and absolute values of the involved vectors is difficult due to the rapidly oscillating integral. To facilitate this implementation, we presented a way how the integration can be regularized non-perturbatively by adding and subtracting a term that is linear in the initial power spectrum. Moreover, we derived the asymptotics of these factors at small scales. However, our asymptotic method does not provide a limit when only the vector appearing in the complex phase of the integration kernel becomes large. It is subject to future work to find or develop an asymptotic method which is appropriate for this case. Once the factors can be computed for arbitrary vectors, we are able to calculate the free density moments of high orders by convolutions of these factors and thus calculate higher order terms in perturbation theory.

To summarize, we provided novel mathematical tools that apply to KFT and beyond. We derived the small-scale asymptotics of the cosmic density fluctuation power spectrum and the scales characteristic for small-scale stream crossing. With these results we lay the foundations for future work to constrain possible dark matter candidates from observations and to understand the formation of universal halo density profiles in simulations. Finally, our asymptotics results will guide the numerical implementation of KFT such that the plethora of existing expressions for higher order correlation functions and perturbation series can eventually be numerically evaluated.

Part III

APPENDIX

APPENDIX: KINETIC FIELD THEORY FOR COSMIC STRUCTURE FORMATION

A.1 DERIVATION OF THE HAMILTONIAN PROPAGATOR

We start with the modified free Hamiltonian

$$\mathcal{H}_0' = \frac{\mathbf{p}^2}{2m(t)} - \langle \mathbf{K}, \mathcal{J}\mathbf{x} \rangle \,, \tag{A.1}$$

satisfying the following equations of motion.

$$\dot{\mathbf{q}} = \partial_p \mathcal{H}_0' = \frac{1}{m(t)}\mathbf{p} - \mathbf{K}_q \tag{A.2}$$

$$\dot{\mathbf{p}} = -\partial_q \mathcal{H}_0' = -\mathbf{K}_p \,. \tag{A.3}$$

We integrate (A.3) directly and obtain

$$\mathbf{p}(t) = \mathbf{p}^{(i)} - \int_{t_i}^{t} dt' \, \mathbf{K}_p(t) \,, \tag{A.4}$$

where $\mathbf{p}^{(i)}$ are the initial momenta at time $t = t_i$. With (A.4), we integrate (A.2)

$$
\begin{aligned}
\mathbf{q}(t) &= \mathbf{q}^{(i)} + \int_{t_i}^{t} dt' \left[\frac{1}{m(t')}\mathbf{p}(t') - \mathbf{K}_q(t') \right] \\
&= \mathbf{q}^{(i)} + \int_{t_i}^{t} dt' \left[\frac{1}{m(t')} \left(\mathbf{p}^{(i)} - \int_{t_i}^{t'} dt'' \, \mathbf{K}_p(t'') \right) - \mathbf{K}_q(t') \right] \\
&= \mathbf{q}^{(i)} + \mathbf{p}^{(i)} \int_{t_i}^{t} \frac{dt'}{m(t')} - \int_{t_i}^{t} dt' \left[\mathbf{K}_q(t') + \frac{1}{m(t')} \int_{t_i}^{t'} dt'' \, \mathbf{K}_p(t'') \right] \,.
\end{aligned} \tag{A.5}
$$

By partial integration, we obtain

$$
\begin{aligned}
\int_{t_i}^{t} \frac{dt'}{m(t')} \int_{t_i}^{t'} dt'' \, \mathbf{K}_p(t'') &= \int_{t_i}^{t'} dt'' \, \mathbf{K}_p(t'') \int_{t_i}^{t'} \frac{dt''}{m(t'')} \bigg|_{t'=t_i}^{t'=t} - \int_{t_i}^{t} dt' \, \mathbf{K}_p(t') \int_{t_i}^{t'} \frac{dt''}{m(t'')} \\
&= \int_{t_i}^{t} dt' \, \mathbf{K}_p(t') \int_{t_i}^{t} \frac{dt'}{m(t')} - \int_{t_i}^{t} dt' \, \mathbf{K}_p(t') \int_{t_i}^{t'} \frac{dt''}{m(t'')} \\
&= \int_{t_i}^{t} dt' \, \mathbf{K}_p(t') \left[\int_{t_i}^{t} \frac{dt'}{m(t')} - \int_{t_i}^{t'} \frac{dt''}{m(t'')} \right] \\
&= \int_{t_i}^{t} dt' \, \mathbf{K}_p(t') \int_{t'}^{t} \frac{dt''}{m(t'')} \,.
\end{aligned} \tag{A.6}
$$

We define the propagator

$$g_{qp}(t, t') := \int_{t'}^{t} \frac{dt''}{m(t'')} \,, \tag{A.7}$$

and write (A.5) as

$$\mathbf{q}(t) = \mathbf{q}^{(i)} + g_{qp}(t,t_i)\mathbf{p}^{(i)} - \int_{t_i}^{t} dt' \left[\mathbf{K}_q(t') + g_{qp}(t,t')\mathbf{K}_p(t') \right] . \tag{A.8}$$

A.2   HAMILTONIAN FOR PARTICLES IN AN EXPANDING SPACETIME

This section is a review of the derivations shown in [50] and [5].
We start with the Lagrangian of an individual particle with mass m_0 in a gravitational field Φ, where space expands isotropically accordingly to the scale factor $a(t)$

$$L(\vec{q}, \dot{\vec{q}}, t) = \frac{1}{2} m \left(a(t)\dot{\vec{q}} + \dot{a}(t)\vec{q} \right)^2 - m_0 \Phi(\vec{q}, t) . \tag{A.9}$$

Here, $\vec{q} = \vec{r}/a$ denotes the comoving coordinate relative to the physical spatial coordinate $\vec{r}$. We apply the canonical transformation

$$L \rightarrow L - \frac{1}{2} \frac{d}{dt} m_0 a\dot{a}q^2 , \tag{A.10}$$

such that the Lagrangian (A.9) reduces to

$$L(\vec{q}, \dot{\vec{q}}, t) = \frac{1}{2} m_0 a^2(t)\dot{q}^2 - m_0 \phi(\vec{q}, t) , \tag{A.11}$$

with the new potential

$$\phi(\vec{q}, t) = \Phi(\vec{q}, t) + \frac{1}{2} a\ddot{a}q^2 . \tag{A.12}$$

The potential satisfies Poisson's equation

$$\Delta \phi(\vec{q}, t) = \frac{4\pi G}{a(t)} \left[\rho_m(\vec{q}, t) - \bar{\rho}_m \right] , \tag{A.13}$$

where ρ_m denotes the comoving mass density and $\bar{\rho}_m$ the average comoving mass density, which is constant in time. (A.13) can be solved with the Green's function that corresponds to the Laplacian in three dimensions,

$$\phi(\vec{q}, t) = -\frac{4\pi G}{a(t)} \int d^3q' \frac{\rho_m(\vec{q}', t) - \bar{\rho}_m}{|\vec{q}' - \vec{q}|} . \tag{A.14}$$

In the point particle picture, the comoving mass density is

$$\rho_m(\vec{q}, t) = m_0 \sum_j \delta_D \left(\vec{q} - \vec{q}_j(t) \right) , \tag{A.15}$$

where the one-particle contribution to the comoving mass density is

$$\rho_{m,j}(\vec{q}, t) = m_0 \delta_D \left(\vec{q} - \vec{q}_j(t) \right) . \tag{A.16}$$

We now define the linear growth factor as new time coordinate $\tau := D_+(t) - D_+(t^{(i)})$. The total differential is given by

$$d\tau = dD_+ = \frac{dD_+}{da} \frac{da}{dt} dt = HD_+ f dt , \tag{A.17}$$

and time derivatives are related by

$$\frac{\mathrm{d}}{\mathrm{d}t} = HD_+ f \frac{\mathrm{d}}{\mathrm{d}\tau} ,\tag{A.18}$$

where H and f denote the usual Hubble function and growth rate, respectively,

$$H = \frac{1}{a}\frac{\mathrm{d}}{\mathrm{d}t}a \quad \text{and} \quad f = \frac{\mathrm{d}\log D_+}{\mathrm{d}\log a} ,\tag{A.19}$$

and H_0 is the value of H evaluated at the time when $a = 1$. Thus, first-order time derivatives transform as

$$\dot{\vec{x}} = \frac{\mathrm{d}\vec{x}}{\mathrm{d}t} = HD_+ f \frac{\mathrm{d}\vec{x}}{\mathrm{d}\tau} .\tag{A.20}$$

Transforming the Lagrangian to the new time coordinate yields

$$L\left(\vec{q}, \frac{\mathrm{d}\vec{q}}{\mathrm{d}\tau}, \tau\right) = \frac{1}{2}ma^2 HD_+ f \left(\frac{\mathrm{d}\vec{q}}{\mathrm{d}\tau}\right)^2 - \frac{m\phi(\vec{q}, \tau)}{HD_+ f} .\tag{A.21}$$

From now on we use the dot for the derivative with respect to the new time coordinate, which we rename back to t and divide the Lagrangian by the constant factor $m_0 H_0$. We define the time-dependent particle mass and the new potential

$$\dot{\vec{q}} := \frac{\mathrm{d}\vec{q}}{\mathrm{d}t} ,\tag{A.22}$$

$$m(t) := a^2 \frac{H}{H_0} D_+ f ,\tag{A.23}$$

$$\varphi(\vec{q}, t) := \frac{a^2 \phi(\vec{q}, t)}{H_0^2 m(t)} .\tag{A.24}$$

With the generalized momentum

$$\vec{p} = \frac{\partial L}{\partial \dot{\vec{q}}} = m(t)\dot{\vec{q}} ,\tag{A.25}$$

we obtain the Hamiltonian of a single particle

$$\mathcal{H} = \vec{p} \cdot \dot{\vec{q}} - L = \frac{\vec{p}^2}{2m(t)} + \varphi(\vec{q}, t) ,\tag{A.26}$$

and the Hamiltonian e.o.m.

$$\dot{\vec{q}} = \frac{\vec{p}}{m(t)}, \quad \dot{\vec{p}} = -\vec{\nabla}\varphi .\tag{A.27}$$

A.3   DERIVATION OF THE INTERACTION POTENTIAL

We consider a general interaction Hamiltonian $\mathcal{H}_I$ that depends only on the pairwise distances of particles, such that we can write

$$\begin{aligned}
\mathcal{H}_I(\mathbf{q}, t) &= A(t) \sum_{1 \leq i < j \leq N} v\left(|\vec{q}_i(t) - \vec{q}_j(t)|\right) \\
&= A(t) \int \mathrm{d}^3 z \mathrm{d}^3 y\, v\left(|\vec{z} - \vec{y}|\right) \sum_{1 \leq i < j \leq N} \delta_D\left(\vec{y} - \vec{q}_i(t)\right) \delta_D(\vec{z} - \vec{q}_j(t)) ,
\end{aligned}\tag{A.28}$$

where $A(t)$ is a time-dependent amplitude. The potential part of the interaction Lagrangian (3.76) then becomes

$$
\begin{aligned}
\mathcal{V}(\chi_p, \mathbf{q}) &= -\langle \chi_p, \nabla_q \mathcal{H}_I(\mathbf{q}, t) \rangle \\
&= -A(t) \int \mathrm{d}^3 z \mathrm{d}^3 y \left\{ v\left(|\vec{z} - \vec{y}|\right) \times \right. \\
&\qquad \left. \sum_{k=1}^{N} \vec{\chi}_{p_k} \cdot \vec{\nabla}_{q_k} \sum_{1 \leq i < j \leq N} \delta_D\left(\vec{y} - \vec{q}_i(t)\right) \delta_D(\vec{z} - \vec{q}_j(t)) \right\} .
\end{aligned}
\tag{A.29}
$$

Applying the derivatives to the sum, we get

$$
\begin{aligned}
&\vec{\chi}_{p_k} \cdot \vec{\nabla}_{q_k} \sum_{1 \leq i < j \leq N} \delta_D\left(\vec{y} - \vec{q}_i\right) \delta_D(\vec{z} - \vec{q}_j) \\
&= \sum_{1 \leq i < k} \delta_D\left(\vec{y} - \vec{q}_i\right) \vec{\chi}_{p_k} \cdot \vec{\nabla}_{q_k} \delta_D\left(\vec{z} - \vec{q}_k\right) \\
&\quad + \sum_{k < j \leq N} \delta_D(\vec{z} - \vec{q}_j) \vec{\chi}_{p_k} \cdot \vec{\nabla}_{q_k} \delta_D\left(\vec{y} - \vec{q}_k\right) .
\end{aligned}
\tag{A.30}
$$

Since the interaction potential depends only on the absolute value of the coordinate difference, we can interchange the integration variables $\vec{y}$ and $\vec{z}$ in the above sum,

$$
\begin{aligned}
\mathcal{V}(\chi_p, \mathbf{q}) &= -A(t) \int \mathrm{d}^3 z \mathrm{d}^3 y \left\{ v\left(|\vec{z} - \vec{y}|\right) \times \right. \\
&\qquad \left. \sum_{k=1}^{N} \sum_{i \neq k} \delta_D\left(\vec{y} - \vec{q}_i\right) \vec{\chi}_{p_k} \cdot \vec{\nabla}_{q_k} \delta_D\left(\vec{z} - \vec{q}_k\right) \right\} .
\end{aligned}
\tag{A.31}
$$

Expressing the interaction potential and the Dirac delta distributions in terms of their Fourier transforms, we can write

$$
\begin{aligned}
\mathcal{V}(\chi_p, \mathbf{q}) &= -A(t) \int_k \hat{v}(\vec{k}) \sum_{k=1}^{N} \sum_{i \neq k} \left(-\mathrm{i} \vec{\chi}_{p_k} \cdot \vec{k}\right) \mathrm{e}^{\mathrm{i}\vec{k} \cdot \vec{q}_i(t)} \mathrm{e}^{-\mathrm{i}\vec{k} \cdot \vec{q}_k(t)} \\
&= -A(t) \sum_{k=1}^{N} \sum_{i \neq k} \int_k \tilde{\rho}_i(\vec{k}, t) \hat{v}(\vec{k}) \left(-\mathrm{i} \vec{\chi}_{p_k} \cdot \vec{k}\right) \tilde{\rho}_k(-\vec{k}, t) ,
\end{aligned}
\tag{A.32}
$$

where we expressed the exponentials in terms of the Fourier transform of the one-particle densities (3.26) in the last step.

A.4   PROPAGATOR-CORRECTION OPERATOR

We start with the full generating functional

$$
Z[\mathbf{J}, \mathbf{K}] = \mathrm{e}^{\mathrm{i}\hat{S}_I} Z_0[\mathbf{J}, \mathbf{K}] ,
\tag{A.33}
$$

where the free generating functional is

$$
Z_0[\mathbf{J}, \mathbf{K}] = \exp\left[\mathrm{i} \int_0^\infty \mathrm{d}t \langle \mathbf{J}(t), \mathbf{x}_0(t) \rangle - \mathrm{i} \int_0^\infty \mathrm{d}t \, \mathrm{d}t' \langle \mathbf{J}(t), \mathcal{G}(t, t') \mathbf{K}(t') \rangle \right] .
\tag{A.34}
$$

We now consider only the propagator correction part of the interaction operator,

$$
\mathrm{i}\hat{S}_I^{\mathcal{C}} = \mathrm{i} \int_0^\infty \mathrm{d}t \left\langle \frac{\delta}{\delta \mathbf{K}_q(t)}, \frac{\delta}{\delta \mathbf{J}_p(t)} \right\rangle \left(\frac{1}{m(t)} - 1\right) ,
\tag{A.35}
$$

such that the first-order correction to particle trajectories are

$$
\begin{aligned}
\mathbf{q}^{(1)}(t) &= \mathrm{i}\hat{S}_I^{\mathcal{C}}\left(-\mathrm{i}\frac{\delta}{\delta\mathbf{J}_q(t)}\right) Z_0[\mathbf{J},\mathbf{K}]\big|_{\mathbf{J}=0=\mathbf{K}} \\
&= \int_0^\infty \mathrm{d}t'\left\langle \frac{\delta}{\delta\mathbf{K}_q(t)}, \frac{\delta}{\delta\mathbf{J}_p(t)}\right\rangle \frac{\delta}{\delta\mathbf{J}_p(t')}\left(\frac{1}{m(t')}-1\right) Z_0[\mathbf{J},\mathbf{K}]\big|_{\mathbf{J}=0=\mathbf{K}} \\
&= \mathrm{i}\int_0^\infty \mathrm{d}t'\left\langle \frac{\delta}{\delta\mathbf{K}_q(t)}, \frac{\delta}{\delta\mathbf{J}_p(t)}\right\rangle\left(\frac{1}{m(t')}-1\right)\left[\mathbf{p}^{(\mathrm{i})}-\int_0^\infty \mathrm{d}t'' g_{pp}(t,t'')\mathbf{K}_p(t'')\right] Z_0[\mathbf{J},\mathbf{K}]\big|_{\mathbf{J}=0=\mathbf{K}} \\
&= -\int_0^\infty \mathrm{d}t'\left\{ \frac{\delta}{\delta\mathbf{K}_q(t')}\left(\frac{1}{m(t')}-1\right)\left[\mathbf{p}^{(\mathrm{i})}-\int_0^\infty \mathrm{d}t'' g_{pp}(t',t'')\mathbf{K}_p(t'')\right]\right. \\
&\qquad\qquad \left. \times \left[\mathbf{q}^{(\mathrm{i})}+g_{qp}(t,0)\mathbf{p}^{(\mathrm{i})}-\int_0^\infty \mathrm{d}t'' \mathcal{G}_{qa}(t,t'')\mathbf{K}_a(t'')\right]\right\} Z_0[\mathbf{J},\mathbf{K}]\big|_{\mathbf{J}=0=\mathbf{K}},
\end{aligned}
$$

(A.36)

where we used $g_{pq}=0$, and summation over $a\in\{q,p\}$ is implied in the last line. The application of the last functional derivative, together with $g_{qq}=\Theta(t-t')$, finally yields

$$
\begin{aligned}
\mathbf{q}^{(1)}(t) &= \int_0^\infty \mathrm{d}t'\left(\frac{1}{m(t')}-1\right)\mathbf{p}^{(\mathrm{i})}g_{qq}(t,t') \\
&= -t\mathbf{p}^{(\mathrm{i})}+\mathbf{p}^{(\mathrm{i})}\int_0^t \mathrm{d}t'\frac{1}{m(t')}.
\end{aligned}
$$

(A.37)

A.5 ERRONEOUS REPRESENTATION OF $C_{p_j p_k}$

In [9], an erroneous transformation of the integration kernel of the factors

$$
I_{jk}(\vec{L}_{p_j},\vec{L}_{p_k},\vec{k}_{jk}) := \int_{q_{jk}} \mathrm{e}^{-\vec{L}_{p_j}^\top \hat{C}_{pp}(\vec{q}_{jk})\vec{L}_{p_k}+\mathrm{i}\vec{k}_{jk}\cdot\vec{q}_{jk}}
$$

(A.38)

of the factorized free moments was performed. There, the following relation for the momentum correlations C_{pp} was introduced,

$$
C_{p_j p_k} \equiv \hat{C}_{pp}(\vec{q}) = -\tilde{\pi}_\parallel \xi_\psi''(q) - \tilde{\pi}_\perp \frac{\xi_\psi'(q)}{q},
$$

(A.39)

where $\vec{q}$ is the separation vector between particles j and k, and

$$
\tilde{\pi}_\parallel = \frac{\vec{q}\otimes\vec{q}}{q^2}, \qquad \tilde{\pi}_\perp = \mathbb{I}_3 - \tilde{\pi}_\parallel
$$

(A.40)

are the parallel and perpendicular projection operators with respect to $\vec{q}$. Furthermore, the projection operators with respect to the internal wave vector $\vec{k}_{jk}$ (see (3.122)) were introduced,

$$
\pi_{jk}^\parallel = \frac{\vec{k}_{jk}\otimes\vec{k}_{jk}}{k_{jk}^2}, \qquad \pi_{jk}^\perp = \mathbb{I}_3 - \pi_{jk}^\parallel.
$$

(A.41)

The idea in [9] was to represent the momentum correlation matrix in terms of the latter set of projectors. This was done by an expansion of the Hessian of the potential correlation function,

$$\hat{C}_{pp}(q) = D^2 \xi_\psi(q) = \tilde{\pi}_\parallel \xi''_\psi(q) + \tilde{\pi}_\perp \frac{\xi'_\psi(q)}{q} = a_\parallel \pi^\parallel_{jk} + a_\perp \pi^\perp_{jk} \,, \tag{A.42}$$

such that the integral (A.38) can be written as

$$I_{jk}(\vec{L}_{p_j}, \vec{L}_{p_k}, \vec{k}_{jk}) := \int_{q_{jk}} e^{\vec{L}^\top_{p_j} \pi^\parallel_{jk} \vec{L}_{p_k} a_\parallel + \vec{L}^\top_{p_j} \pi^\perp_{jk} \vec{L}_{p_k} a_\perp + i\vec{k}_{jk} \cdot \vec{q}_{jk}} \,. \tag{A.43}$$

The functions $a_\parallel$ and $a_\perp$ were determined by multiplying the above equation by $\pi^\parallel_{jk}$ and $\pi^\perp_{jk}$, and taking the trace of the resulting two equations, which yields

$$\begin{aligned}
a_\parallel &= \xi''_\psi(q) \mathrm{tr}\tilde{\pi}_\parallel \pi^\parallel_{jk} + \frac{\xi'_\psi(q)}{q} \mathrm{tr}\tilde{\pi}_\perp \pi^\parallel_{jk} \,, \\
2a_\perp &= \xi''_\psi(q) \mathrm{tr}\tilde{\pi}_\parallel \pi^\perp_{jk} + \frac{\xi'_\psi(q)}{q} \mathrm{tr}\tilde{\pi}_\perp \pi^\perp_{jk} \,.
\end{aligned} \tag{A.44}$$

The cosine $\mu := \frac{\vec{q} \cdot \vec{k}_{jk}}{q k_{jk}}$ of the angle between $\vec{q}$ and $\vec{k}_{jk}$ was introduced, yielding the traces

$$\mathrm{tr}\tilde{\pi}_\parallel \pi^\parallel_{jk} = \mu^2, \quad \mathrm{tr}\tilde{\pi}_\perp \pi^\parallel_{jk} = 1 - \mu^2 = \mathrm{tr}\tilde{\pi}_\parallel \pi^\perp_{jk}, \quad \mathrm{tr}\tilde{\pi}_\perp \pi^\perp_{jk} = 1 + \mu^2 \,, \tag{A.45}$$

and thus

$$\begin{aligned}
a_\parallel &= \mu^2 \xi''_\psi(q) + (1 - \mu^2) \frac{\xi'_\psi(q)}{q} \,, \\
2a_\perp &= (1 - \mu^2) \xi''_\psi(q) + (1 + \mu^2) \frac{\xi'_\psi(q)}{q} \,.
\end{aligned} \tag{A.46}$$

This result implies that in the integral (A.43) polar coordinates can be introduced such that $\vec{k}_{jk}$ is parallel to the z-axis and the integrand is independent of the angle ϕ, for arbitrary vectors $\vec{L}_{p_j}$, $\vec{L}_{p_k}$ and $\vec{k}_{jk}$.

The erroneous nature of this transformation becomes clear when we choose a similar but different way to compute $a_\parallel$ and $a_\perp$. First, we multiply (A.42) by the projectors with respect to $\vec{q}$, and then take the trace,

$$\begin{aligned}
\xi''_\psi(q) &= a_\parallel \mathrm{tr}\tilde{\pi}_\parallel \pi^\parallel_{jk} + a_\perp \mathrm{tr}\tilde{\pi}_\parallel \pi^\perp_{jk} \\
&= a_\parallel \mu^2 + a_\perp (1 - \mu^2), \\
2\frac{\xi'_\psi(q)}{q} &= a_\parallel \mathrm{tr}\tilde{\pi}_\perp \pi^\parallel_{jk} + a_\perp \mathrm{tr}\tilde{\pi}_\perp \pi^\perp_{jk} \\
&= a_\parallel (1 - \mu^2) + a_\perp (1 + \mu^2).
\end{aligned} \tag{A.47}$$

Using (A.45), we solve these two equation analogously for $a_\parallel$ and $a_\perp$ and arrive at

$$\begin{aligned}
a_\parallel &= \frac{1 + \mu^2}{3\mu^2 - 1} \xi''_\psi(q) - \frac{2(1 - \mu^2)}{3\mu^2 - 1} \frac{\xi'_\psi(q)}{q} \,, \\
a_\perp &= \frac{\mu^2 - 1}{3\mu^2 - 1} \xi''_\psi(q) + \frac{2\mu^2}{3\mu^2 - 1} \frac{\xi'_\psi(q)}{q} \,.
\end{aligned} \tag{A.48}$$

First, note that these results differ from (A.46). Second, for $\mu^2 \to \frac{1}{3}$, $a_\parallel$ and $a_\perp$ diverge. Therefore, we conclude that $a_\parallel$ and $a_\perp$ do not induce a formally correct transformation for the kernel in (A.38) as shown in (A.42).

When two-point correlation functions are considered, the above transformation does not fail. In this case all three involved vectors point in the same direction: $\vec{L}_{p_j} = -\vec{L}_{p_i}$ due to the Dirac delta distribution in front of the generating functional, and $\vec{L}_{p_j} \parallel \vec{k}_{jk}$. Thus, we can align all three vectors along the z-axis, and the original expressions (A.39) and (A.40) yield

$$-\vec{L}_{p_j}^\intercal \hat{C}_{pp}(\vec{q}) \vec{L}_{p_k} = -L_{p_j}^2 \mu^2 \xi_\psi''(q) - L_{p_j}^2 \frac{\xi_\psi'(q)}{q} + L_{p_j}^2 \mu^2 \frac{\xi_\psi'(q)}{q} \ . \tag{A.49}$$

Using the transformed expression (A.43) together with (A.46) yields the same result,

$$\vec{L}_{p_j}^\intercal \pi_{jk}^\parallel \vec{L}_{p_k} a_\parallel + \vec{L}_{p_j}^\intercal \pi_{jk}^\perp \vec{L}_{p_k} a_\perp = -L_{p_j}^2 a_\parallel \tag{A.50}$$

$$= -L_{p_j}^2 \left[\mu^2 \xi_\psi''(t) + (1 - \mu^2) \frac{\xi_\psi'(q)}{q} \right] \ . \tag{A.51}$$

APPENDIX: ASYMPTOTICS OF CERTAIN TYPES OF INTEGRALS

B.1 HESSIAN IN MORSE'S LEMMA

Let Q denote the Hessian matrix of $(f \circ h)(y)$ at $y = 0$, with the diffeomorphism h from Morse's Lemma 4.2. Recall from (4.60), that

$$A_{ij} = \left. \frac{\partial^2 f(x)}{\partial x_i \partial x_j} \right|_{x=x_0} \tag{B.1}$$

denotes the Hessian matrix of A at the critical point x_0. From (4.61) we infer that Q is the diagonal matrix

$$Q_{ij} = \left. \frac{\partial^2}{\partial y_i \partial y_j} (f \circ h)(y) \right|_{y=0} = \mu_i \delta_{ij} \,, \tag{B.2}$$

with μ_i being the eigenvalues of A. We now compute Q via the chain rule

$$
\begin{aligned}
Q_{ij} &= \left. \frac{\partial^2}{\partial y_i \partial y_j} f(h(y)) \right|_{y=0} \\
&= \left. \frac{\partial}{\partial y_i} \sum_{a=1}^{N} \frac{\partial f(h(y))}{\partial h_a(y)} \frac{\partial h_a(y)}{\partial y_j} \right|_{y=0} \\
&= \sum_{a=1}^{N} \frac{\partial h_a(y)}{\partial y_j} \frac{\partial}{\partial y_i} \left. \frac{\partial f(h(y))}{\partial h_a(y)} \right|_{y=0} + \sum_{a=1}^{N} \frac{\partial f(h(y))}{\partial h_a(y)} \left. \frac{\partial^2 h_a(y)}{\partial y_i \partial y_j} \right|_{y=0} \\
&= \sum_{a=1}^{N} \sum_{b=1}^{N} \frac{\partial h_a(y)}{\partial y_j} \frac{\partial h_b(y)}{\partial y_i} \left. \frac{\partial^2 f(h(y))}{\partial h_b(y) \partial h_a(y)} \right|_{y=0} \,,
\end{aligned} \tag{B.3}
$$

where the second term vanished because $\vec{nabl}a f(x)|_{x=x_0} = 0$. With

$$\left. \frac{\partial^2 f(h(y))}{\partial h_a(y) \partial h_b(y)} \right|_{y=0} \equiv \left. \frac{\partial^2 f(x)}{\partial x_a \partial x_b} \right|_{x=x_0} = A_{ab} \,, \tag{B.4}$$

and the Jacobian matrix of the diffeomorphism

$$\left[h'(y) \right]_{aj} := \frac{\partial h_a(y)}{\partial y_j} \,, \qquad \left[h_0' \right]_{aj} := \left. \frac{\partial h_a(y)}{\partial y_j} \right|_{y=0} \,, \tag{B.5}$$

(B.3) becomes

$$
\begin{aligned}
Q_{ij} &= \sum_{a=1}^{N} \sum_{b=1}^{N} \left[h_0' \right]_{aj} A_{ab} \left[h_0' \right]_{bi} \\
&= \sum_{a=1}^{N} \sum_{b=1}^{N} \left[h_0' \right]_{ja}^{\mathsf{T}} A_{ab} \left[h_0' \right]_{bi} \\
&= \left[[h_0']^{\mathsf{T}} A \, h_0' \right]_{ij} \,.
\end{aligned} \tag{B.6}
$$

This result shows, that $\left[h_0'\right]^\mathsf{T}$ and h_0' diagonalize A,

$$Q = \left[h_0'\right]^\mathsf{T} A\, h_0' = \operatorname{diag}(\mu_1,\dots,\mu_N)\,, \tag{B.7}$$

and since $\det h_0' = 1$, it follows that

$$\left[h_0'\right]^{-1} = \left[h_0'\right]^\mathsf{T}\,. \tag{B.8}$$

Furthermore, we arrive at the following representation of the inverse of the Hessian,

$$
\begin{aligned}
& Q = \left[h_0'\right]^\mathsf{T} A\, h_0' \\
\Leftrightarrow\quad & \mathbb{I}_N = \left[h_0'\right]^\mathsf{T} A\, h_0'\, Q^{-1} \\
\Leftrightarrow\quad & h_0' = A\, h_0'\, Q^{-1} \\
\Leftrightarrow\quad & A^{-1} h_0' = h_0'\, Q^{-1} \\
\Leftrightarrow\quad & A^{-1} = h_0'\, Q^{-1}\, \left[h_0'\right]^\mathsf{T} \\
\Rightarrow\quad & k^\mathsf{T} A^{-1} k = (k^\mathsf{T} h_0')\, Q^{-1}\, (\left[h_0'\right]^\mathsf{T} k),\quad \forall k \in \mathbb{R}^N.
\end{aligned}
\tag{B.9}
$$

From this, we conclude the following result,

$$k^\mathsf{T} A^{-1} k = \sum_{j=1}^N \frac{\left[k \cdot h_0'\right]_j^2}{\mu_j} = \sum_{j=1}^N \frac{1}{\mu_j} \left[\left.\frac{\partial}{\partial y_j} k \cdot h(y)\right|_{y=0}\right]^2. \tag{B.10}$$

B.2 SIMPLIFYING TERMS

We use the result (B.10) to simplify the sum, appearing in (4.77)

$$S(\lambda,k) :=$$

$$
\begin{aligned}
&\sum_{n=0}^{\infty} \sum_{|\alpha|=2n} \frac{\delta(\alpha)}{\alpha!} \left(\frac{-k^2}{\lambda}\right)^n \left(\frac{2}{\mu}\right)^{\frac{\alpha+1}{2}} \Gamma\left(\frac{\alpha+1}{2}\right) \prod_{j=1}^N \left.\left(\frac{\partial}{\partial y_j} \hat{k} \cdot h(y)\right)^{\alpha_j}\right|_{y=0} \\
&= \sqrt{\frac{(2\pi)^N}{\det A}} \sum_{n=0}^{\infty} \sum_{|\alpha|=2n} \prod_{j=1}^N \frac{\delta(\alpha_j)}{(\alpha_j/2)!} \left[-\frac{k^2}{2\lambda\mu_j} \left(\frac{\partial}{\partial y_j} \hat{k} \cdot h(y)|_{y=0}\right)^2\right]^{\alpha_j/2} \\
&= \sqrt{\frac{(2\pi)^N}{\det A}} \sum_{n=0}^{\infty} \sum_{|\alpha|=n} \prod_{j=1}^N \frac{1}{\alpha_j!} \left[-\frac{k^2}{2\lambda\mu_j} \left(\frac{\partial}{\partial y_j} \hat{k} \cdot h(y)|_{y=0}\right)^2\right]^{\alpha_j},
\end{aligned}
\tag{B.11}
$$

where we used (4.13) and, since all α_j are even numbers, $\Gamma\left(\frac{\alpha_j+1}{2}\right) = \frac{\alpha_j!}{(\alpha_j/2)!\,2^{\alpha_j}}\sqrt{\pi}$. The last expression is identical to the Taylor expansion of a multivariate exponential, such that

$$S(\lambda,k) = \sqrt{\frac{(2\pi)^N}{\det A}}\exp\left[-\frac{k^2}{2\lambda}\sum_{j=1}^N \frac{1}{\mu_j}\left(\frac{\partial}{\partial y_j}\hat{k}\cdot h(y)|_{y=0}\right)^2\right]. \tag{B.12}$$

With (B.10), we finally arrive at

$$S(\lambda,k) = \sqrt{\frac{(2\pi)^N}{\det A}}\exp\left(-\frac{k^2}{2\lambda}\,\hat{k}^\mathsf{T} A^{-1}\hat{k}\right). \tag{B.13}$$

APPENDIX: SMALL-SCALE ASYMPTOTICS OF THE FREE POWER SPECTRUM

C.1 DERIVATION OF $\mathcal{P}^{(0)}$ AND $\mathcal{P}^{(1)}$

We start with the expression for the time-dependent coefficients $\mathcal{P}^{(m)}$ from (6.25),

$$\mathcal{P}^{(m)}(t) = 8 \cdot 3^{3/2} \pi \left(\frac{5}{2\tau_2^2(t)} \right)^{3/2} \int_{-1}^{1} \mathrm{d}\mu \, \frac{I_m(\mu)}{(2\mu^2 + 1)^{3/2}} , \tag{C.1}$$

with the functions from (6.20),

$$I_m(\mu) = \frac{-\mathrm{e}^{\frac{i}{2}\pi m}}{\mu^m} \sum_{n=m}^{\infty} \Gamma\left(\frac{n+3}{2} \right) \left(\frac{\mu}{\sqrt{a_0(\mu)}} \right)^n \frac{\mathrm{e}^{\frac{i}{2}\pi n} d_{m,n}(\mu)}{m!(n-m)!} , \tag{C.2}$$

and the coefficients $d_{m,n}$ are given in (6.21),

$$d_{m,n}(\mu) = \lim_{x \to 0^+} \frac{\mathrm{d}^m}{\mathrm{d}x^m} \left(1 + \sum_{j=1}^{\infty} \frac{a_j(\mu)}{a_0(\mu)} x^j \right)^{-\frac{n+3}{2}} . \tag{C.3}$$

The μ-dependent coefficients $a_m(\mu)$ follow from inserting expansions (5.29) and (5.30) of $a_1(q)$ and $a_2(q)$ into the definition (6.4) of f_μ, and identifying terms with (6.22),

$$a_{2m}(\mu) = g_{qp}^2(t, 0) \left[2(m+1)\mu^2 + 1 \right] a_{m+1} , $$
$$a_{2m+1}(\mu) = 0 , \tag{C.4}$$

with the μ-dependent coefficients a_m defined in (5.28),

$$a_m = \frac{(-1)^{m+1} \sigma_{m+1}^2}{(3 + 2m)(1 + 2m)!} . \tag{C.5}$$

The first three coefficients in (C.4) are then given by

$$a_0(\mu) = (2\mu^2 + 1) \frac{\tau_2^2(t)}{30} , \tag{C.6}$$

$$a_1(\mu) = 0 , \tag{C.7}$$

$$a_2(\mu) = -(4\mu^2 + 1) \frac{\tau_3^2(t)}{840} , \tag{C.8}$$

with $\tau_n^2(t) = g_{qp}^2(t, 0)\sigma_n^2$, such that we get for the first three coefficients in (C.3)

$$d_{0,n}(\mu) = 1 , \tag{C.9}$$

$$d_{1,n}(\mu) = 0 , \tag{C.10}$$

$$d_{2,n}(\mu) = -(n+3) \frac{a_2(\mu)}{a_0(\mu)} = \frac{n+3}{28} \frac{4\mu^2 + 1}{2\mu^2 + 1} \frac{\sigma_3^2}{\sigma_2^2} . \tag{C.11}$$

C.1.1   *Evaluation of $\mathcal{P}^{(0)}$*

With

$$I_0(\mu) = -\sum_{n=0}^{\infty} \frac{\Gamma\left(\frac{n+3}{2}\right)}{n!} \left(\frac{\sqrt{30}\mu\mathrm{i}}{\sqrt{(2\mu^2+1)\tau_2^2(t)}}\right)^n, \tag{C.12}$$

we calculate

$$\int_{-1}^{1} \mathrm{d}\mu \frac{I_0(\mu)}{(2\mu^2+1)^{3/2}} \tag{C.13}$$

$$= -\sum_{n=0}^{\infty} \frac{\Gamma\left(\frac{n+3}{2}\right)}{n!} \int_{-1}^{1} \frac{\mathrm{d}\mu}{(2\mu^2+1)^{3/2}} \left(\frac{\sqrt{30}\mu\mathrm{i}}{\sqrt{(2\mu^2+1)\tau_2^2(t)}}\right)^n \tag{C.14}$$

$$= -\sum_{n=0}^{\infty} \frac{\Gamma\left(n+\frac{3}{2}\right)}{(2n)!} \int_{-1}^{1} \frac{\mathrm{d}\mu}{(2\mu^2+1)^{3/2}} \left(-\frac{30\mu^2}{(2\mu^2+1)\tau_2^2(t)}\right)^n, \tag{C.15}$$

where we used in the last step that odd powers of μ vanish in the integral. Using the result

$$\int_{-1}^{1} \mathrm{d}\mu \frac{\mu^{2n}}{(2\mu^2+1)^{2n+3/2}} = \frac{2}{3^{n+1/2}(2n+1)}, \tag{C.16}$$

with the help of the computer algebra software Wolfram Mathematica [38], we arrive at

$$\int_{-1}^{1} \mathrm{d}\mu \frac{I_0(\mu)}{(2\mu^2+1)^{3/2}} \tag{C.17}$$

$$= -\frac{2}{\sqrt{3}} \sum_{n=0}^{\infty} \frac{\Gamma\left(n+\frac{3}{2}\right)}{(2n+1)!} \left(-\frac{10}{\sigma_2^2}\right)^n \tag{C.18}$$

$$= -\sqrt{\frac{\pi}{3}} \exp\left(-\frac{5}{2\tau_2^2(t)}\right). \tag{C.19}$$

In the last step we used the relation

$$\sum_{n=0}^{\infty} \frac{\Gamma\left(n+\frac{3}{2}\right)}{(2n+1)!} x^n = \frac{\sqrt{\pi}}{2} e^{x/4}, \tag{C.20}$$

which we obtained with [38].

We finally arrive at the following result for the first coefficient in the asymptotic expansion (6.24) of $\mathcal{P}$,

$$\mathcal{P}^{(0)}(t) = 3(4\pi)^{3/2} \left(\frac{5}{2\tau_2^2(t)}\right)^{3/2} \exp\left(-\frac{5}{2\tau_2^2(t)}\right). \tag{C.21}$$

Evaluation of $\mathcal{P}^{(1)}$

For the second term in the asymptotics, we start with

$$I_1(\mu) = \frac{1}{14\mu^2} \frac{\sigma_3^2}{\sigma_2^2} \frac{4\mu^2 + 1}{2\mu^2 + 1} \sum_{n=2}^{\infty} \frac{\Gamma\left(\frac{n+3}{2} + 1\right)}{2(n-2)!} \left(\frac{\sqrt{30}\mu i}{\sqrt{(2\mu^2 + 1)\tau_2^2(t)}} \right)^n \tag{C.22}$$

and calculate

$$\int_{-1}^{1} d\mu \frac{I_1(\mu)}{(2\mu^2 + 1)^{3/2}} \tag{C.23}$$

$$= \frac{1}{28} \frac{\sigma_3^2}{\sigma_2^2} \sum_{n=2}^{\infty} \frac{\Gamma\left(\frac{n+5}{2}\right)}{(n-2)!} \int_{-1}^{1} d\mu \frac{4\mu^2 + 1}{\mu^2(2\mu^2 + 1)^{5/2}} \left(\frac{\sqrt{30}\mu i}{\sqrt{(2\mu^2 + 1)\tau_2^2(t)}} \right)^n \tag{C.24}$$

$$= \frac{1}{28} \frac{\sigma_3^2}{\sigma_2^2} \sum_{n=1}^{\infty} \frac{\Gamma\left(n + \frac{5}{2}\right)}{(2n-2)!} \left(-\frac{30}{\tau_2^2(t)} \right)^n \int_{-1}^{1} d\mu \frac{(4\mu^2 + 1)\mu^{2n-2}}{(2\mu^2 + 1)^{5/2+n}} , \tag{C.25}$$

where we again used that terms with odd powers of μ vanish in the integration. We obtained the solution for the integral

$$\int_{-1}^{1} d\mu \frac{(4\mu^2 + 1)\mu^{2n-2}}{(2\mu^2 + 1)^{5/2+n}} = \frac{2}{3^{n+3/2}} \frac{31 + 10n}{2n(2n+2) - 3} \tag{C.26}$$

from [38], which yields

$$\int_{-1}^{1} d\mu \frac{I_1(\mu)}{(2\mu^2 + 1)^{3/2}} \tag{C.27}$$

$$= \frac{1}{28k^2} \frac{2}{3^{3/2}} \frac{\sigma_3^2}{\tau_2^2(t)} \sum_{n=1}^{\infty} \frac{\Gamma\left(n + \frac{5}{2}\right)}{(2n-2)!} \left(-\frac{10}{\sigma_2^2} \right)^n \frac{31 + 10n}{2n(2n+2) - 3} . \tag{C.28}$$

Again from [38], we obtained the sum

$$\sum_{n=1}^{\infty} \frac{\Gamma\left(n + \frac{5}{2}\right)}{(2n-2)!} x^n \frac{31 + 10n}{2n(2n+2) - 3} = \frac{\sqrt{\pi}x}{32} e^{x/4} \left(492 + 132x + 5x^2 \right) , \tag{C.29}$$

which yields

$$\int_{-1}^{1} d\mu \frac{I_1(\mu)}{(2\mu^2 + 1)^{3/2}}$$

$$= \frac{\sqrt{\pi}}{28 \cdot 3^{3/2}} \frac{\sigma_3^2}{\sigma_2^2} \left(\frac{5}{2\tau_2^2(t)} \right) \exp\left(-\frac{5}{2\tau_2^2(t)} \right) \tag{C.30}$$

$$\times \left[123 - 132 \left(\frac{5}{2\tau_2^2(t)} \right) + 20 \left(\frac{5}{2\tau_2^2(t)} \right)^2 \right] .$$

With (C.1), we finally arrive at the second coefficient in the asymptotic series (6.24) of $\mathcal{P}$

$$
\begin{aligned}
\mathcal{P}^{(1)}(t) = \frac{2\pi^{3/2}}{7} \frac{\sigma_3^2}{\sigma_2^2} & \left(\frac{5}{2\tau_2^2(t)}\right)^{5/2} \exp\left(-\frac{5}{2\tau_2^2(t)}\right) \\
& \times \left[123 - 132\left(\frac{5}{2\tau_2^2(t)}\right) + 20\left(\frac{5}{2\tau_2^2(t)}\right)^2\right].
\end{aligned}
\tag{C.31}
$$

D

APPENDIX: FACTORS OF THE GENERATING FUNCTIONAL

D.1 IDENTIFICATION OF THE CRITICAL POINTS

Let $q > 0$ and set $\vec{\nabla} f_{\tilde{\mu}} = 0$, then from (7.13) we arrive at the following set of equations

$$\frac{q_x}{q}\left[\left(q_x^2 - \tilde{\mu}^2(q_x^2 + q_z^2)\right)\left(\frac{a_2'(q)}{q^2} - 2\frac{a_2(q)}{q^3}\right) + (3 - 4\tilde{\mu}^2)\frac{a_2(q)}{q}\right] = 0 , \tag{D.1}$$

$$\frac{q_y}{q}\left[\left(q_x^2 - \tilde{\mu}^2(q_x^2 + q_z^2)\right)\left(\frac{a_2'(q)}{q^2} - 2\frac{a_2(q)}{q^3}\right) + (1 - 2\tilde{\mu}^2)\frac{a_2(q)}{q}\right] = 0 , \tag{D.2}$$

$$\frac{q_z}{q}\left[\left(q_x^2 - \tilde{\mu}^2(q_x^2 + q_z^2)\right)\left(\frac{a_2'(q)}{q^2} - 2\frac{a_2(q)}{q^3}\right) + (1 - 4\tilde{\mu}^2)\frac{a_2(q)}{q}\right] = 0 . \tag{D.3}$$

The second equation, (D.2), implies that either

$$\left(q_x^2 - (q_x^2 + q_z^2)\right)\left(\frac{a_2'(q)}{q^2} - 2\frac{a_2(q)}{q^3}\right) + (1 - 2\tilde{\mu}^2)\frac{a_2(q)}{q} = 0 , \tag{D.4}$$

or $q_y = 0$.

- If (D.4) is satisfied, then (D.1) and (D.3) reduce to

$$\frac{q_x}{q}\left(1 - \tilde{\mu}^2\right) = 0 , \tag{D.5}$$

$$\frac{q_z}{q}\tilde{\mu}^2 = 0 . \tag{D.6}$$

Equation (D.5) implies $q_x = 0$ or $\tilde{\mu}^2 = 1$.

  – If $q_x = 0$, then (D.6) implies either $\tilde{\mu} = 0$ or $q_z = 0$. But if $\tilde{\mu} = 0 = q_x$, then (D.3) implies $\frac{a_2(q)}{q} = 0$, contradicting $q > 0$. If instead $q_z = 0$, then (D.2) implies

$$(1 - 2\tilde{\mu}^2)\frac{a_2(q_y)}{q_y} = 0 , \tag{D.7}$$

  which is possible only for $\tilde{\mu}^2 = \frac{1}{2}$. We conclude that for $\tilde{\mu}^2 = \frac{1}{2}$, all points on the q_y-axis are critical points.

  – If $\tilde{\mu}^2 = 1$, then (D.6) implies $q_z = 0$. Then (D.1) implies $\frac{a_2(q)}{q} = 0$, again contradicting $q > 0$.

- If $q_y = 0$ instead, (D.1) and (D.3) remain unchanged.

– If $q_x = 0$, then (D.3) reduces to

$$(1 - 2\tilde{\mu}^2)\frac{a_2(q_z)}{q_z} = \tilde{\mu}^2 a_2'(q_z) \, . \tag{D.8}$$

We conclude that a pair of critical points lies on the z-axis, at positions $(0, 0, \pm q_z(\tilde{\mu})$, where $q_z(\tilde{\mu}$ has to satisfies (D.8).

– If $q_x \neq 0$, then (D.1) and (D.3) imply $q_z = 0$, since $\frac{a_2(q)}{q} > 0$ which is not possible due to our requirement $q > 0$. With $q_y = 0 = q_z$, (D.1) implies

$$(1 - 2\tilde{\mu}^2)\frac{a_2(q_x)}{q_x} = -(1 - \tilde{\mu}^2)a_2'(q_x) \, . \tag{D.9}$$

Therefore, we conclude that a pair of critical points is located on the x-axis at positions $(\pm q_x(\tilde{\mu}), 0, 0)$, where $q_x(\tilde{\mu})$ satisfies (D.9).

D.2   DERIVATION OF THE HESSIAN AT THE CRITICAL POINTS

We start by defining

$$Q_1 := \frac{1 - 2\tilde{\mu}^2}{2} \, ,$$

$$Q_2 := (1 - \tilde{\mu}^2)\frac{q_x^2}{q^2} - \tilde{\mu}^2\frac{q_z^2}{q^2} \, ,$$

$$B := 2\frac{a_2(q)}{q} \, ,$$

$$A := Q_2\left(a_2'(q) - B\right) + Q_1 B \, ,$$

$$\vec{v} := (1 - \tilde{\mu}^2)\frac{q_x}{q}\vec{e}_x - \tilde{\mu}^2\frac{q_z}{q}\vec{e}_z \, .$$

With these definitions , $f_{\tilde{\mu}}$ and $\vec{\nabla}f_{\tilde{\mu}}$ as defined in (7.11) and (7.13), respectively, can be re-written as

$$f_{\tilde{\mu}}(\vec{q}) = Q_2 a_2(q) + 2Q_1 a_1(q) \, , \tag{D.10}$$

$$\vec{\nabla}f_{\tilde{\mu}}(\vec{q}) = A\frac{\vec{q}}{q} + B\vec{v} \, . \tag{D.11}$$

For the Hessian of $f_{\tilde{\mu}}$ we then get

$$(\vec{\nabla} \otimes \vec{\nabla})f_{\tilde{\mu}}(\vec{q}) = \vec{\nabla}A \otimes \frac{\vec{q}}{q} + \frac{A}{q}\left(\mathbb{I}_3 - \frac{\vec{q} \otimes \vec{q}}{q^2}\right) + B'\frac{\vec{q}}{q} \otimes \vec{v} + B\vec{\nabla} \otimes \vec{v} \, , \tag{D.12}$$

with

$$\vec{\nabla}A = \frac{\vec{q}}{q}\left\{Q_2\left[a_2''(q) - B' - \frac{2}{q}\left(a_2'(q) - B\right)\right] + Q_1 B'\right\} + \frac{2}{q}\left(a_2'(q) - B\right)\vec{v} \, , \tag{D.13}$$

and

$$\vec{\nabla} \otimes \vec{v} = \frac{1}{q}\left[\left(1 - \tilde{\mu}^2\right)E_{11} - \tilde{\mu}^2 E_{33} - \frac{\vec{q}}{q} \otimes \vec{v}\right] \, , \tag{D.14}$$

where we defined $E_{11} = \mathrm{diag}(1,0,0)$ and $E_{33} = \mathrm{diag}(0,0,1)$. We thus arrive at

$$(\vec{\nabla} \otimes \vec{\nabla})f_{\tilde{\mu}}(\vec{q}) = \frac{A}{q}\mathbb{I}_3 + \left\{ Q_2\left[a_2''(q) - B' - \frac{2}{q}\left(a_2'(q) - B\right)\right] + Q_1 B' - \frac{A}{q} \right\} \frac{\vec{q} \otimes \vec{q}}{q^2}$$

$$+ \frac{2\left(a_2'(q) - B\right)}{q}\vec{v} \otimes \frac{\vec{q}}{q} + \left(B' - \frac{B}{q}\right)\frac{\vec{q}}{q} \otimes \vec{v} + \frac{B}{q}\left[\left(1 - \tilde{\mu}^2\right)E_{11} - \tilde{\mu}^2 E_{33}\right] .$$

$$(\text{D.15})$$

Next, we evaluate the Hessian at the critical points.

Hessian at the origin $\vec{q} = (0,0,0)$:

Since

$$\lim_{q \to 0} a_2''(q) = \lim_{q \to 0} 2\frac{a_2'(q)}{q} = \lim_{q \to 0} 2\frac{a_2(q)}{q^2} = 2\frac{\sigma_2^2}{15} , \tag{D.16}$$

the Hessian at the origin becomes

$$A^{(0)} := \lim_{q \to 0}(\vec{\nabla} \otimes \vec{\nabla})f_{\tilde{\mu}}(\vec{q}) = \frac{\sigma_2^2}{15}\begin{pmatrix} 3 - 4\tilde{\mu}^2 & 0 & 0 \\ 0 & 1 - 2\tilde{\mu}^2 & 0 \\ 0 & 0 & 1 - 4\tilde{\mu}^2 \end{pmatrix} . \tag{D.17}$$

Hessian on the x-axis $\vec{q} = (\pm q_x, 0, 0)$:

We now set $q_z = 0 = q_y$, implying $q = q_x$ and

$$Q_2 = 1 - \tilde{\mu}^2 \quad \text{and} \quad \vec{v} = Q_2\vec{e}_x , \tag{D.18}$$

such that the Hessian $A^{(x)} := (\vec{\nabla} \otimes \vec{\nabla})f_{\tilde{\mu}}(\vec{q})\Big|_{q_y=0=q_z}$ reduces to

$$A^{(x)} = \frac{A}{q}\left(\mathbb{I}_3 - E_{11}\right) + \left[\left(1 - \tilde{\mu}^2\right)a_2''(q) + Q_1 B'\right]E_{11} - \frac{B}{q}\tilde{\mu}^2 E_{33} . \tag{D.19}$$

Inserting condition (D.9) that is valid at the critical points, yields

$$A^{(x)} = \begin{pmatrix} (1 - \tilde{\mu}^2)a_2''(q_x) + (2 - 3\tilde{\mu}^2)\frac{a_2'(q_x)}{q_x} & 0 & 0 \\ 0 & 2(\tilde{\mu}^2 - 1)\frac{a_2(q_x)}{q_x^2} & 0 \\ 0 & 0 & -2\frac{a_2(q_x)}{q_x^2} \end{pmatrix} , \tag{D.20}$$

where $q_x = q_x(\tilde{\mu})$ is implicitly given by (D.9).

Hessian on the y-axis $\vec{q} = (0, \pm q_y, 0)$:

For $\vec{q} = (0, \pm q_y, 0)$ and $\tilde{\mu}^2 = \frac{1}{2}$, we have

$$\vec{v} = 0 \quad \text{and} \quad Q_2 = 0 = Q_1 \quad \Rightarrow A = 0 , \tag{D.21}$$

such that the Hessian $A^{(y)} := (\vec{\nabla} \otimes \vec{\nabla}) f_{\tilde{\mu}}(\vec{q})\big|_{q_x=0=q_z}$ reduces to

$$
\begin{aligned}
A^{(y)} &= \frac{B}{q}\left[\left(1 - \tilde{\mu}^2\right) E_{11} - \tilde{\mu}^2 E_{33}\right] \\
&= \frac{a_2(q_y)}{q_y^2}\begin{pmatrix} 1 & 0 & 0 \\ 0 & 0 & 0 \\ 0 & 0 & -1 \end{pmatrix}.
\end{aligned}
\tag{D.22}
$$

Hessian on the z-axis $\vec{q} = (0, 0, \pm q_z)$:

Finally, for $q_x = 0 = q_y$, we have

$$
Q_2 = -\tilde{\mu}^2 \quad \text{and} \quad \vec{v} = Q_2 \vec{e}_z ,
\tag{D.23}
$$

such that the Hessian $A^{(z)} := (\vec{\nabla} \otimes \vec{\nabla}) f_{\tilde{\mu}}(\vec{q})\big|_{q_x=0=q_y}$ reduces to

$$
A^{(z)} = \frac{A}{q}\left(\mathbb{I}_3 - E_{33}\right) + \left(-\tilde{\mu}^2 a_2''(q) + Q_1 B'\right) E_{33} + \frac{B}{q}\left(1 - \tilde{\mu}^2\right) E_{11} .
\tag{D.24}
$$

Making use of (D.8) that is satisfied at the critical points along the z-axis, we get

$$
A^{(z)} = \begin{pmatrix} 2\frac{a_2(q_z)}{q_z^2} & 0 & 0 \\ 0 & 2\tilde{\mu}^2\frac{a_2(q_z)}{q_z^2} & 0 \\ 0 & 0 & -\tilde{\mu}^2 a_2''(q_z) + (1 - 3\tilde{\mu}^2)\frac{a_2'(q_z)}{q_z} \end{pmatrix} ,
\tag{D.25}
$$

where $q_z = q_z(\tilde{\mu})$ is implicitly given by (D.8).

E

PARAMETERS AND FUNCTIONS USED

E.1 POWER SPECTRA AND TRANSFER FUNCTIONS

- Linearly evolved power spectra are obtained by

$$P_\delta^{\text{lin.}}(k,t) = \frac{D_+^2(t)}{D_+^2(t^{(\text{i})})} \mathcal{A}(\sigma_8) T^2(k) k^{n_s} , \tag{E.1}$$

where $\mathcal{A}(\sigma_8)$ is the power spectrum amplitude that is determined by σ_8 (see 2.45) by using an exponential filter. $T(k)$ denotes the transfer function, for which we use either the cold dark matter transfer function (E.4) from Bardeen et al [4], a damped cold dark matter transfer function (E.6) or a non-cold dark matter-type (E.7) from Murgia et al [45].

- Linearly evolved damped power spectra,

$$P_\delta^{\text{lin.(d)}}(k,t) = e^{-\frac{\sigma_1^2}{3} k^2 g_{qp}^2} \frac{D_+^2(t)}{D_+^2(t^{(\text{i})})} \mathcal{A}(\sigma_8) T^2(k) k^{n_s} , \tag{E.2}$$

are obtained by multiplying (E.1) with the damping factor from KFT as described in Section 6.2.3 of Chapter 6.

- Free power spectra,

$$\mathcal{P}(k,t) = e^{-\frac{\sigma_1^2}{3} k^2 g_{qp}^2(t,0)} \int \mathrm{d}^3 q \ \left(e^{g_{qp}^2(t,0)\vec{k}^\top \hat{C}_{pp}(\vec{q})\vec{k}} - 1 \right) e^{i\vec{k}\cdot\vec{q}} , \tag{E.3}$$

are obtained from KFT as described in Section 3.5.3 of Chapter 3.

- The transfer function from Bardeen et al [4] for cold dark matter is

$$T_{\text{CDM,ad,X}}(k) = \frac{\ln(1 + 2.34q)}{2.34q} \left[1 + 3.89q + (16.1q)^2 + (5.46q)^3 + (6.71q)^4 \right]^{-1/4} \tag{E.4}$$

with

$$q = \frac{k}{h\text{Mpc}^{-1}} \Omega_{\text{X0}}^{-1} \exp\left[\Omega_{\text{b0}} \left(1 + \sqrt{2h}\Omega_{\text{X0}}^{-1} \right) \right] , \tag{E.5}$$

where $\Omega_{\text{X0}} = \Omega_{\text{m0}} - \Omega_{\text{b0}}$ denotes the dark matter density parameter, today.

- The transfer function for smoothed cold dark matter is

$$T(k) = T_{\text{CDM,ad,X}}(k) e^{-k/(2k_s)} , \tag{E.6}$$

where k_s corresponds to the smoothing wave number.

- The parameterized transfer function non-cold dark matter-type power spectra from Murgia et al [45] is

$$T^{\text{nCDM}}(k) = T_{\text{CDM,ad,X}}(k) \left[1 + (\alpha k)^\beta \right]^\gamma , \tag{E.7}$$

where α, β and γ are free parameters, specifying the dark matter type.

E.2   PARAMETER TABLES FOR FIGURES

$\Omega_{\Lambda 0}$	Ω_{m0}	Ω_{b0}	h	σ_8	n_s	a	$T(k)$	$k_s \, [h \, \mathrm{Mpc}^{-1}]$	Figure
0.7	0.3	0.04	0.7	0.8	0.96	0.001	(E.6)	10	5.1 (a)
								1000	5.1 (b)
$\Omega_{\Lambda 0}$	Ω_{m0}	Ω_{b0}	h	σ_8	n_s	a	$P_\delta^{(i)}(k)$	$k_s \, [h \, \mathrm{Mpc}^{-1}]$	Figure
-	-	-	-	-	-	-	$k \, \mathrm{e}^{-k/k_s}$	1	5.2

Table E.1: Cosmological and power spectrum parameters used in Figures 5.1 and 5.2.

$\Omega_{\Lambda 0}$	Ω_{m0}	Ω_{b0}	h	σ_8	n_s	$a^{(i)}$	Figure(s)
0.7	0.3	0.04	0.7	0.8	0.96	0.001	6.1, 6.2, 6.3, 6.4
							6.5 (blue lines), 6.6, 6.7
							7.2, 7.3, 7.4
0.0	0.999	0.001	0.7	0.8	0.96	0.001	6.5 (red lines)
0.7	0.3	0.04	0.3	0.8	0.96	0.001	6.5 (purple lines)

Table E.2: Cosmological parameters that are used in Figures 6.1 – 6.7 and Figures 7.2 – 7.4.

a	z	$T(k)$	power spectrum	k_s [h Mpc^{-1}]	Figure	Line
1/11	10	(E.6)	(E.3)	10	6.1 (a), 6.2 (a)	purple
		(E.4)	(E.1)	10	6.1 (a)	grey
		(E.6)	(E.2)	10	6.2 (a)	golden
		(E.6)	(E.3)	1000	6.1 (b), 6.2 (b)	purple
		(E.4)	(E.1)	1000	6.1 (b)	grey
		(E.6)	(E.2)	1000	6.2 (b)	golden
1/3	2	(E.6)	(E.3)	10	6.1 (c), 6.2 (c)	purple
		(E.4)	(E.1)	10	6.1 (c)	grey
		(E.6)	(E.2)	10	6.2 (c)	golden
		(E.6)	(E.3)	1000	6.1 (d), 6.2 (d)	purple
		(E.4)	(E.1)	1000	6.1 (d)	grey
		(E.6)	(E.2)	1000	6.2 (d)	golden

Table E.3: Power spectrum parameters that are used in Figures 6.1 and 6.2.

z	$T(k)$	power spectrum	k_s [h Mpc^{-1}]	Figure	Line
(see Fig.)	(E.6)	(E.3)	1000	6.3	(see Fig.)
0	(E.6)	(E.3)	(see Fig.)	6.4	(see Fig.)
	(E.4)	(E.1)	-	6.4	black
z^{sc}	(E.6)	(E.3)	$\in [10^{-1}, 10^4]$	6.5	(see Fig.)
$z^{sc} = 2.17$	(E.6)	(E.3)	1	6.6 (a), 6.6 (c)	purple
	(E.4)	(E.1)	-	6.6 (a), 6.6 (c)	black
$z^{sc} = 21.0$	(E.6)	(E.3)	1000	6.6 (b), 6.6 (d)	purple
	(E.4)	(E.1)	-	6.6 (b), 6.6 (d)	black

Table E.4: Power spectrum parameters that are used in Figures 6.3 – 6.6.

z	$T(k)$	α	β	γ	power spectrum	k_s [h Mpc^{-1}]	Figure	Line
z^{sc}	(E.6)	-	-	-	(E.3)	$\in [10^{-1}, 10^2]$	6.7	blue
	(E.7)	1.0	2.0	$\in [-20.0, -0.02]$	(E.3)	10^6	6.7	golden

Table E.5: Power spectrum parameters that are used in Figure 6.7.

a	$T(k)$	k_s [h Mpc^{-1}]	Figures
0.001	(E.6)	10	7.2, 7.3, 7.4

Table E.6: Cosmological and power spectrum parameters used in Figures 7.2 – 7.4.

BIBLIOGRAPHY

[1] Milton Abramowitz. *Pocketbook of mathematical functions*. H. Deutsch, 1984.

[2] Nabila Aghanim, Yashar Akrami, M Ashdown, J Aumont, C Baccigalupi, M Ballardini, AJ Banday, RB Barreiro, N Bartolo, S Basak, et al. "Planck 2018 results-VI. Cosmological parameters." In: *Astronomy & Astrophysics* 641 (2020), A6.

[3] Y Akrami, M Ashdown, J Aumont, C Baccigalupi, M Ballardini, AJ Banday, RB Barreiro, N Bartolo, S Basak, K Benabed, et al. "Planck 2018 results-VII. Isotropy and statistics of the CMB." In: *Astronomy & Astrophysics* 641 (2020), A7.

[4] James M Bardeen, JR Bond, Nick Kaiser, and AS Szalay. "The statistics of peaks of Gaussian random fields." In: *The Astrophysical Journal* 304 (1986), pp. 15–61.

[5] Matthias Bartelmann. "Trajectories of point particles in cosmology and the Zel'dovich approximation." In: *Physical Review D* 91.8 (2015), p. 083524.

[6] Matthias Bartelmann. *Das Kosmologische Standardmodell*. Springer, 2019.

[7] Matthias Bartelmann, Felix Fabis, Daniel Berg, Elena Kozlikin, Robert Lilow, and Celia Viermann. "A microscopic, non-equilibrium, statistical field theory for cosmic structure formation." In: *New Journal of Physics* 18.4 (2016), p. 043020. ISSN: 1367-2630. DOI: 10.1088/1367-2630/18/4/043020. URL: http://dx.doi.org/10.1088/1367-2630/18/4/043020.

[8] Matthias Bartelmann, Felix Fabis, Sara Konrad, Elena Kozlikin, Robert Lilow, Carsten Littek, and Johannes Dombrowski. "Analytic calculation of the non-linear cosmic density-fluctuation power spectrum in the Born approximation." In: *arXiv preprint arXiv:1710.07522* (2017).

[9] Matthias Bartelmann, Felix Fabis, Elena Kozlikin, Robert Lilow, Johannes Dombrowski, and Julius Mildenberger. "Kinetic field theory: effects of momentum correlations on the cosmic density-fluctuation power spectrum." In: *New Journal of Physics* 19.8 (2017), p. 083001. ISSN: 1367-2630. DOI: 10.1088/1367-2630/aa7e6f. URL: http://dx.doi.org/10.1088/1367-2630/aa7e6f.

[10] Matthias Bartelmann, Elena Kozlikin, Robert Lilow, Carsten Littek, Felix Fabis, Ivan Kostyuk, Celia Viermann, Lavinia Heisenberg, Sara Konrad, and Daniel Geiss. "Cosmic structure formation with kinetic field theory." In: *Annalen der Physik* 531.11 (2019), p. 1800446.

[11] Francis Bernardeau, S Colombi, E Gaztanaga, and R Scoccimarro. "Large-scale structure of the Universe and cosmological perturbation theory." In: *Physics reports* 367.1-3 (2002), pp. 1–248.

[12] Norman Bleistein and Richard A Handelsman. *Asymptotic expansions of integrals*. Courier Corporation, 1986.

[13] John P Boyd. "The Fourier Transform of the quartic Gaussian exp (-Ax4): Hypergeometric functions, power series, steepest descent asymptotics and hyperasymptotics and extensions to exp (-Ax2n)." In: *Applied Mathematics and Computation* 241 (2014), pp. 75–87.

[14] Thomas Buchert. "Lagrangian theory of gravitational instability of Friedman-Lemaître cosmologies and the 'Zel'dovich approximation'." In: *Monthly Notices of the Royal Astronomical Society* 254.4 (1992), pp. 729–737.

[15] Robin Bühler. "Algorithms for the evaluation of correlationsin Kinetic Field Theory." In: *Master Thesis* (2018).

[16] Tara Butler. "Approaches for calculating rapidly oscillatory integrals in kinetic field theory." In: *Bachelor Thesis* (2020).

[17] Richard Chapling. *Asymptotic methods*. 2016.

[18] Shi-Fan Chen and Massimo Pietroni. "Asymptotic expansions for the Large Scale Structure." In: *arXiv preprint arXiv:2002.11357* (2020).

[19] Leonid Chuzhoy. "Impact of Dark Matter Annihilation on the High-Redshift Intergalactic Medium." In: *The Astrophysical Journal Letters* 679.2 (2008), p. L65.

[20] Peter Coles, Adrian L. Melott, and Sergei F. Shandarin. "Testing approximations for non-linear gravitational clustering." In: *Monthly Notices of the Royal Astronomical Society* 260.4 (Feb. 1993), pp. 765–776. DOI: 10.1093/mnras/260.4.765.

[21] Pedro Colin, Vladimir Avila-Reese, Alejandro Gonzalez-Samaniego, and Hector Velazquez. "Simulations of galaxies formed in warm dark matter halos of masses at the filtering scale." In: *The Astrophysical Journal* 803.1 (2015), p. 28.

[22] Asantha Cooray and Ravi Sheth. "Halo models of large scale structure." In: *Physics reports* 372.1 (2002), pp. 1–129.

[23] Albert Einstein. "Die Feldgleichungen der Gravitation." In: *Sitzung der physikalische-mathematischen Klasse* 25 (1915), pp. 844–847.

[24] Albert Einstein. "Kosmologische Betrachtungen zur allgemeinen Relativitätstheorie." In: *Sitzungsberichte der Königlich Preußischen Akademie der Wissenschaften (Berlin* (Jan. 1917), pp. 142–152.

[25] A. Erdélyi. *Asymptotic Expansions*. New York: Dover Publications Inc., 1956, pp. vi+108.

[26] Carmelo Evoli, Andrei Mesinger, and Andrea Ferrara. "Unveiling the nature of dark matter with high redshift 21 cm line experiments." In: *Journal of Cosmology and Astroparticle Physics* 2014.11 (2014), p. 024.

[27] Felix Fabis, Elena Kozlikin, Robert Lilow, and Matthias Bartelmann. "Kinetic field theory: exact free evolution of Gaussian phase-space correlations." In: *Journal of Statistical Mechanics: Theory and Experiment* 2018.4 (2018), p. 043214.

[28] Carlos S Frenk and Simon DM White. "Dark matter and cosmic structure." In: *Annalen der Physik* 524.9-10 (2012), pp. 507–534.

[29] A. Friedmann. "Über die Krümmung des Raumes." In: *Zeitschrift fur Physik* 10 (Jan. 1922), pp. 377–386. DOI: 10.1007/BF01332580.

[30] A. Friedmann. "Über die Möglichkeit einer Welt mit konstanter negativer Krüm-mung des Raumes." In: *Zeitschrift fur Physik* 21.1 (Dec. 1924), pp. 326–332. DOI: 10.1007/BF01328280.

[31] Watson Fulks and JO Sather. "Asymptotics. II. Laplace's method for multiple integrals." In: *Pacific Journal of Mathematics* 11.1 (1961), pp. 185–192.

[32] Daniel Geiss, Ivan Kostyuk, Robert Lilow, and Matthias Bartelmann. "Re-summed Kinetic Field Theory: a model of coupled baryonic and dark matter." In: *arXiv preprint arXiv:2007.09484* (2020).

[33] Daniel Geiss, Robert Lilow, Felix Fabis, and Matthias Bartelmann. "Resummed Kinetic Field Theory: using Mesoscopic Particle Hydrodynamics to describe baryonic matter in a cosmological framework." In: *Journal of Cosmology and Astroparticle Physics* 2019.05 (2019), p. 017.

[34] Carlo Giocoli, Matthias Bartelmann, Ravi K Sheth, and Marcello Cacciato. "Halo model description of the non-linear dark matter power spectrum at k » 1 Mpc-1." In: *Monthly Notices of the Royal Astronomical Society* 408.1 (2010), pp. 300–313.

[35] ENNIO Gozzi, M Reuter, and WD Thacker. "Hidden BRS invariance in classical mechanics. II." In: *Physical Review D* 40.10 (1989), p. 3363.

[36] I. S. Gradshteyn and I. M. Ryzhik. *Table of integrals, series, and products*. Seventh. Translated from the Russian, Translation edited and with a preface by Alan Jeffrey and Daniel Zwillinger, With one CD-ROM (Windows, Macintosh and UNIX). Elsevier/Academic Press, Amsterdam, 2007, pp. xlviii+1171. ISBN: 978-0-12-373637-6; 0-12-373637-4.

[37] *IAU members vote to recommend renaming the Hubble law as the Hubble-Lemaître law*. https://www.iau.org/news/pressreleases/detail/iau1812/. Accessed: 2020-09-28.

[38] Wolfram Research, Inc. *Mathematica, Version 12.1*. Champaign, IL, 2020. URL: https://www.wolfram.com/mathematica.

[39] Henrietta S. Leavitt and Edward C. Pickering. "Periods of 25 Variable Stars in the Small Magellanic Cloud." In: *Harvard College Observatory Circular* 173 (Mar. 1912), pp. 1–3.

[40] G. Lemaître. "Un Univers homogène de masse constante et de rayon croissant rendant compte de la vitesse radiale des nébuleuses extra-galactiques." In: *Annales de la Société Scientifique de Bruxelles* 47 (Jan. 1927), pp. 49–59.

[41] Robert Lilow, Felix Fabis, Elena Kozlikin, Celia Viermann, and Matthias Bartel-mann. "Resummed Kinetic Field Theory: general formalism and linear structure growth from Newtonian particle dynamics." In: *Journal of Cosmology and Astroparticle Physics* 2019.04 (2019), p. 001.

[42] Carsten Littek. "Kinetic Field Theory: Momentum-Density Correlations and Fuzzy Dark Matter." PhD thesis. 2018.

[43] Mark R Lovell, Carlos S Frenk, Vincent R Eke, Adrian Jenkins, Liang Gao, and Tom Theuns. "The properties of warm dark matter haloes." In: *Monthly Notices of the Royal Astronomical Society* 439.1 (2014), pp. 300–317.

[44] Viatcheslav F Mukhanov and GV Chibisov. "Quantum fluctuations and a non-singular universe." In: *JETP Letters* 33.10 (1981), pp. 532–535.

[45] Riccardo Murgia, Alexander Merle, Matteo Viel, Maximilian Totzauer, and Aurel Schneider. ""Non-cold" dark matter at small scales: a general approach." In: *Journal of Cosmology and Astroparticle Physics* 2017.11 (2017), p. 046.

[46] Julio F Navarro, Carlos S Frenk, and Simon DM White. "A universal density profile from hierarchical clustering." In: *The Astrophysical Journal* 490.2 (1997), p. 493.

[47] Gergő Nemes. "An explicit formula for the coefficients in Laplace's method." In: *Constructive Approximation* 38.3 (2013), pp. 471–487.

[48] Go Ogiya and Oliver Hahn. "What sets the central structure of dark matter haloes?" In: *Monthly Notices of the Royal Astronomical Society* 473.4 (2018), pp. 4339–4359.

[49] Frank WJ Olver, Daniel W Lozier, Ronald F Boisvert, and Charles W Clark. *NIST handbook of mathematical functions hardback and CD-ROM*. Cambridge university press, 2010.

[50] Phillip James Edwin Peebles. *The large-scale structure of the universe*. Vol. 98. Princeton university press, 1980.

[51] Riccardo Penco and Danilo Mauro. "Perturbation theory via Feynman diagrams in classical mechanics." In: *European journal of physics* 27.5 (2006), p. 1241.

[52] A. A. Penzias and R. W. Wilson. "A Measurement of Excess Antenna Temperature at 4080 Mc/s." In: *Astrophysical Journal* 142 (July 1965), pp. 419–421. DOI: 10.1086/148307.

[53] S. Perlmutter et al. "Measurements of Ω and Λ from 42 High-Redshift Supernovae." In: *Astrophysical Journal* 517.2 (June 1999), pp. 565–586. DOI: 10.1086/307221. arXiv: astro-ph/9812133 [astro-ph].

[54] T Poston and Ian Stewart. "Catastrophe theory and its applications. Surveys and reference works in mathematics." In: *Pitman, London* (1978).

[55] Adam G. Riess et al. "Observational Evidence from Supernovae for an Accelerating Universe and a Cosmological Constant." In: *Astronomical Journal* 116.3 (Sept. 1998), pp. 1009–1038. DOI: 10.1086/300499. arXiv: astro-ph/9805201 [astro-ph].

[56] Vera C Rubin and W Kent Ford Jr. "Rotation of the Andromeda nebula from a spectroscopic survey of emission regions." In: *The Astrophysical Journal* 159 (1970), p. 379.

[57] Peter Schneider. *Einführung in die extragalaktische Astronomie und Kosmologie*. Springer-Verlag, 2006.

[58] Peter Schneider and Matthias Bartelmann. "The power spectrum of density fluctuations in the Zel'dovich approximation." In: *Monthly Notices of the Royal Astronomical Society* 273.2 (1995), pp. 475–483.

[59] Volker Springel, Rüdiger Pakmor, Annalisa Pillepich, Rainer Weinberger, Dylan Nelson, Lars Hernquist, Mark Vogelsberger, Shy Genel, Paul Torrey, Federico Marinacci, et al. "First results from the IllustrisTNG simulations: matter and galaxy clustering." In: *Monthly Notices of the Royal Astronomical Society* 475.1 (2018), pp. 676–698.

[60] Volker Springel, Simon DM White, Adrian Jenkins, Carlos S Frenk, Naoki Yoshida, Liang Gao, Julio Navarro, Robert Thacker, Darren Croton, John Helly, et al. "Simulations of the formation, evolution and clustering of galaxies and quasars." In: *nature* 435.7042 (2005), pp. 629–636.

[61] James E Taylor and Joseph Silk. "The clumpiness of cold dark matter: implications for the annihilation signal." In: *Monthly Notices of the Royal Astronomical Society* 339.2 (2003), pp. 505–514.

[62] Matteo Viel, K Marković, Marco Baldi, and Jochen Weller. "The non-linear matter power spectrum in warm dark matter cosmologies." In: *Monthly Notices of the Royal Astronomical Society* 421.1 (2012), pp. 50–62.

[63] Mark Vogelsberger, Federico Marinacci, Paul Torrey, and Ewald Puchwein. "Cosmological simulations of galaxy formation." In: *Nature Reviews Physics* 2.1 (2020), pp. 42–66.

[64] J Wang, S Bose, CS Frenk, L Gao, A Jenkins, V Springel, and SDM White. "Universal structure of dark matter haloes over a mass range of 20 orders of magnitude." In: *Nature* 585.7823 (2020), pp. 39–42.

[65] DH Weinberg and JE Gunn. "Largescale structure and the adhesion approximation." In: *Monthly Notices of the Royal Astronomical Society* 247 (1990), p. 260.

[66] John Wojdylo. "Computing the Coefficients in Laplace's Method." In: *Siam Review - SIAM REV* 48 (Mar. 2006), pp. 76–96. DOI: 10.1137/S0036144504446175.

[67] John Wojdylo. "On the coefficients that arise from Laplace's method." English. In: *Journal of Computational and Applied Mathematics* 196.1 (2006), pp. 241–266. ISSN: 0377-0427. DOI: 10.1016/j.cam.2005.09.004.

[68] R. Wong. *Asymptotic Approximation of Integrals*. Classics in Applied Mathematics. Society for Industrial and Applied Mathematics, 2001. ISBN: 9780898714975. URL: https://books.google.de/books?id=KQHPHPZs8k4C.

[69] Jesús Zavala and Carlos S Frenk. "Dark matter haloes and subhaloes." In: *Galaxies* 7.4 (2019), p. 81.